UNIVERSIDADE FEDERAL FLUMINENSE

INSTITUTO DE FÍSICA

PROGRAMA DE PÓS-GRADUAÇÃO EM FÍSICA

MESTRADO EM FÍSICA

JAYANA ANTUNES SAES DE LIMA

EQUATION-OF-STATE INDEPENDENT RELATIONS FOR NEUTRON STARS

Niterói
2022

JAYANA ANTUNES SAES DE LIMA

EQUATION-OF-STATE INDEPENDENT RELATIONS FOR NEUTRON STARS

Dissertação de Mestrado apresentada ao Programa de Pós-Graduação em Física da Universidade Federal Fluminense, como parte dos requisitos necessários para a obtenção do Título de Mestre em Física.

Orientadora: Raissa Fernandes Pessoa Mendes

Niterói-RJ

2022

Ficha catalográfica automática - SDC/BIF
Gerada com informações fornecidas pelo autor

S127e Saes de lima, Jayana Antunes
Equation-of-State Independent Relations For Neutron Stars / Jayana Antunes Saes de lima ; Raissa Fernandes Pessoa Mendes, orientadora. Niterói, 2022.
109 p. : il.

Dissertação (mestrado)-Universidade Federal Fluminense, Niterói, 2022.

DOI: http://dx.doi.org/10.22409/PPGF.2022.m.15310958797

1. Estrela de nêutrons. 2. Relatividade geral (Física). 3. Produção intelectual. I. Mendes, Raissa Fernandes Pessoa, orientadora. II. Universidade Federal Fluminense. Instituto de Física. III. Título.

CDD -

Bibliotecário responsável: Debora do Nascimento - CRB7/6368

EQUATION-OF-STATE INDEPENDENT RELATIONS FOR NEUTRON STARS

Dissertação apresentada ao Curso de Mestrado em Física da Universidade Federal Fluminense, como requisito parcial para obtenção do Grau de Mestre. Área de Concentração: Gravitação e Astrofísica.

Aprovada em MARÇO de 2022.

Prof. Dra. RAISSA FERNANDES PESSOA MENDES - Orientadora
UFF

Prof. Dra. CECÍLIA BERTONI MARTHA HADLER CHIRENTI
UFABC

Prof. Dr. RODRIGO PICANÇO NEGREIROS
UFF

Niterói-RJ
2022

I dedicate this work to my brothers Gabriel and Nino and my sisters Flora, Liria and Indaiá.

Acknowledgements

I would like to thank my parents for the kind words of encouragement and support through the last couple of years. I would also like to thank my godmother for being a constant supporter of my academic career and sharing its few ups and numerous downs with me. I'd like to thank my uncle André for the supportive presence and I'd like to thank my grandmother who is responsible for so much of what I am today and without whom I would certainly not be here.

I would like to thank Marcelo for once again enduring me during the last two years, which may not have been easy, and cheering me with the most nonchalant attitude possible — as usual.

I would like to thank Bernardo who was fundamental in my adjustment to the university and helped me greatly with all possible difficulties I had in the past years, including all general breakdowns and crisis involved in the process of writing this thesis.

I would like to thank Kathie for all the support, company and love, and for being such a warm presence in my life. I couldn't have done without you helping me and (occasionally) making tortillas for me.

I'd like to more than thank Vitor for being there for me during absolutely every step of the way, holding my hand (even without a bike), for being my absolute greatest cheerleader and not doubting me for a second (even during the many times that I did). I am extremely grateful and lucky to share my life with you.

Lastly, I would like to immensely thank my supervisor Prof. Raissa, who is the best supervisor I could ask for and teaches by example about being an amazing researcher and person. I am honored of you having accepted to guide me through my Masters studies.

I acknowledge financial support by CNPq.

Contents

Resumo

Relações independentes de equações de estado entre duas ou mais propriedades macroscópicas de estrelas de nêutrons se mostraram de extrema utilidade. Exemplos incluem a relação "I-Love-Q" e a relação entre as deformabilidades por maré das componentes de um sistema binário de estrelas de nêutrons (*binary love relations*). Estas relações são amplamente utilizadas para extrair informações relevantes sobre estrelas de nêutrons a partir de observações. Relações universais entre propriedades macroscópicas e microscópicas de estrelas de nêutrons, por outro lado, podem ser de extrema relevância do ponto de vista de serem capaz de prover informação sobre as propriedades microfísicas da estrela a partir de dados obsevacionais. Essa informação pode ser utilizada para expandir o nosso conhecimento do ainda desconhecido interior de estrelas de nêutrons. Nesse trabalho, nós discutimos diversas relações independentes da equação de estado tanto entre propriedades macroscópicas quanto entre propriedades microscópicas e macroscópicas. Notavelmente, nós apresentamos e analisamos uma nova relação entre certos observáveis macroscópicos, a compacidade da estrela, sua deformabilidade por maré e seu momento de inérica e uma medida microscópica da dureza da matéria nuclear. Nós também investigamos o efeito que diferentes suposições têm na relação.

Palavras-chave: Estrelas de nêutrons. Relatividade Geral. Relações Universais.

Abstract

Equation of state (EoS) insensitive relations between macroscopic properties of neutron stars have proven to be extremely useful. Examples include the I-Love-Q relation, and the binary love relation, which is the relation between the tidal deformabilities of the components of a neutron star-neutron star binary system. These relations have been widely used to extract relevant neutron star data from observations. EoS-insensitive relations between macroscopic and microscopic properties of neutron stars, on the other hand, can be quite relevant in the sense of informing us of the microphysical properties of the star, given the observational data. This information can be used to further expand our knowledge of the still unknown interior of neutron stars. In this work we discuss several EoS-insensitive relations both between different macroscopic and microscopic properties of neutron stars. Notably, we uncover and analyze a tight relation between certain macroscopic observables, the star compactness, its tidal deformability and its moment of inertia and a microscopic measure of the stiffness of nuclear matter. We also further investigate the effect that different assumptions have on the relation.

Keywords: Neutrons Stars. General Relativity. Universal Relations.

Chapter 1

Introduction

Neutron star (NS) are astrophysical objects remnant of the process of gravitational collapse of a massive main sequence star. They are extremely compact objects with a mass close to the solar mass ($M_\odot$) but with a radius of the order of 10 km, with central densities that can exceed $\sim 10^{14}\mathrm{g/cm}^3$.

In such an extreme environment, General Relativity is necessary in order to explain the behavior of these objects, since Newtonian gravity is no longer adequate to do so. Also it is not known how matter behaves at such high densities, since they are not reachable in Earth experiments at the temperatures that are present inside the star. Besides this, there is also a difficulty in making accurate theoretical predictions, since densities in the core of NSs exceed those where nuclear models are well tested, and is far below those where perturbative Chromodynamic (QCD) calculations can be performed. This means that the equation that describes the properties of neutron stars, its equation of state (EoS), is not known.

Since their existence was proposed in 1934 [1] efforts to understand the interior structure and behavior of neutron stars (examples include Refs. [2–6]) and several methods to constrain the neutron star equation of state through observational data were developed (examples include Refs. [7–21]).

Currently the field of compact objects – black holes and neutron stars – is very active, with several observational efforts underway. Particularly, the first detection of gravitational waves (GW) from neutron stars in 2017 by the LIGO/VIRGO collaboration [22] and the launching of the Neutron Star Interior Composition Explorer, NICER, telescope (analyses made of data from this mission include Refs. [23, 24] and [25, 26]) were

responsible for boosting the study and understanding of neutron stars. GW observations lead to deformability and mass measurements whilst the data from NICER has lead to radius and mass measurements of pulsars. And with the growing number of measurements of macroscopic properties of neutron stars, the constraints to the equation of state will also increase.

Universal relations play an important part on how the parameters of neutron stars can be measured through observational data. These are relations that connect two or more NS properties whose behavior remain unchanged independently of the choice of equation of state; they are also called EoS-independent relations, examples include the universal relation between the tidal deformabilities of a binary neutron star system [27], the relations between the multipole tidal deformabilities of a NS [28] and the relations "I-Love-Q", between the tidal deformability, moment of inertia and quadrupole moment of a NS [29]. Some of these relations, specifically the ones between macroscopic parameters, are what make it possible for certain observables to be measured and some are responsible for decreasing the uncertainties associated with the measurements. For example, the "binary love relations" [27] make it possible to measure individual deformabilities from a gravitational wave detection from a binary system and the "I-Love-Q" relations [29] break important degeneracies in the GW phase.

If universal relations between macroscopic quantities are so fundamental in the current measurements of NS properties, relations that connect macroscopic quantities to microscopic ones independently of the EoS (e.g. Ref. [30], that connects the pressure at densities close to the nuclear saturation density and the radius of a star with specific values of mass) can be an equally important tool in the understanding of the equation of state. Unfortunately, the number of micro-macro universal relations is much lower when compared to the macro-macro relations, since the internal properties of an object tend to depend strongly on the matter inside it.

In the sense of exploring internal neutron star properties we propose and analyze three approximate EoS-insensitive relations. They are between an average parameter for the EoS stiffness $\alpha_c = p_c/\epsilon_c$ where p_c and ϵ_c are respectively the pressure and the energy density at the center of the star and three macroscopic observables, the compactness of the star $C = GM/(Rc^2)$, where M is the star mass and R is the star radius, the dimensionless tidal deformability $\overline{\Lambda}$, that characterizes the deformability of a neutron star

to a given moment of the tidal field, and the dimensionless moment of inertia $\overline{I}$ of the star. These relations are then analyzed with different assumptions on the observables and the microscopic quantities.

The following work is divided as follows: in Chapter 2 we discuss the structure of neutron stars and the equations used to calculate the macroscopic properties of the star used here; we study both the equilibrium configuration and the perturbations of neutron stars. In Chapter 3 we discuss the equation of state of neutron stars, the difficulties in determining it and possible parametrizations to it. In Chapter 4 a literature survey of universal relations is presented along with the demonstration and analysis of the $\alpha_c - C/\overline{\Lambda}/\overline{I}$ relations. Chapter 5 gathers our main conclusions. In what follows, natural units where $G = c = 1$ are adopted unless stated otherwise.

Chapter 2

Neutron Star Equilibrium and Perturbations

Neutron stars were first thought of shortly after the discovery of the neutron [1], as a method of explaining the existence of supernovae, in which the occurrence of a supernova would be representative of the transition of an ordinary, what is now called a main-sequence, star into a neutron star.

It is now known that neutron stars are formed as a result of the gravitational collapse of a star, in which a supernova typically occurs. Main sequence stars are able to maintain equilibrium by performing stellar nucleosynthesis that generates radiation, which exercises pressure outwardly, and also maintaining the temperature of the gas, which determines its pressure. This pressure is responsible for balancing the inward pull caused by the gravitational field. Nuclear fusion inside the star core consists in hydrogen nucleus being fused into helium and helium being burned into heavier elements, liberating energy.

In these stars, when hydrogen fuel starts to become scarce, stars begin fusing helium atoms and in massive stars ($M > 8M_{\odot}$, where $M_{\odot}$ is the mass of the Sun), the fusion process continues up until iron is generated, at which point it is no longer energetically favorable to fuse the atoms due to the high binding energy of iron, which is the highest of the periodic table. As the amount of iron in the core begins to grow, energy due to nuclear fusion is no longer released and the gravitational force takes over, increasing the density in the star's core, forcing electrons to occupy same energy levels, and because electrons are fermions, this generates degeneracy pressure, that is capable of

balancing out the gravitational force; the final object is called a white dwarf [31]. With the initial mass $M > 8M_\odot$, this iron core is generally over the Chandrasekhar limit [31] $M \gtrsim 1.39M_\odot$, the maximum mass for which it is possible for this object to remain stable. This limit can also be reached by a white dwarf, previously in equilibrium, that accretes matter up until it exceeds its mass limit. As the outer layer of the star burns, mass is deposited in the core, and the electron degeneracy pressure is no longer capable of sustaining the star, which becomes hotter causing the breaking of iron nuclei, liberating protons that ignite the process of electron capture that consists in a proton capturing an electron and releasing a neutrino and a neutron. The increase of neutrons in the core causes them to become degenerate and the degeneracy pressure stops the collapse of outer layers, which leads them to be expelled in a supernova explosion. If the neutron core that remains has $M \lesssim 3M_\odot$ it no longer collapses and is able to maintain equilibrium using both the neutron degeneracy pressure and the interaction between nucleons [32], with a radius of only a few kilometers. This core is called a neutron star.

2.1 Equilibrium Configuration

These stars are extremely compact, with densities of the order of $\rho \sim 10^{14}$ g/cm^3, whereas the average density of the Sun is $\rho_\odot = 1.4$ g/cm^3. For this reason Newtonian gravity is not capable of accurately describing them and the use of General Relativity is necessary.

Describing material objects in the formalism of General Relativity requires two different aspects of these objects. The first aspect regards the geometry of the spacetime where it is located and around it, and the second regards the object's behavior as matter or radiation.

The geometry of the spacetime is described by the metric, that is defined from the line element ds [33]:

$$ds^2 = g_{\mu\nu} dx^\mu dx^\nu, \tag{2.1}$$

where x represents the spacetime coordinates, with $\mu, \nu \in \{0, 1, 2, 3\}$, 0 being the time-like coordinate, $(1, 2, 3)$ being the 3-dimensional space-like coordinates, and the metric being

the second order tensor $g_{\mu\nu}$. From now on, Greek indices represent numbers from 0 to 3, and Latin indices numbers from 1 to 3; there is also a convention, that will be used in this entire work, called the Einstein notation, where a repeated index imply in a sum over such indices.

The simplest (without considering rotation, which will be treated later on) condition of gravitational equilibrium for a fluid, in this case, a neutron star, will result in matter that has a static and spherically symmetric distribution, so we choose the spherical coordinates r, θ and φ. The spacetime in this case is described by the following line element [34]:

$$ds^2 = -e^{\nu}dt^2 + e^{\lambda}dr^2 + r^2 d\theta^2 + r^2 \sin^2\theta d\varphi^2, \tag{2.2}$$

where ν and λ are functions to be determined, that depend only on the radial coordinate r, in agreement with the hypothesis of spherical symmetry. Outside the star, meaning $r > R$, where R is the radius of the star, the spacetime is described by the Schwarzschild metric:

$$ds^2 = -\left(1 - \frac{2M}{r}\right) dt^2 + \left(1 - \frac{2M}{r}\right)^{-1} dr^2 + r^2 d\theta^2 + r^2 \sin^2\theta \, d\varphi^2, \tag{2.3}$$

where M is the total mass of the star.

The second part needed in this description is the energy-momentum tensor. It is a second order tensor that carries information regarding the momentum and energy, it also enables a more general description of the conservation of these quantities. This tensor is represented by $T^{\mu\nu}$, and is symmetric in General Relativity, meaning $T^{\mu\nu} = T^{\nu\mu}$.

It can be separated in different components, the meaning of which are as follows, without sum over repeated indices [32]:

- T^{00} represents the energy density;
- T^{0i} represents energy flux — the amount of energy passing through a surface with constant x^i in an amount of time;

- T^{ik} is the so-called *stress tensor* and it represents shear stress. Its components mean the amount of the i-th component of the momentum passing through a surface with constant x^k per amount of time;
- T^{ii} represent each of the components of the stress, if they are the same in every direction, this is called pressure.

The conservation of energy and momentum is given by four equations, that can be condensed as one:

$$\nabla_\mu T^{\mu\nu} = 0. \tag{2.4}$$

This equation says that the four-divergence of the energy-momentum tensor vanishes. ∇_μ is the covariant derivative, which is a generalization of the regular derivative. It is useful in General Relativity because, differently than the regular derivative, the covariant derivative maps tensors into tensors. It is defined, when applied to a 2^{nd} order tensor with both contravariant indices as:

$$\nabla_\mu T^{\mu\nu} = \partial_\mu T^{\mu\nu} + \Gamma^\nu_{\rho\mu} T^{\rho\mu} + \Gamma^\mu_{\rho\mu} T^{\nu\rho}, \tag{2.5}$$

where ∂_μ is an abbreviated form of the regular derivative $\frac{\partial}{\partial x^\mu}$ and $\Gamma^\nu_{\rho\mu}$ is the Christoffel symbol, a useful object in General Relativity used to define several important concepts, such as geodesics, parallel transport and the covariant derivative. This symbol is defined as [33]:

$$\Gamma^\nu_{\rho\mu} = \frac{1}{2} g^{\nu\sigma} (\partial_\rho g_{\mu\sigma} + \partial_\mu g_{\sigma\rho} - \partial_\sigma g_{\mu\rho}), \tag{2.6}$$

where $g^{\nu\sigma}$ is the inverse metric, that is defined as:

$$g^{\mu\nu} g_{\nu\sigma} = \delta^\mu_\sigma \tag{2.7}$$

where $\delta^\mu{}_\sigma$ is the Kronecker delta, a second order tensor that has components $\delta^\sigma{}_\sigma = 1$ and

$\delta^{\mu}{}_{\sigma} = 0$ if $\mu \neq \sigma$.

A fluid without viscosity, shear stress or heat conduction is called a perfect fluid, and that is a good way to describe the matter inside a neutron star. A perfect fluid can be entirely described by its energy density and its isotropic pressure. The energy-momentum tensor for such a fluid is written as [35]:

$$T^{\mu\nu} = (p + \epsilon)u^{\mu}u^{\nu} + pg^{\mu\nu}, \tag{2.8}$$

where p is the pressure, ϵ is the energy density (as measured in the fluid's rest frame) and u^{μ} is the 4-velocity of the fluid elements, it is defined as:

$$u^{\mu} = \frac{dx^{\mu}}{d\tau}, \tag{2.9}$$

where τ is the proper time, a more fitting way to describe movement in General Relativity because it is frame-independent, whereas the usual time t is not. The proper time can be thought of as the time in the locality of a clock, its formal definition is given by $d\tau^2 = -ds^2$ along the clock's worldline.

Using Equations (2.9) alongside the metric defined in (2.2), it is possible to find that $u^i = 0$ (as we are considering a static equilibrium configuration, all space-like coordinates are stationary) and $u^0 = -e^{\nu/2}$. Leading to, in indices of mixed types, that are obtained by contracting the tensor with the covariant metric:

$$\begin{aligned} T^{0}{}_{0} &= -\epsilon, \\ T^{1}{}_{1} = T^{2}{}_{2} &= T^{3}{}_{3} = p, \\ T^{\mu}{}_{\nu} &= 0, \text{ for } \mu \neq \nu. \end{aligned} \tag{2.10}$$

One of the greatest changes brought by Einstein's theory of General Relativity is the idea that instead of a gravitational force acting on massive bodies, massive bodies distort the spacetime, creating the effects perceived as gravity. This idea is mathematically expressed as the Einstein field equations, that are 10 independent equations that can be expressed as one tensorial equation [36]:

$$G^{\mu}{}_{\nu} = 8\pi T^{\mu}{}_{\nu}, \tag{2.11}$$

where $G^{\mu}{}_{\nu}$ is the Einstein tensor, defined as:

$$G^{\mu}{}_{\nu} = R^{\mu}{}_{\nu} - \frac{1}{2} R g^{\mu}{}_{\nu}, \tag{2.12}$$

where $R^{\mu}{}_{\nu}$ is the Ricci tensor defined as:

$$R_{\mu\nu} = \partial_{\nu}\Gamma^{\sigma}_{\mu\sigma} - \partial_{\sigma}\Gamma^{\sigma}_{\mu\nu} + \Gamma^{\alpha}_{\mu\sigma}\Gamma^{\sigma}_{\alpha\nu} - \Gamma^{\alpha}_{\mu\nu}\Gamma^{\sigma}_{\alpha\sigma}. \tag{2.13}$$

The tensor with mixed components $R^{\mu}{}_{\nu}$ can be obtained by contracting the one in this equation with the inverse metric. R is the Ricci scalar, defined as the trace, meaning the sum of the diagonal values, of the mixed-type Ricci tensor: $R = R^{\mu}{}_{\mu}$.

With these definitions, is then possible to find the equations that describe the behavior of a neutron star in equilibrium. This calculation and analysis was first performed by Tolman [2], Oppenheimer and Volkoff [3], which is why these equations are called the TOV equations. They can be obtained by solving the Equations (2.11) and Equations (2.4).

By computing the Einstein tensor we find that only its diagonal components are non-zero, and as only the diagonal terms are non-zero for the energy-momentum tensor as well, this reduces the 16 equations contained in (2.11) to 4. We also find that $G^{2}{}_{2} = G^{3}{}_{3}$, remaining, then, only 3 equations:

$$G^{0}{}_{0} = -e^{-\lambda}\left(-\frac{1}{r^2} + \frac{\lambda'}{r}\right) - \frac{1}{r^2} = -8\pi\epsilon \tag{2.14}$$

$$G^{1}{}_{1} = e^{-\lambda}\left(-\frac{1}{r^2} + \frac{\nu'}{r}\right) - \frac{1}{r^2} = 8\pi p \tag{2.15}$$

$$G^{2}{}_{2} = e^{-\lambda}\left[-\frac{(\lambda' - \nu')(2 + r\nu')}{4r} + \frac{\nu''}{2}\right] = 8\pi p, \tag{2.16}$$

where one prime mark indicates total derivative in relation to the r coordinate and two primes indicate second-order total derivative in relation to the same coordinate.

Equation (2.14) can be rewritten as:

$$1 - 8\pi\epsilon r^2 = \frac{d}{dr}(re^{-\lambda}), \tag{2.17}$$

which can be integrated from 0 to r, using the definition of mass aspect function:

$$m(r) = \int_0^r 4\pi\epsilon(r')r'^2 dr', \tag{2.18}$$

to obtain

$$e^{-\lambda} = 1 - \frac{2m}{r}. \tag{2.19}$$

Substituting this in Equation (2.15), we obtain:

$$\frac{d\nu}{dr} = \frac{2(4p\pi r^3 + m)}{r(r - 2m)}. \tag{2.20}$$

From Equation (2.4), we find that $\nabla_\mu T^\mu{}_0 = \nabla_\mu T^\mu{}_2 = \nabla_\mu T^\mu{}_3$ are identically zero and the only non-zero component leads to:

$$\frac{d\nu}{dr} = -\frac{2}{(p + \epsilon)}\frac{dp}{dr}, \tag{2.21}$$

that can be used to rewrite (2.20) as:

$$\frac{dp}{dr} = -(p + \epsilon)\frac{(4p\pi r^3 + m)}{r(r - 2m)}. \tag{2.22}$$

Equation (2.18) in its differential form

$$\frac{dm}{dr} = 4\pi r^2\epsilon, \tag{2.23}$$

alongside Equations (2.22) and (2.20) are the TOV equations.

As these equations describe the interior of the star, the interior metric needs to match the exterior metric (2.3) at the surface of the star. We can define this surface at $r = R$, where R is the radius at which the pressure drops to zero, $p(R) = 0$. The boundary is defined this way because outside the star the pressure generated by it is zero, so defining it as zero at the surface is required in order to maintain a finite pressure gradient. At the surface of the star, we have:

$$e^{-\lambda(R)} = 1 - \frac{2M}{R}, \tag{2.24}$$

and

$$e^{\nu(R)} = 1 - \frac{2M}{R}. \tag{2.25}$$

Consequently:

$$e^{\nu(R)} = e^{-\lambda(R)}. \tag{2.26}$$

Solving the TOV equations gives us the total mass M, radius R, pressure profile of the star and values of ν and λ inside the star. This procedure is done by integrating the differential Equations (2.23), (2.20) and (2.22). To perform it, a relation in the form

$$F(p, \epsilon) = 0, \tag{2.27}$$

is necessary. This relation is called the Equation of State, EoS, that will be discussed in details in the next chapter. It is fundamental in the understanding the properties of matter in general. The EoS that describes the matter inside NSs is not yet fully determined.

These equations are integrated from the center of the star, $r = 0$, or in actuality, a very small cutoff radius, $r = r_0$, of the order of a centimeter, to the radius R, this radius is, as mentioned, defined by $p(R) = 0$. We begin by determining the boundary conditions for each of the equations:

- The central pressure p_c is determined by picking a value for the central energy density ϵ_c and using (2.27) to connect it to the corresponding pressure.
- Assuming that $m(r)$ is regular around the stellar center, using the cutoff radius,

the central mass is determined by $m(r_0) = \frac{4}{3}\pi r_0^3 \epsilon_c + \mathcal{O}(r_0^5)$, where ϵ_c is the central energy density.

- The function ν is determined at the radius of the star by (2.25), so we choose an arbitrary value for $\nu(r_0)$ and integrate the equations. Then, we correct it by a constant throughout the star so it matches the value found by substituting the total mass and radius that were obtained in the integration in (2.25). This procedure is possible since the TOV equations are invariant under a $\nu \to \nu + cte$ transformation.

These steps can be performed numerically through several different methods for solving differential equations, such as Runge-Kutta, the Euler method and others. Here, the ordinary differential equations are solved using a 4-th order Runge-Kutta method.

2.2 Perturbed Configuration

The equilibrium configuration considered so far, although useful, does not accurately represent most astrophysical objects, including neutron stars. A more realistic description can be found through the use of perturbations that are implemented on top of the equilibrium description. In the next sections we discuss perturbations of this description, specifically, perturbations caused by tidal forces and rotation.

From here on we shall consider small perturbations of the star. This configuration is described by the displacement of the fluid in relation to the coordinate system. As a result of this motion the spacetime both externally and internally no longer corresponds to the equilibrium configurations shown in (2.1) and (2.2). The perturbed configuration of the star can be described using a linear expansion, such as:

$$g_{\mu\nu} = g^{(0)}_{\mu\nu} + h_{\mu\nu}, \tag{2.28}$$

in which $g^{(0)}_{\mu\nu}$ is the background, non-perturbed, metric (2.2) and $h_{\mu\nu}$ is the perturbation of the metric, which will be better described when a specific perturbation is considered. As the displacement of the fluid is not large, we use only a first order approximation, so that any terms that are quadratic in the perturbed metric are considered sufficiently small when compared to the background metric and can be discarded.

The differential perturbation equations that $h_{\mu\nu}$ obeys are determined by solving

the perturbed Einstein equations:

$$\delta G^{\mu}{}_{\nu} = 8\pi\, \delta T^{\mu}{}_{\nu}, \tag{2.29}$$

in which the δ indicates the perturbation of the quantity that it precedes. After finding them, and providing an equation of state, they can be, often numerically, solved in order to find the coefficients of the perturbation $h_{\mu\nu}$.

The perturbed Einstein tensor is obtained by performing the same calculations done in the previous section using Equation (2.12), except the equilibrium metric is replaced by the one on (2.28):

$$\delta G^{\mu}{}_{\nu} = \delta R^{\mu}{}_{\nu} - \frac{1}{2}\,\delta R\, g^{\mu}{}_{\nu}{}^{(0)}, \tag{2.30}$$

where $\delta R^{\mu}{}_{\nu}$ can be found by contracting the inverse metric with [37]

$$\delta R_{\nu\mu} = -\nabla_{\beta}\,\delta\Gamma^{\beta}_{\nu\mu} + \nabla_{\nu}\,\delta\Gamma^{\beta}_{\beta\mu} \tag{2.31}$$

and

$$\delta\Gamma^{\beta}_{\nu\mu} = \frac{1}{2}\, g^{\alpha\beta(0)}(\nabla_{\nu}\, h_{\mu\alpha} + \nabla_{\mu}\, h_{\nu\alpha} - \nabla_{\alpha}\, h_{\nu\mu}). \tag{2.32}$$

The total energy-momentum tensor is given by:

$$T^{\mu}{}_{\nu} = (\epsilon + p)\, u_{\nu} u^{\mu} + p\, \delta^{\mu}{}_{\nu} \tag{2.33}$$

where $\epsilon = \epsilon^{(0)} + \delta\epsilon$ is the total energy density, with $\epsilon^{(0)}$ being the energy density of the equilibrium configuration and $\delta\epsilon$ being its increment, $p = p^{(0)} + \delta p$ is the total pressure with $p^{(0)}$ being the pressure of the equilibrium configuration and δp being its increment.

Calculating the Einstein tensor and the energy-momentum tensor and using them in Equation (2.29), we find the perturbation equations, that need to be solved to give a clear view of the perturbed behavior of the neutron star.

2.2.1 Tidal Deformation

Tidal forces are caused by the non-homogeneity in the gravitational attraction between two bodies. A well-known example of this force are tides, caused by the attraction between the Moon, Sun and the Earth. As points of the planet are closer to the Moon, the gravitational impact they are subject to is greater than the one on points further away from it. Points that are not aligned with the Earth-Moon direction, also have components of acceleration caused by the tidal force in the direction of the center of the Earth. This configuration results in a quadrupolar pattern, meaning the Earth acquires a quadrupolar momentum.

Besides the effects that tidal forces have on oceans, they also have a less visible effect on the entirety of Earth's structure. This effect can be observed by measuring the different values of g, the acceleration of the gravitational force, throughout the surface of the Earth [38]. The different responses a body can have to tidal forces are directly related to its interior structure. This type of deformation, of the object as a whole, is what we study. The analysis of tidal deformabilities, in the Newtonian context, was first made by [39], a more recent account was made by [38]. In the context of relativistic stars there are also several studies regarding the tidal proprieties of NSs, such as [40–44].

As a considerable number of neutron stars are part of a binary system, either with its companion being also a neutron star or other stellar object, the analysis of this configuration is extremely important and the external field considered is usually generated by these objects. The tidal deformability of neutron stars has been measured recently, via gravitational waves, for a NS-NS binary system [45]. This could be obtained because the neutron star tidal distortion has effects on the orbital dynamics and the gravitational waves of a binary system: the tidal deformability is connected to a tidal phase correction for the phase of the GW signal, this correction is of post-5-Newtonian order. More details on how the tidal deformability can be extracted from GW signals can be found in Ref. [15], Ref. [46], Ref. [47], that uses not only the GW data but also microscopic modeling to extract information on the tidal deformability, Ref. [48], that consider realistic equations of state and Ref. [49].

In this section we consider static tides, meaning that the variation of the external field responsible for the tides in a body is so slow, the body remains in hydrostatic equilibrium. In practice, what is required is that the timescale in which the external field

varies is much slower than the dynamical timescale of the neutron star, measured, for instance, by the frequency of its oscillation modes.

For simplicity, here we first consider the Newtonian case. An external gravitational potential U_{ext} generates a quadrupolar tidal moment $\mathcal{E}_{ij}$ in the form of:

$$\mathcal{E}_{ij}(t) \equiv -\,\partial_i \partial_j U_{ext}(t, \mathbf{0}); \tag{2.34}$$

here the coordinate system has its origin in the center of the body affected by the potential, meaning this is evaluated in the center of the star. As outside the star the potential obeys the Laplace equation $\nabla^2 U_{ext} = 0$, the tidal moment $\mathcal{E}_{ij}$ is symmetric and traceless. It causes a response of the body that generates an internal gravitational potential U_{body} that can be characterized by the symmetric and traceless quadrupole moment:

$$Q_{ij}(t) \equiv \int_{\mathbb{R}^3} \delta\rho(t, \mathbf{x}) \left(x^i x^j - \frac{1}{3} r^2 \delta_{ij} \right) d^3x \,, \tag{2.35}$$

where $\delta\rho$ is the perturbation to the mass density that is caused by the tidal field and $r \equiv |\mathbf{x}|$. The potential generated by a deformed star is:

$$U(t, \mathbf{x}) = \int d^3x' \, \frac{\rho(r') + \delta\rho(t, \mathbf{x}')}{|\,\mathbf{x} - \mathbf{x}'\,|}, \tag{2.36}$$

ρ is the mass density in the equilibrium configuration and it depends only on r as in equilibrium the star is spherically symmetric; the coordinates with the prime mark are integration variables ranging from the center to the surface of the star. Outside the star we can perform a multipole expansion, around the center of the star:

$$\frac{1}{|\,\mathbf{x} - \mathbf{x}'\,|} = \frac{1}{r} + \frac{x_i}{3}\, x_i' + \frac{3 n_i n_j - \delta_{ij}}{2 r^3} x_i' x_j' + \dots \,, \tag{2.37}$$

where $n_i \equiv \frac{x_i}{r}$. This expansion is valid at any point for which $r > r'$, meaning that it is valid outside the star. The first order term of the expansion (2.37) is the gravitational potential for a point source. Outside the star, the gravitational potential U_{ext} is added.

We can add it as an expansion around the center of mass:

$$U_{ext}(t, \mathbf{x}) = -\frac{1}{2}\,\mathcal{E}_{ij}\,x_i\,x_j + \mathcal{O}(x^3). \tag{2.38}$$

Substituting (2.37) in the Equation (2.36) and adding (2.38) we find:

$$U(t, \mathbf{x}) = \frac{M}{r} + \frac{3}{2r^3}\,n_i\,n_j\,Q_{ij}(t) + O\left(\frac{1}{r^4}\right) - \frac{1}{2}\,\mathcal{E}_{ij}(t)\,x_i\,x_j + \mathcal{O}(r^3), \tag{2.39}$$

where we have used the fact that the second term of the expansion (2.37) is null when substituted in the potential and that $Q_{ij}\,\delta^{ij} = 0$, since the quadrupole moment is a traceless tensor. As we are considering static perturbations, $\mathcal{E}_{ij}$ is static, which leads to the induced quadrupole Q_{ij} being time independent. In this case, to linear order, the quadrupole moment and the tidal moment are proportional to one another as:

$$Q_{ij} = -\Lambda\,\mathcal{E}_{ij}, \tag{2.40}$$

where Λ is a constant called tidal deformability. The second tidal Love number is defined as:

$$k_2 = \frac{3}{2\,R^5}\,\Lambda. \tag{2.41}$$

The gravitational potential (2.39) can be connected to the metric using a Newtonian approximation, which is valid far away from the star; in this case the metric can be written as:

$$ds^2 \simeq -(1 + 2\Phi)\,dt^2 + (1 - 2\Phi)\,\delta_{ij}\,dx^i\,dx^j, \tag{2.42}$$

where $\Phi = -U$ is the gravitational potential. With this relation we write [40]:

$$\frac{(1-g_{00})}{2} = \frac{M}{r} + \frac{3}{2r^3}\, n_i\, n_j\, Q_{ij}(t) + O\left(\frac{1}{r^4}\right) - \frac{1}{2}\,\mathcal{E}_{ij}(t)\, x_i\, x_j + \mathcal{O}(r^3). \tag{2.43}$$

By finding the components of the perturbed metric it is then possible to use this equation to determine the tidal Love number k_2 or the tidal deformability Λ.

All of the components of the perturbed metric, in principle, are non zero and depend on all spatial coordinates, since we are considering a static perturbation, there is no time dependence, so we can write $h_{\mu\nu} = h_{\mu\nu}(r, \theta, \varphi)$. The angular part of each component of the metric can be expanded into spherical harmonics $Y_l^m(\theta, \varphi)$. For example, if the component is a scalar given by $h_{00}(r, \theta, \varphi)$, this expansion is:

$$h_{00}(r, \theta, \varphi) = f(r)\, Y_l^m(\theta, \varphi). \tag{2.44}$$

Spherical harmonics are characterized by two parities, an even parity: $Y_l^m(\theta, \varphi) = Y_l^m(\pi - \theta, \pi + \varphi)$ and odd parity: $Y_l^m(\theta, \varphi) = -Y_l^m(\pi - \theta, \pi + \varphi)$. This difference is determined by the value of l, so that generically, we can write: $Y_l^m(\pi - \theta, \pi + \varphi) = (-1)^l Y_l^m(\theta, \phi)$. With this, the problem can then be separated into two, each one representing one of the possible parities of the spherical harmonics. As in this work we are interested in the Love number connected to the tidal deformability, which is the *electric* or *even* second tidal Love number k_2, we focus on the even parity perturbations with $l = 2$.

Gauge transformations can bring several simplifications to the metric. In its simplest form, the even components of the metric $h_{\mu\nu}$ can be written in the Regge-Wheeler gauge as [37]:

$$h_{\mu\nu} = \begin{bmatrix} -e^{\nu(r)} H_0(r) & H_1(r) & 0 & 0 \\ H_1(r) & e^{\lambda(r)} H_2(r) & 0 & 0 \\ 0 & 0 & r^2 K(r) & 0 \\ 0 & 0 & 0 & r^2 \sin^2\theta K(r) \end{bmatrix} Y_2^m(\theta, \varphi), \tag{2.45}$$

where the functions H_0, H_1, H_2 and K are determined by solving the perturbed Einstein Equations (2.30), and the functions $\nu(r)$ and $\lambda(r)$ are the ones used in the equilibrium configuration, meaning (2.20) and (2.19). With the explicit form of the perturbed metric, we may proceed to the calculation of the Einstein equations. The four-velocity components are given by $u^i = 0$ as the perturbation considered is stationary and the explicit form of u^0 can be determined by the normalization condition $g_{\mu\nu}u^\mu u^\mu = -1$; however we only use this component as $u_0\, u^0$, which is -1. The non-zero components of the perturbed energy-momentum tensor are:

$$\begin{aligned} T^0{}_0 &= \epsilon^{(0)} - \delta\epsilon, \\ T^1{}_1 = T^2{}_2 = T^3{}_3 &= p^{(0)} + \delta p, \\ T^\mu{}_\nu &= 0, \text{ for } \mu \neq \nu, \end{aligned} \tag{2.46}$$

where δp and $\delta\epsilon$ are the increments in pressure and energy density caused by the perturbation. The increment of the energy-momentum tensor, that we can call $\delta T^0{}_0$, can be rewritten as $\delta T^0{}_0 = -\delta\epsilon = -\left(\dfrac{dp}{d\epsilon}\right)^{-1}\delta p$, where we assume that the perturbed equation of state and the equilibrium equation of state are the same. From the equation $\delta G^1{}_0 = 8\pi\delta T^1{}_0 = 0$ we find:

$$-e^{-\lambda(r)}H_1(r)\frac{\csc^2\theta\,\partial_\varphi^2\,Y_2^m(\theta,\varphi) + \cot\theta\,\partial_\theta\,Y_2^m(\theta,\varphi) + \partial_\theta^2\,Y_2^m(\theta,\varphi)}{2r^2} = 0, \tag{2.47}$$

as the exponential is never 0 and neither are the spherical harmonics for arbitrary angles, this leads to $H_1(r) = 0$, simplifying the following calculations. From $\delta G^2{}_2 - \delta G^3{}_3 = 8\pi(\delta T^2{}_2 - \delta T^3{}_3) = 0$, we find:

$$-[H_0(r) - H_2(r)]\frac{1}{2r^2}\,\csc^2\theta\,\partial_\varphi^2\,Y_2^m(\theta,\varphi) + \cot\theta\,\partial_\theta\,Y_2^m(\theta,\varphi) - \partial_\theta^2\,Y_2^m(\theta,\varphi) = 0, \tag{2.48}$$

from which we obtain $H_2(r) = H_0(r) \equiv H(r)$. From equation $\delta G^2{}_1 = 8\pi\,\delta T^2{}_1 = 0$ we obtain:

$$\frac{1}{2r^2}\left[-K'(r) + H(r)\,\nu'(r) + H'(r)\right]\partial_\theta\, Y_2^m(\theta,\varphi) = 0, \tag{2.49}$$

that leads to $K'(r) = H(r)\,\nu'(r) + H'(r)$. The equation $\delta G^2{}_2 + \delta G^3{}_3 = 8\pi\,(\delta T^2{}_2 + \delta T^3{}_3)$ can be reduced to:

$$\frac{e^{-\lambda(r)}\,H(r)\,(\lambda' + \nu')}{16\pi r}\,Y_2^m(\theta,\varphi) = \delta p, \tag{2.50}$$

that, using the expressions for the function $\lambda(r)$ (2.19), its derivative and the expression for $\nu'(r)$ (2.20), equals:

$$\delta p = \frac{1}{2}(p+\epsilon)\,H(r)\,Y_2^m(\theta,\varphi). \tag{2.51}$$

We have now eliminated most of the unknown functions leaving only one, $H(r)$. Finding the equation that H obeys is to find the equation that describes the perturbation. To find it, we take $\delta G^0{}_0 - \delta G^1{}_1 = 8\pi\delta\, p\left(1 + 1/\frac{dp}{d\epsilon}\right)$, alongside all the simplifications found and using the definitions of the equilibrium functions:

$$\begin{aligned} H'' + H'\left\{\frac{2}{r} + e^{\lambda}\left[\frac{2m(r)}{r^2} + 4\pi r\,(p-\epsilon)\right]\right\} + \\ H\left[-\frac{6e^{\lambda}}{r^2} + 4\pi e^{\lambda}\left(5\epsilon + 9p + \frac{\epsilon+p}{dp/d\epsilon}\right) - \nu'(r)\right] = 0. \end{aligned} \tag{2.52}$$

This equation depends on equilibrium functions throughout the star, so in order for it to be solved, we need to integrate it alongside the equilibrium Equations (2.23), (2.22), (2.20). This is done, given an equation of state, from the center of the star, using a very small cutoff radius $r = r_0$ to the total radius R of the star. The initial conditions for the equilibrium functions are the same described in the previous section. The initial conditions for H and H' can be determined by solving this equation for values of r that are near zero and requiring regularity in the function, this yields

$$H(r) = a_0 r^2 \left[1 - \frac{2\pi}{7}\left(5\epsilon(0) + 9p(0) + \frac{\epsilon(0)+p(0)}{(dp/d\epsilon)(0)}\right) r^2 + \mathcal{O}(r^3)\right] \tag{2.53}$$

as the most general and regular solution near the center of the star, where a_0 is an arbitrary constant. We can then take $H(r_0) \simeq a_0 r_0^2$ as the initial value for H, but the general expression above can also be used. The constant a_0 is arbitrary, as the differential equation is homogeneous, so the solution is determined up to a multiplying constant, so we will determine a_0 by matching the external and internal solution at the surface $r = R$ of the star evaluating the following function at the surface:

$$y^{\text{int}}(r) \equiv \frac{r\, H'(r)}{H(r)}. \tag{2.54}$$

We can write initial conditions for the perturbation function as $H(r_0) = r_0^2$ and $H'(r_0) = 2r_0$, that will permit to solve Equation (2.52) to find the internal value of the quantity (2.54), $y^{\text{int}}(R)$.

The equation of the perturbation outside the star can be found by making $p = \epsilon = 0$, $m(r) = M$ and using the expressions (2.25) and (2.24). This results in this differential equation:

$$H'' + \left(\frac{2}{r} - \lambda'\right) H' - \left(\frac{6e^{\lambda}}{r^2} + \lambda'^2\right) H = 0, \tag{2.55}$$

and, by changing variables from r to $x = -1 + \dfrac{r}{M}$, this equation becomes an associated Legendre equation with $l = m = 2$:

$$\left(x^2 - 1\right) H'' + 2xH' - \left(6 + \frac{4}{x^2 - 1}\right) H = 0, \tag{2.56}$$

where the prime mark now indicates total derivative in relation to the variable x. The solutions to this equation are the associated Legendre polynomials $P_{22}(x)$ and $Q_{22}(x)$, that can be linearly combined as one general solution:

$$H(x) = a_Q\,\hat{Q}_{22}(x) + a_P\,\hat{P}_{22}\,(x)\,. \tag{2.57}$$

The hats in this case indicate some changes in the functions: both $Q_{22}(x)$ and $P_{22}(x)$ were normalized so that when $x \to \infty$ or $r \to \infty$, $\hat{P}_{22} \simeq x^2 \simeq (\frac{r}{M})^2$ and $\hat{Q}_{22} \simeq x^{-3} \simeq (\frac{M}{r})^3$, this means writing them as:

$$\hat{P}_{22} = -\frac{1}{3}\,P_{22} \tag{2.58}$$

$$\hat{Q}_{22} = -\frac{5}{8}\,Q_{22}. \tag{2.59}$$

Also, the usual $Q_{22}(x)$ was changed so that it is related to the interval $x > 1$ instead of $-1 < x < 1$. This is necessary because the quantity $-1+\frac{r}{M}$ is at least 1, since the external solution is valid for $r > R$ and $R > 2M$; this means changing $\log\left(\frac{1+x}{1-x}\right)$ to $\log\left(\frac{x+1}{x-1}\right)$. a_Q and a_P are integration constants that will be determined by matching the internal and external solutions.

The external quantity analogous to (2.54) is:

$$y^{\text{ext}}(x) = (1+x)\frac{\hat{P}'_{22}(x) + a\,\hat{P}_{22}(x)}{\hat{Q}'_{22}(x) + a\,\hat{Q}_{22}(x)}, \tag{2.60}$$

where $a \equiv \frac{a_Q}{a_P}$ and $C \equiv \frac{M}{R}$ is the compactness of the star.

The next step is to match the internal and external values of y at the surface of the star. This can be done if both the function H and its derivative H' are regular at the surface. It is correct to assume that the function is continuous and differentiable at the surface [43], even though the thermodynamic variables pressure and energy density are not analytic around the star's surface and the fact that the radius of the perturbed star and the radius R we use, of the star in the equilibrium configuration, are likely different, even if only on a small scale. Matching both expressions we have:

$$a = -\left.\frac{\hat{P}'_{22}(x) - C\,y^{\text{int}}\,\hat{P}_{22}(x)}{\hat{Q}'_{22}(x) - C\,y^{\text{int}}\,\hat{Q}_{22}(x)}\right|_{x=\frac{1}{C}-1}. \tag{2.61}$$

In order to connect the ratio between the two constants a_Q and a_P to the multipole

moments, Equation (2.40) can be simplified by expanding Q_{ij} and $\mathcal{E}_{ij}$:

$$\mathcal{E}_{ij} = \sum_{m=-2}^{2} \mathcal{E}_m \mathcal{Y}_{ij}^{2m}, \tag{2.62}$$

and

$$Q_{ij} = \sum_{m=-2}^{2} Q_m \mathcal{Y}_{ij}^{2m}, \tag{2.63}$$

where $\mathcal{Y}_{ij}^{2m}$ are symmetric traceless tensors, defined by [50] as:

$$Y_{2m}(\theta, \varphi) = \mathcal{Y}_{ij}^{2m} n^i n^j, \tag{2.64}$$

where $\mathbf{n} = (\sin\theta\cos\varphi, \sin\theta\sin\varphi, \cos\theta)$. This leads to:

$$Q_m = -\Lambda \mathcal{E}_m, \tag{2.65}$$

from which it is possible to assume that only one $\mathcal{E}_m$ is not zero, which is sufficient to compute Λ [41].

The ratio a can then be connected to the quadrupolar moments Q and $\mathcal{E}$ by matching the asymptotic behavior at large r of the external part of the function $H(r)$:

$$H = a_P \left(\frac{r}{M}\right)^2 + O\left(\left(\frac{r}{M}\right)^3\right) + a_Q \left(\frac{M}{r}\right)^3 + O\left(\left(\frac{M}{r}\right)^4\right), \tag{2.66}$$

to the expansion in the Equation (2.43). We find that:

$$\begin{aligned} a_P &= \frac{1}{2} M^2 \mathcal{E}, \\ a_Q &= \frac{3}{2} M^3 \Lambda \mathcal{E}, \end{aligned} \tag{2.67}$$

which we can use to rewrite the external function y^{ext}:

$$y^{\text{ext}}(x) = (1+x) \frac{\hat{P}'_{22}(x) + \frac{3\Lambda}{M^5} \hat{P}_{22}(x)}{\hat{Q}'_{22}(x) + \frac{3\Lambda}{M^5} \hat{Q}_{22}(x)}, \tag{2.68}$$

and by matching $y^{\text{int}}(R) = y^{\text{ext}}(R) \equiv y$, after the interior function is numerically solved,

we find for Λ:

$$\Lambda = \frac{M^5}{3} \left. \frac{\hat{P}'_{22}(x) - C\, y\, \hat{P}_{22}(x)}{\hat{Q}'_{22}(x) - C\, y\, \hat{Q}_{22}(x)} \right|_{x=\frac{1}{C}-1}, \tag{2.69}$$

explicitly:

$$\begin{aligned} \Lambda = -16(1-2C)^2 C^5 R^5 \Big\{ & 30\, C\big[C\left(2C\left(C\left(2C\left(y+1\right)+\right.\right.\right. \\ & \left.\left.\left. 3y-2\right)-11y+13\right)+3(5y-8)\right)-3y+6\big] \\ & +45\left(1-2C\right)^2\left(\,2C\left(y-1\right)-y+2\right)\log(1-2C)\Big\}^{-1}, \end{aligned} \tag{2.70}$$

or, in terms of the second tidal Love number k_2, using the definition (2.41):

$$\begin{aligned} k_2 = {} & \frac{8C^5}{5}\left(1-2C\right)^2\left[2+2C\left(y-1\right)-y\right]\times \\ & \Big\{2C\left(6-3y+3C(5y-8)\right)+4C^3\left[13-11y+C(3y-2)+2C^2(1+y)\right] \\ & +3(1-2C)^2\left[2-y+2C(y-1)\right]\log\left(1-2C\right)\Big\}^{-1}. \end{aligned} \tag{2.71}$$

The dimensionless deformability, which will be used in the following chapters can be found using the normalization:

$$\overline{\Lambda} = \frac{3}{2C^5}\, k_2. \tag{2.72}$$

2.2.2 Rotating Neutron Stars

As main sequence stars rotate, they have angular momentum, and even the slowest rotation, through the conservation of the angular momentum, causes the remnant of the gravitational collapse to spin considerably more, as its size is generally much smaller than the original star. Newly formed NSs can have periods of hundreds of rotations per second, because of this, considering the effect of this rotation is significant. Here we are

interested in the moment of inertia of a neutron star. Currently, there are no observational measurements of this quantity, but it is expected to be measured in the near future with the observation of pulsars and double pulsar systems [51].

To treat neutron stars that rotate arbitrarily fast is numerically very challenging. As we are interested in the moment of inertia we restrict ourselves to slow rotations. With this, we can consider rotation as a perturbation of the equilibrium configuration as described in equations (2.28)-(2.33). This analysis was first made by Hartle [52].

The slow rotation approximation we consider means that the star rotates at angular velocity Ω small enough so that the perturbation it causes in pressure, energy density and in the gravitational field are negligible. This also means that all terms quadratic in the angular velocity can be discarded. Besides being slow, we consider rotation to be uniform, meaning that Ω is constant throughout the star.

The rate of rotation of a fluid element in relation to an inertial frame is what determines the forces that each element is subject to, both in Newtonian gravitation and General Relativity. In the latter, however, the inertial frames inside a relativistic fluid are not at rest in relation to distant observers. This happens because the motion of the fluid drags along the spacetime and consequently the frames of reference.

In this configuration we no longer consider a spherically symmetric spacetime, because due to the angular velocity, it is no longer isotropic, so we consider it to be only axially symmetric and stationary. This spacetime may then be written using quasi-Schwarzschild coordinates (t, r, θ, φ) [53]:

$$ds^2 = -H^2\, dt^2 + Q^2\, dr^2 + r^2\, K^2\, [\, d\theta^2 + \sin^2(\theta)\, (d\varphi - \, L\, dt)^2], \tag{2.73}$$

where r is the radial coordinate that matches the equilibrium radius to first order. To ensure that this metric describes an axially symmetric and stationary spacetime, we require that the components of the metric don't depend on t and φ. This results in the functions H, Q, K and L being functions of r and θ alone. $L(r, \theta)$ can be interpreted as the angular velocity of a particle of zero angular momentum falling from infinity to the coordinates (r, θ); we shall call this quantity the rate of dragging of inertial frames.

The components of the metric can be expanded in terms of the angular velocity Ω; as the metric is invariant under a reversal in both the time and rotation directions,

the diagonal functions H, Q and K have only even powers of Ω, while the function L has only odd powers. The expansion of $L(r,\theta)$ to first order can be written as:

$$L(r,\theta) = \omega\,(r,\theta) + \mathcal{O}(\Omega^3), \tag{2.74}$$

whereas the diagonal components have their values unchanged from the equilibrium configuration. The metric can be simplified as:

$$ds^2 = -e^{\nu}\,dt^2 + e^{\lambda}\,dr^2 + r^2\,[\,d\theta^2 + \sin^2(\theta)\,(\,d\varphi^2 - 2\,\omega\,(r,\theta)\,dt\,d\varphi\,)\,]. \tag{2.75}$$

The problem now consists in finding the equation that governs the behavior of the function ω. The only relevant component of the Einstein equations is:

$$R^{t}{}_{\varphi} = 8\pi T^{t}{}_{\varphi}, \tag{2.76}$$

where for simplicity we can multiply both sides by $(-g)^{\frac{1}{2}}$ where g is the determinant of the metric (2.2):

$$g = -r^4 \sin^2(\theta) e^{(\lambda+\nu)}. \tag{2.77}$$

For the left side of the Einstein equation we find, discarding terms that are quadratic or higher in ω:

$$-r^2\,\sin(\theta)\,e^{\frac{(\lambda+\nu)}{2}}\,R^{t}{}_{\varphi} = \partial_r\,[e^{\frac{-(\lambda+\nu)}{2}}\,r^4\,\sin^3(\theta)\,\partial_r\,\omega] + \partial_\theta\,[\,e^{\frac{(\lambda-\nu)}{2}}\,r^2\sin^3(\theta)\,\partial_\theta\,\omega]. \tag{2.78}$$

The component $T^{t}{}_{\varphi}$ is found using the expression (2.33):

$$T^{t}{}_{\varphi} = (\epsilon + p)\,u^t\,u_\varphi = (\epsilon + p)\,u^t\,(\,u^t\,g_{t\varphi} + u^\varphi\,g_{\varphi\varphi}\,), \tag{2.79}$$

the 4-velocity components are given by (2.9):

$$u^t = [-(\, g_{tt} + 2\,\Omega\, g_{t\varphi} + \Omega^2\, g_{\varphi\varphi}\,)]^{-1/2}, \tag{2.80}$$

$$u^\varphi = \Omega u^t, \tag{2.81}$$

and with this we write $T^t{}_\varphi$:

$$T^t{}_\varphi = r^2\,(\,p+\epsilon)\,(\,\Omega-\omega\,)\,\sin^2(\theta)\,e^{\,-\nu(r)}, \tag{2.82}$$

where terms quadratic and higher in Ω were discarded and the total quantities ϵ and p are used now to represent the equilibrium quantities $\epsilon^{(0)}$ and $p^{(0)}$ (as we are considering they are unchanged, they are without the superscript for simplicity).

It is convenient to define the angular velocity of a fluid element seen by a free falling observer; this is given by the difference between the angular velocity Ω and the dragging of the inertial frames ω, we denote this quantity as $\varpi\,(r,\theta) \equiv \Omega - \omega\,(r,\theta)$. Equation (2.76) becomes, using (2.78) and (2.82):

$$\frac{1}{r^4}\,\partial_r\,[e^{\frac{-(\lambda+\nu)}{2}}\,r^4\,\partial_r\,\varpi\,] + \frac{e^{\frac{(\lambda-\nu)}{2}}}{r^2\,\sin^3(\theta)}\,\partial_\theta\,[\sin^3(\theta)\,\partial_\theta\,\varpi\,] - 16\pi\,(\epsilon+p)\,e^{\frac{(\lambda-\nu)}{2}}\,\varpi = 0. \tag{2.83}$$

By defining a function $j(r) \equiv \exp[-(\nu+\lambda)/2]$ alongside the use of the unperturbed equations we find:

$$\frac{1}{r^4}\,\partial_r\,[j\,r^4\,\partial_r\,\varpi\,] + \frac{e^{\frac{(\lambda-\nu)}{2}}}{r^2\,\sin^3(\theta)}\,\partial_\theta\,[\sin^3(\theta)\,\partial_\theta\,\varpi\,] + \frac{4}{r}\frac{dj}{dr}\,\varpi = 0, \tag{2.84}$$

which can be further simplified if the function ϖ is expanded in terms of spherical harmonics:

$$\varpi\,(r,\theta) = \sum_{l=1}^{\infty} \varpi_l(r)\,\left(-\frac{1}{\sin\theta}\,\frac{d\,P_l}{d\,\theta}\right) \tag{2.85}$$

leading to:

$$\frac{1}{r^4}\,\partial_r\left[j\,r^4\,\partial_r\,\overline{\omega}_l\right]+\left[\frac{4}{r}\,\frac{dj}{dr}-e^{\frac{(\lambda-\nu)}{2}}\,\frac{l(l+1)-2}{r^2}\right]\overline{\omega}_l=0. \tag{2.86}$$

We demand that the geometry described is regular at small values of r and that it is flat at large r. It can be shown [52] that this asymptotically flat and regular solution is only obtained if all the coefficients of the expansion are zero except for $l=1$, which means that $\overline{\omega}$ depends only on the radial coordinate r. Equation (2.86) becomes the second order ordinary differential equation:

$$\frac{1}{r^4}\,\frac{d}{dr}\left[j\,r^4\,\frac{d\,\overline{\omega}}{dr}\right]+\frac{4}{r}\,\frac{dj}{dr}\,\overline{\omega}=0. \tag{2.87}$$

Outside the star $j=1$ and the equation becomes:

$$\frac{d}{dr}\left(r^4\,\overline{\omega}'\right)=0, \tag{2.88}$$

leading to $r^4\,\overline{\omega}'=$ constant, that we choose to be $6\,J$, and to $\overline{\omega}=-\frac{2\,J}{r^3}+c_1$ where c_1 is an integration constant that can be identified as Ω, resulting in:

$$\overline{\omega}=-\frac{2\,J}{r^3}+\Omega, \tag{2.89}$$

where J can be identified as the total angular momentum of the star. This identification can be made because at the asymptotic region $r\gg R$ of the spacetime we are considering (asymptotically flat, stationary and axially symmetric) the component $g^{t\varphi}$ can be expressed as [54]:

$$g^{t\varphi}=-\frac{2\,j}{r^3}, \tag{2.90}$$

where j is the spacetime angular momentum parameter, that can be used to define the angular momentum.

The general relativistic generalization of the moment of inertia can be found as the constant of proportionality between the angular momentum and the angular velocity:

$$J = I\,\Omega. \tag{2.91}$$

The explicit expression to calculate the moment of inertia can be found using the fact that at the surface ($r = R$) of the star $\overline{\omega}'(R) = \frac{6\,J}{R^4}$ and $\Omega = \overline{\omega}(R) + \frac{2\,J}{R^3}$, which can be combined as:

$$I = \frac{J}{\Omega} = \overline{\omega}'(R)\,\frac{R^4}{6}\,\frac{1}{\overline{\omega}(R) + \frac{R}{3}\,\overline{\omega}'(R)}. \tag{2.92}$$

The value for I can be determined by integrating Equation (2.87), alongside the equilibrium equations (2.20), (2.22), (2.23), from the center of the star with $r = r_0 \gtrsim 0$, to the star's surface. The initial conditions for the equilibrium configuration are the ones described in the previous section and by requiring that the solution is regular at the center of the star we find the initial condition $\overline{\omega}'(r = 0) = 0$ and $\overline{\omega}(r = 0) = k$, where k is a constant. As we are using a small cutoff radius, r_0, we use a Taylor approximation for both $\overline{\omega}(r_0)$ and $\overline{\omega}'(r_0)$, that results in the conditions $\overline{\omega}(r_0) = k + k\frac{8}{5}\,r_0^2\,(\epsilon_0 + p_0)$ and $\overline{\omega}'(r_0) = k\,\frac{16}{5}\,r_0\,(\epsilon_0 + p_0)$. The Equation (2.87) is homogeneous and any constant that multiplies $\overline{\omega}$ will be eventually canceled in Equation (2.92), this means that the constant k is arbitrary and for simplicity we set it as $k = 1$. Its dimensionless version will be used in the following chapters and is defined as:

$$\overline{I} \equiv \frac{I}{M^3}, \tag{2.93}$$

Chapter 3

Equation of State of Neutron Stars

The equation of state (EoS), in a general way, is the term used to describe any mathematical relation between two or more thermodynamic quantities; an example of this is the ideal gas law that is the equation of state for ideal gases. More specifically, we use this expression to describe the equation or equations that can completely determine the state of matter given a specific set of conditions. An EoS that describes an astrophysical object can only be used if the system described is in thermodynamic equilibrium (or sufficiently close to equilibrium). This means that the thermodynamic variables such as pressure and temperature need to be well defined in this system.

The internal structure of neutron stars is then described by its equation of state, as it contains the information on the behavior of matter inside the star. This matter is, in fact, with the exception of the early universe, in the most extreme conditions in the universe; neutron stars is where matter is at its compactest, on the verge of collapsing into a black hole. As these densities easily exceed, as mentioned, $\rho \sim 10^{14}$ g/cm^3, they are not yet reachable by nuclear physics experiments on Earth at the same temperature levels present in neutron stars.

Even though neutron stars have extremely dense cores, each of the layers of the star has its own range of densities. The outer layers are less dense, the star's crust ranging from 10^6 g/cm$^3 \lesssim \rho \lesssim 10^{14}$ g/cm^3 whilst the inner ones are denser, with $\rho \gtrsim 10^{14}$ g/cm^3 [55]. Up until $\rho \sim 10^{11}$ g/cm^3, in the outer crust, the behavior of the atomic nuclei is expected to be the same as the one observed in laboratory; in the inner crust, with density in the range 10^{11} g/cm$^3 \lesssim \rho \lesssim 10^{14}$ g/cm^3 the behavior is described by theoretical models. When densities are below 10^{13} g/cm^3, the temperature of the star is high enough

so that it has effects on the properties of matter [55]. At higher densities, these thermal effects are no longer relevant [55] so that the pressure depends only on the mass density, meaning a cold EoS has only one parameter and the form $p(\rho)$; or, connecting the mass density to the energy density ϵ trough the first law of thermodynamics, the form $\epsilon(p)$.

For a better understanding of the equation of state problem in neutron stars, we can consider a simple model for it: We study the quantum mechanical pressure as the only source of outward pressure in neutron stars. For this purpose we consider a fermion gas, as neutrons are fermions, they are ruled by the same quantum statistic, Fermi-Dirac statistics, and the fermion gas provides a simple description.

We begin by considering the fermion gas in a box of volume V. The uncertainty of its momentum $\Delta\, k$, given the uncertainty principle of Heisenberg, can be written as:

$$\Delta\, k = h\, V^{-\frac{1}{3}}, \tag{3.1}$$

where h is the Plank constant. The region in the space of momentum with momentum between k and $k+dk$ has volume $4\,\pi\, k^2\, dk$ and the number of possible states, that occupy, at least, $(\Delta k)^3$ each, in this volume is:

$$d\, N = 4\,\pi\, k^2\, \frac{dk}{(\Delta\, k)^3}, \tag{3.2}$$

that using Equation (3.1), becomes:

$$d\, N = \, V\, 4\,\pi\, k^2\, \frac{dk}{h^3}. \tag{3.3}$$

As we are considering a fermion gas, the particles obey the principle of exclusion of Fermi, which states that two fermions cannot occupy the exact same momentum state. As fermions have spin $\frac{1}{2}$, a fermion has two possible values for its spin, up or down, meaning each state of momentum can be occupied by two fermions, one with spin-up and other with spin-down. So the maximum number of fermions in the volume V is actually double the value in Equation (3.3). If we reduce the temperature of this gas as much as possible we also reduce the fermion momentum to nearly zero, meaning that at $T = 0$K, only the lowest momentum states, between $k = 0$ and a given momentum $k = k_f$, will be occupied. This allows us to integrate Equation (3.3) using these limits:

$$\frac{N}{V} = \int_0^{k_f} \frac{8\,\pi\,k^2}{h^3}\,dk. \tag{3.4}$$

The ration $\frac{N}{V}$ is the number density n and, solving the integral we find:

$$n = \frac{8\,\pi\,k_f^3}{3\,h^3}, \tag{3.5}$$

or in terms of the momentum k_f:

$$k_f\,(n) = \left(\frac{3\,h^3}{8\,\pi}\right)^{\frac{1}{3}}\,n^{\frac{1}{3}}. \tag{3.6}$$

The energy density ϵ can be calculated by finding the ratio between the total energy E_{tot} and the volume V, and as we are considering relativistic particles, the energy of a single one is given by $E^2 = k^2 + m^2$ where m is the fermion mass, and consequently the total energy is found by making $dE_{tot} = E \cdot dN$ and integrating:

$$E_{tot} = \int dE_{tot} \;= \int_0^{k_f} V\,\frac{8\,\pi\,k^2}{h^3}\,(k^2+m^2)^{\frac{1}{2}}\,dk, \tag{3.7}$$

and the energy density can be calculated by dividing this by the volume V:

$$\epsilon = \int \frac{dE_{tot}}{V} \;= \int_0^{k_f} \frac{8\,\pi\,k^2}{h^3}\,(k^2+m^2)^{\frac{1}{2}}\,dk, \tag{3.8}$$

where we can make a substitution $u \equiv \frac{k}{m}$ and $u_f \equiv \frac{k_f}{m}$:

$$\epsilon = \frac{8\,\pi\,m^4}{h^3}\int_0^{u_f} u^2\,(u^2+1^2)^{\frac{1}{2}}\,du. \tag{3.9}$$

Integrating this equation we find:

$$\epsilon(n) \;=\; \frac{\pi\,m^4}{h^3}\left[(2\,u_f^3+u_f)\,(1+u_f)^{1/2} - \operatorname{arcsinh}(u_f)\right]. \tag{3.10}$$

The pressure p can be found using the first law of thermodynamics:

$$\Delta Q = \Delta\,E_{tot} + \,p\,\Delta V, \tag{3.11}$$

where ΔQ is the energy added to the system as heat. As we are considering an isolated

system, it is 0, which leads to:

$$p = -\frac{d\,E_{tot}}{d\,V} = -\frac{d}{dV}(\epsilon\,V) = -\epsilon - V\frac{d\,\epsilon}{d\,V} = -\epsilon - V\frac{d\,\epsilon}{d\,k_f}\frac{d\,k_f}{d\,V}. \tag{3.12}$$

The term $\frac{d\epsilon}{dk_f}$ is:

$$\frac{d\epsilon}{dk_f} = \frac{8\,\pi\,k_f^2}{h^3}\,(k_f^2 + m^2)^{\frac{1}{2}}, \tag{3.13}$$

while the term $\frac{d\,k_f}{d\,V}$ can be obtained by using the chain rule and considering that the number of fermions N is constant:

$$V\frac{d}{d\,V} = -n\,\frac{d}{d\,n}, \tag{3.14}$$

that can be applied to k_f using Equation (3.6) and leads to:

$$-n\,\frac{d\,k_f}{d\,n} = \frac{1}{3}\,k_f. \tag{3.15}$$

With this, the pressure can be written as:

$$p(n) = \frac{8\,\pi\,k_f^3}{3h^3}\,(k_f^2 + m^2)^{\frac{1}{2}} - \epsilon, \tag{3.16}$$

or, writing the expression in terms of the variable u_f and writing $\epsilon(n)$ explicitly:

$$p(n) = \frac{\pi}{3h^3}\,m^4\left[(1+u_f^2)^{1/2}(2\,u_f^3 - 3\,u_f) + 3\,\mathrm{arcsinh}(u_f)\right]. \tag{3.17}$$

The Equations (3.17) and (3.10) together are the equation of state of this gas.

Computing the equilibrium equations described in the previous chapter along with these equations, using m as the neutron mass m_c, we find that they allow for a maximum mass of approximately $0.7M_\odot$ as shown in Figure 3.1. This is much lower than the mass limit of a stable white dwarf and, more importantly, lower than the average observed mass of a neutron star that is $\gtrsim 1.4M_\odot$ with recent measures reaching $2M_\odot$ [56–58]. This

shows that this description is clearly wrong, which leads to the question: What is the problem or problems with it?

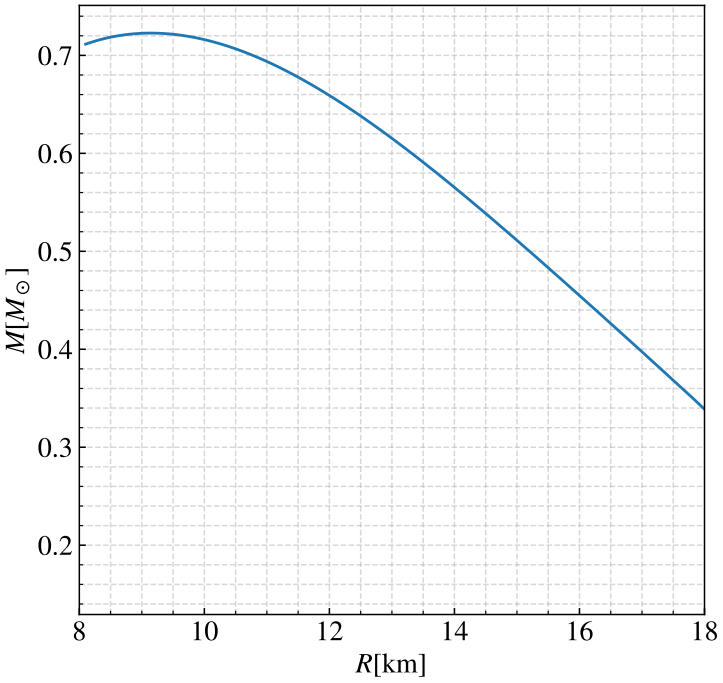

Figure 3.1: Mass-radius curve generated with Equations (3.10) and (3.17). The maximum mass found is $M_{\max} \approx 0.72\, M_{\odot}$.

The main thing to consider is that this description is of a non-interacting gas, meaning it does not consider the interaction between neutrons: Is this realistic?

We can approximate the volume occupied by a single neutron as $V \sim \frac{1}{n}$, where n is the number density. To understand the possibility of neutron-neutron interactions we can compare the value of this volume to the wavelength of a neutron: if the volume occupied by a neutron is smaller than its wavelength λ_n, $V < \lambda_n^3$, this means the neutrons interact with one another. If we consider the Compton wavelength of the neutron, given by $\lambda_n = \frac{h}{m_n c}$ where c is the speed of light, we find $\lambda_n^3 \simeq 2.3 \times 10^{-39}\text{cm}^3$. For this to be greater than the volume V, the mass density ρ, related to the number density through $n = \frac{\rho}{m_n}$, needs to be $\rho \gtrsim 3\,\rho_{\text{sat}}$.

As it is expected that densities this high are reached inside neutron stars, neutrons inside them do interact with each other. Even though their interaction is clear, modeling it is not easy. This leads to a variety of equations of state that propose to do so.

3.1 EoS Representations

Different equations of state result in different predictions regarding macroscopic properties and behavior of neutrons stars, such as radius, mass, tidal deformability and others. This difference, illustrated in Figures 3.2 and 3.3, means that observational measurements of these properties can inform us about the true form of the equation of state, an example on how this can be done is given in [8].

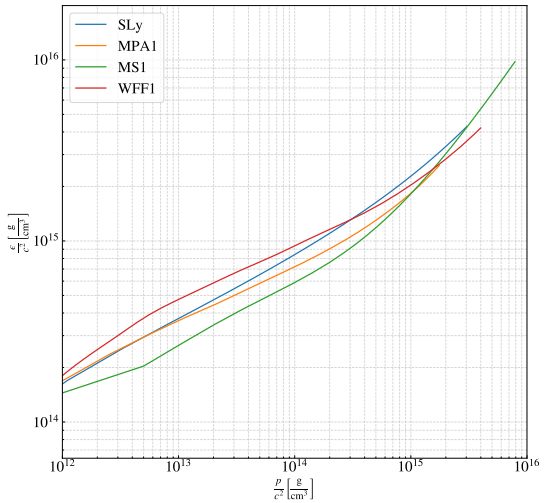

Figure 3.2: Illustration of the $\epsilon(p)$ relation for a set of four realistic equations of state: SLy [59], MPA1 [60], MS1 [61] and WFF1 [62]. The EoS data used here are from the tables from [63].

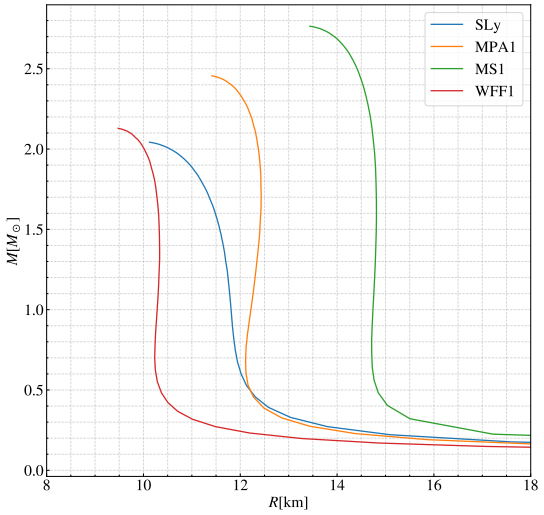

Figure 3.3: The correspondent Mass-Radius curves for each of the equations of state in Figure 3.2. Each point in a curve represents a different star with a different central density.

In this context, there are realistic equations of state; they are derived from different microphysical approaches that consider different interactions and models for the matter inside the neutron star. Their description varies and comparison between them is not necessarily trivial. In this sense, using a parametric representation of the equation of state that can combine different EoS into the same format can be extremely useful. Having parameterized EoS means that the space of EoS is also parameterized: this is important as observational data can lead to direct constraints in regions of this space, narrowing the number of EoS possibilities. Because of this it is necessary that a representation has parameters enough and that it is flexible enough to reproduce any behavior an EoS may have, such as phase transitions. However, it should not have an excessively large number of parameters so that the constraints are the most restrictive of the space as possible.

Several different representations have been created: the widely used piecewise poly-

tropic parametrization by Jocelyn Read et al. [64], a generalization of this parametrization proposed by O'Boyle et al. [65], the spectral parametrization by Lindblom [66], a speed of sound interpolation by Annala et al. [67], among several others. Despite the differences between them, they must result in the same macroscopic properties when fitting the same realistic equation of state, as anything different would mean the representation is not a useful tool in the study of NS EoS.

Here, we describe and analyze a few of these representations that will be used in the following chapter.

3.1.1 Generalized Piecewise Polytropic Parametrization

The piecewise polytropic parametrization is based on the polytropic equation of state, which is defined as:

$$p(\rho) = K\,\rho^{\Gamma}, \tag{3.18}$$

where ρ is the rest-mass density and Γ is the adiabatic exponent, which is defined in general as:

$$\Gamma\,(p) \;=\; \frac{\epsilon + p}{p}\,\frac{dp}{d\epsilon}. \tag{3.19}$$

With the first law of thermodynamics,

$$d\frac{\epsilon}{\rho} = -p\,d\frac{1}{\rho}, \tag{3.20}$$

the energy density ϵ can be fixed. Using Eq. (3.18), Eq. (3.20) has an immediate integral:

$$\frac{\epsilon}{\rho} = (1 + a) + \frac{1}{\Gamma - 1} K \rho^{\Gamma - 1}, \tag{3.21}$$

where a is a constant of integration that can be determined using the requirement $\lim_{\rho\to 0} \frac{\epsilon}{\rho} = 1$, which implies that $a = 0$, leading to:

$$\epsilon = \rho + \frac{1}{\Gamma - 1} p. \tag{3.22}$$

The piecewise polytropic (PP) parametrization (see, e.g. Ref. [64]) consists in defining density intervals above a density ρ_0, $\rho_0 < \rho_1 < \rho_2 < ...$, each one with its own K_i and Γ_i, in such a way that the pressure and energy density are continuous everywhere and are determined by:

$$p(\rho) = K_i \rho^{\Gamma_i}, \quad \rho_{i-1} \leq \rho \leq \rho_i, \tag{3.23}$$

and

$$\epsilon(\rho) = (1 + a_i)\rho + \frac{K_i}{\Gamma_i - 1} \rho^{\Gamma_i}, \quad \Gamma_i \neq 1, \tag{3.24}$$

where a_i can be determined using continuity:

$$a_i = \frac{\epsilon(\rho_{i-1})}{\rho_{i-1}} - 1 - \frac{K_i}{\Gamma_i - 1} \rho_{i-1}^{\Gamma_i - 1}. \tag{3.25}$$

The generalized piecewise polytropic (GPP) parametrization [65] is based on a generalization of the prescription above. This generalization has the purpose of guaranteeing continuity of the sound speed across the dividing densities. Indeed, one can easily see that the sound speed, generally defined as:

$$c_s^2 = \frac{d\,p}{d\,\epsilon}, \tag{3.26}$$

is given by:

$$c_s(\rho) = \sqrt{\frac{\Gamma_i p}{\epsilon + p}} \tag{3.27}$$

in the PP parametrization, and in general it will be discontinuous across ρ_i.

In the GPP parametrization, Eqs. (3.18) and (3.21) become:

$$p(\rho) = K\rho^{\Gamma} + \Lambda \tag{3.28}$$

and

$$\epsilon(\rho) = \frac{K}{\Gamma - 1}\rho^{\Gamma} + (1 + a)\rho - \Lambda. \tag{3.29}$$

In these equations Γ is no longer identified as the adiabatic exponent. If one used (3.28) throughout the interior of the star, Λ would be related to the mass density at the surface of the star, where pressure vanishes.

The GPP parametrization consists in considering, in the same manner as the PP parametrization, density intervals each one with its own parameters, K_i, Γ_i, Λ_i and a_i, for an interval $[\rho_{i-1}, \rho_i]$. The EoS has the piecewise form:

$$p(\rho) = K_i\rho^{\Gamma_i} + \Lambda_i, \qquad \rho_{i-1} \leq \rho \leq \rho_i \tag{3.30}$$

and

$$\epsilon(\rho) = \frac{K_i}{\Gamma_i - 1}\rho^{\Gamma_i} + (1 + a_i)\rho - \Lambda_i. \tag{3.31}$$

Demanding continuity and differentiability for both the pressure and energy density in all dividing densities results in the following relations:

$$K_{i+1} = K_i\frac{\Gamma_i}{\Gamma_{i+1}}\rho_i^{\Gamma_i - \Gamma_{i+1}}, \tag{3.32}$$

$$\Lambda_{i+1} = \Lambda i + \left(1 - \frac{\Gamma_i}{\Gamma_{i+1}}\right) K_i\rho_i^{\Gamma_i}, \tag{3.33}$$

$$a_{i+i} = a_i + \Gamma_i\frac{\Gamma_{i+1} - \Gamma_i}{(\Gamma_{i+1} - 1)(\Gamma_i - 1)}K_i\rho_i^{\Gamma_{i-1}}. \tag{3.34}$$

In particular, the requirement of differentiabillity implies that the speed of sound, now given by

$$c_s(\rho) = \sqrt{\frac{\Gamma_i\, p - \Lambda_i}{\epsilon + p}}, \tag{3.35}$$

is continuous throughout the star.

The equations above are used to parameterize the unknown core and match it to a known crust EoS. Following Ref. [65], the parameterized core is characterized by three density intervals and four free parameters, K_1 and Γ_i, $i \in \{1, 2, 3\}$.

The density at which the inner crust EoS and the outer core EoS intersect is designated as ρ_0. At this density, one requires differentiability, resulting in:

$$\frac{dp_{\text{crust}}}{d\rho}(\rho_0) = K_1\Gamma_1\rho_0^{\Gamma_1-1}, \tag{3.36}$$

where p_{crust} is the crust EoS. Now we use Λ_1 to ensure continuity at $\rho = \rho_0$:

$$\Lambda_1 = p_{\text{crust}}(\rho_0) - K_1\rho_0^{\Gamma_1}. \tag{3.37}$$

Similarly, a_1 can be determined by demanding continuity in $\epsilon(\rho)$:

$$a_1 = \frac{\epsilon_c(\rho_0)}{\rho_0} - \frac{K_1}{\Gamma_1 - 1}\rho_0^{\Gamma_1-1} + \frac{\Lambda_1}{\rho_0} - 1. \tag{3.38}$$

Appropriate diving densities are determined in Ref. [65] by minimizing errors in observables. The preferred densities found in that work are $\rho_1 = 10^{14.87}\text{g/cm}^3$ and $\rho_2 = 10^{14.99}$ g/cm^3.

3.1.2 Spectral Parametrization

An equation of state in the form $\epsilon(p)$, where ϵ is the energy density and p is the pressure can be fully described by its adiabatic index:

$$\Gamma\left(p\right) \;=\; \frac{\epsilon + p}{p}\,\frac{dp}{d\epsilon}. \tag{3.39}$$

It can be determined, given an initial condition, by solving the differential equation:

$$\frac{d\epsilon(p)}{dp} \;=\; \frac{\epsilon + p}{p\,\Gamma(p)}. \tag{3.40}$$

The spectral parametrization is based on the idea of writing the unknown part of the neutron star equation of state, its core, trough a spectral expansion of the adiabatic index:

$$\Gamma(p) = \exp\left[\sum_k \gamma_k\,\Phi_k(p)\right], \tag{3.41}$$

where γ_k are constants that characterize different equations of state and $\Phi_k(p)$ is any set of complete functions. A representation of the EoS is obtained by truncating the sum at a value of k and its accuracy increases with the value of k. In Ref [66], the representation is truncated at $k = 4$, and the functions are chosen to be:

$$\Phi_k(p) = \left[\log\left(\frac{p}{p_0}\right)\right]^k, \tag{3.42}$$

where p_0 is a reference pressure that is correspondent to the initial condition $\epsilon_0 \equiv \epsilon(p_0)$. It is defined as the pressure at the dividing density between the low density (crust) EoS and the high density (core) EoS:

$$p_0 = p(\rho_c), \tag{3.43}$$

this density is chosen to be $\rho_c = 2 \times 10^{14}$ g/cm^3. The pressure at this density can be found by solving the following differential equation:

$$\frac{d\,\rho}{\rho} = \frac{1}{\Gamma(p)}\frac{d\,p}{p}, \tag{3.44}$$

found by combining (3.40) and the first law of thermodynamics.

3.1.3 Comparison

Although the parametrizations are differently developed, they share some similarities: both fit the realistic equations of state with four free parameters and the candidate EoS is fitted by the method of minimizing the residual errors of the parameters.

In Ref. [65], where the GPP parametrization was proposed, the errors minimized when determining the ideal parameters to fit an EoS are:

$$\Delta^2(K_1, \{\Gamma_i\}) = \frac{1}{\rho_{\rm u} - \rho_{\rm l}} \sum_{i=1}^{N} \sum_{\rho\in[\rho_{\rm l},\rho_{\rm u}]} \Big(p(\rho) - K_i\rho^{\Gamma_i} - \Lambda_i\Big)^2 \Delta\rho, \tag{3.45}$$

where $p(\rho)$ are the actual values from each realistic EoS, $\rho_{\rm u}$ is the central mass density correspondent to the maximum mass allowed by the candidate equation of state and $\rho_{\rm l}$ is the central mass density correspondent to the lowest mass, set to be $1.25M_\odot$. In Ref. [66],

where the spectral parametrization was proposed, the errors minimized when determining the ideal parameters to fit an EoS are:

$$\Delta^2(\gamma_k) = \sum_{i=1}^{N} \frac{1}{N} \left\{ \log \left[\frac{\epsilon_{\text{fit}}(x_i, \gamma_k)}{\epsilon_i} \right] \right\}^2, \tag{3.46}$$

where $\epsilon_i = \epsilon(x_i)$ are the actual values from each of the candidate EoS.

From these two expressions we can observe some differences: in the GPP expression the objective is to minimize the errors of the entire set of parameters, while in the spectral one, the errors of each of the parameters are calculated separately. Another visible difference is that at (3.45) the absolute error of each point is calculated and subsequently minimized, whilst in (3.46) the relative error is the one used.

The difference in formulation and in the manner the error is minimized leads directly to differences when fitting a particular equation of state. We can use the parameters of the fitted realistic EoS found in Refs. [65] and [66], that are presented in Appendix A to generate Figures 3.4 and 3.5. From them, we can see these differences: the difference on the fits, on the top part of the graph are barely perceptible, however this difference becomes clearer when analyzing the relative errors in the lower part of the graph. As these figures show, neither of the parametrizations seems to be an objectively better choice of representation, each fitting one of the chosen realistic EoS better than the other.

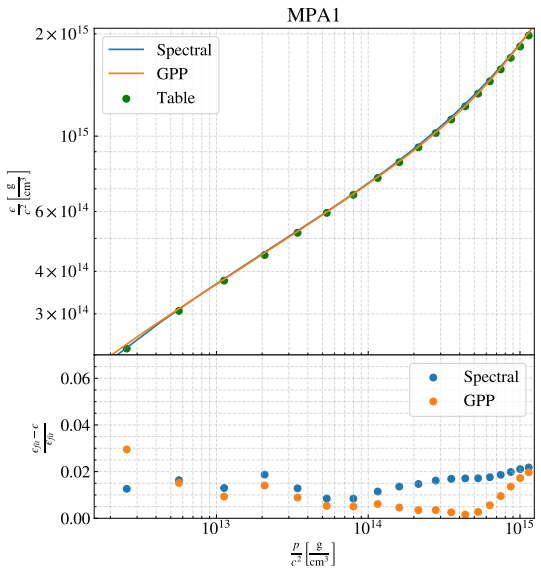

Figure 3.4: Top: Fits of the MPA1 EoS [60] (with the data from [63]) using both the GPP and the spectral representations. Values used in the fits are the ones at A.2 and A.3. Bottom: Correspondent relative error of each fit.

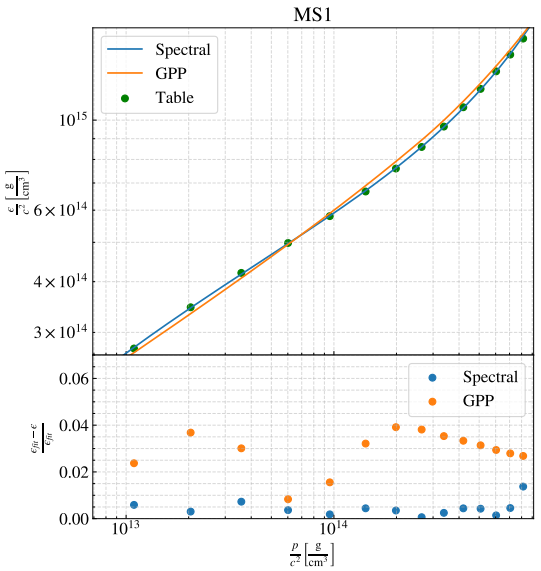

Figure 3.5: Top: Fits of the MS1 EoS [61] (with the data from [63]) using both the GPP and the spectral representations. Values used in the fits are the ones at A.2 and A.3. Bottom: Correspondent relative error of each fit.

Chapter 4

Universal Relations

Universality is a known phenomenon in physics. It appears when a local property of a system does not affect a specific global behavior of this system. For example, in statistical physics phase transitions are sometimes characterized by the same critical exponent for systems that have wildly different compositions and properties.

Black holes, for example, present universality because none of the events that lead to the formation of a black hole and whatever fell into it are significant from an astrophysical perspective since this information is inaccessible behind the event horizon. For astrophysical purposes, the only relevant information to the describe the orbit, for example, of a binary system of black holes, is their mass, angular momentum and electric charge, this is called the no-hair theorem [68–70].

In neutron stars, universality appears in the form of universal relations, meaning relations that do not show strong dependence on the equation of state. In this case, universality is particularly important because it is capable of informing us of properties of the star that would be otherwise inaccessible without the knowledge of the exact neutron star equation of state.

4.1 Literature Survey

In the context of compact stars, and particularly neutron stars, there are several known universal relations. Here we mention a few of these and their respective applications.

I-Love-Q

One of the most well-known universal relations for neutron stars is the I-Love-Q relation. It was first introduced by Yagi and Yunes in Ref. [29]. This is the name of a set of universal relations between the "I", "Love" and "Q" quantities: "I" stands for I in the stellar moment of inertia, "Love" stands for the quadrupolar tidal deformability $\lambda^{(\mathrm{tid})}$ and "Q" stands for the quadrupolar spin-induced moment Q.

The tidal deformability $\lambda^{(\mathrm{tid})}$ of a neutron star is the tidal deformability, that was calculated explicitly in the Subsection 2.2.1 in Equation (2.70) as Λ and is here identified as $\lambda^{(\mathrm{tid})}$. Its dimensionless form, defined in (2.72), and there named $\overline{\Lambda}$, here is called $\overline{\lambda}^{(\mathrm{tid})}$. It characterizes the response of a non-rotating neutron star when subject to an external gravitational field.

The steps to obtain the stellar moment of inertia I are described in Subsection 2.2.2, and this quantity is defined in Equation (2.92). In these relations, however, the dimensionless moment of inertia is used, as defined in (2.93).

The quadrupolar spin-induced moment Q can be found by extending the calculations made in Subsection 2.2.2 to quadratic order in the angular velocity, these calculations are performed in Ref. [52], still, however, considering a slow rotation approximation. In Ref [71] it is given by:

$$Q = -\frac{J^2}{M} - \frac{8}{5} A M^3, \tag{4.1}$$

where A is an integration constant. In the relation, its dimensionless version is used, defined as:

$$\overline{Q} \equiv -\frac{Q}{J^2 M}. \tag{4.2}$$

This quantity characterizes the quadrupolar deformation of a spherical body due to its rotation given a certain spin angular momentum J.

The I-Love-Q relations are three: the I-Love, that connects $\overline{I}$ and $\overline{\lambda}^{(\mathrm{tid})}$, shown in Figure 4.1; the Love-Q relation that connects $\overline{\lambda}^{(\mathrm{tid})}$ and $\overline{Q}$, shown in Figure 4.2, and the I-Q relation that connects $\overline{I}$ and $\overline{Q}$, shown in Figure 4.3.

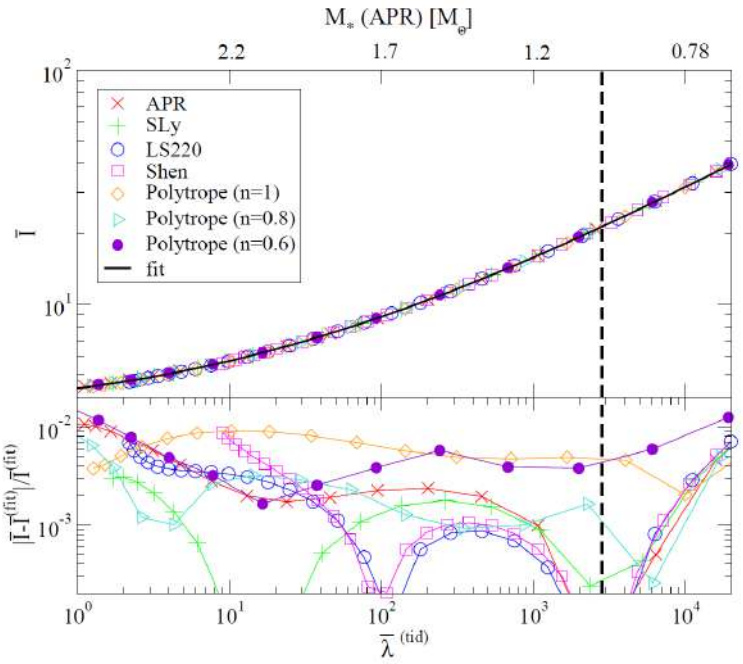

Figure 4.1: Reproduction from Ref. [71]. Top: the universal I-Love relation from slowly rotating neutron stars for a few realistic equations of state as well as polytropic equations of state, and a black line that represents a fit that can be found in [71]. The top axis represents the stellar mass calculated in the APR EoS. Bottom: corresponding fractional error in relation to the fit.

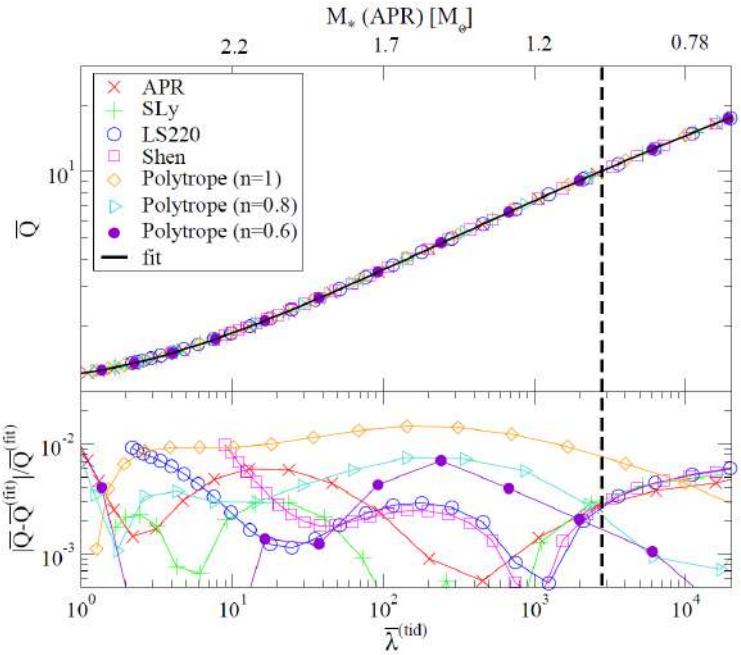

Figure 4.2: Reproduction from Ref. [71]. Top: the universal Love-Q relation for slowly rotating neutron stars for a few realistic equations of state as well as polytropic equations of state, and a black line that represents a fit that can be found in [71]. The top axis represents the stellar mass calculated in the APR EoS. Bottom: corresponding fractional error in relation to the fit.

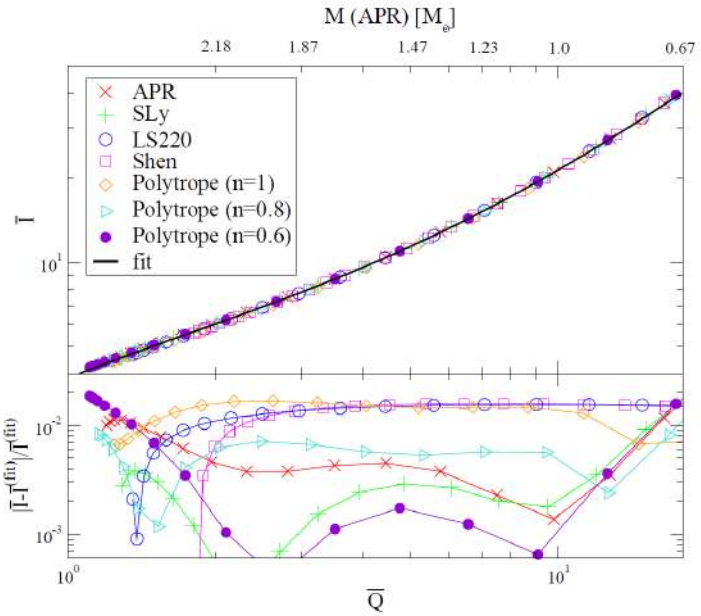

Figure 4.3: Reproduction from Ref. [71]. Top: the universal I-Q relation for slowly rotating neutron stars for a few realistic equations of state as well as polytropic equation of state, and a black line that represents a fit that can be found at [71]. The top axis represents the stellar mass calculated in the APR EoS. Bottom: corresponding fractional error in relation to the fit.

From the bottom part of these figures we can see that these relations are EoS-insensitive, or universal, to $\mathcal{O}(1\%)$. This means that these relations are in fact extremely insensitive to the choice of equation of state.

With the relations presented, there are several applications for these that are important to discuss. One is from the astrophysical perspective: from an observational point of view, these relations allow for a measurement of any of the three quantities to be used to measure the other two. For example, as mentioned in Subsection 2.2.1, the tidal deformability can be measured through gravitational wave data from inspiralling neutron star binary systems and black hole-neutron star binary systems [15,17,46,48,49], this measurement allows us to extract information about the moment of inertia I and the quadrupole moment Q. It will also be possible to use future measurements of the moment of inertia obtained from pulsar timing [13,51] to extract information of tidal deformability and spin-induced quadrupole moment.

Another application is to gravitational-wave astrophysics: this relation is capable of breaking degeneracies found in the GW phase. The neutron star quadrupole moment enters the phase at the same order as a spin-spin interaction term [72], this means that at first it would not be possible to individually measure the quadrupole moment and the spins of the neutron stars. However, using the I-Love-Q relation the quadrupole moment Q can be rewritten in terms of the tidal deformability, and if it is measured using GW detection as just mentioned, it is possible to measure the spins individually. A study on how this relation influences the NS spin measurement with GWs can be found at [29].

The last application we mention here is to fundamental physics: A measurement of two of the components of the relation would allow for a robust test of General Relativity, if these measurements have small enough uncertainties. If the values obtained for the quantities do not lie in the universal I-Love-Q line predicted by GR, this would indicate some sort of deviation from the theory.

The reason why these relations exist was investigated thoroughly in Ref. [73]. The paper concludes that this universality appears due to an emergent symmetry that occurs when moving from a non-compact star region to the region of relativistic stars. It is also important to mention that these relations were also analyzed in different contexts.

- In the context of rapidly rotating neutron stars, with uniform rotation, the I-Q relation was first analyzed in Ref. [74], and then in Refs. [75] and [76].

- The validity of these relations were also evaluated with magnetized neutron stars: this is important because neutron stars can have strong magnetic fields. This analysis can be found in Ref. [77].

- The universality of these relations was also analyzed when the pressure in the star is not isotropic, meaning that the radial pressure is not necessarily equal to the tangential pressure. This analysis can be found in Ref. [78].

- The I-Love-Q relations were also studied using non-barotropic EoS. This scenario is important when considering newly formed neutron stars from supernovae, the so called proto-neutron stars, which are hotter than neutron stars, meaning that temperature effects must be taken in consideration. This study can be found in Ref. [79].

- Non-static tides, or dynamical tides, were also considered. In Ref. [80] the tidal deformability is calculated in the dynamic context and the influence of this on the universality of the I-Love relation is studied.

Binary Love Relation

A neutron star binary system is an astronomical system composed of two neutron stars. The binary Love relation is an approximately equation-of-state-independent relation between the tidal deformabilities, or the Love numbers, of neutron stars in a NS-NS binary system. It was first introduced in Refs. [27] and [81] and connect the quantities $\bar{\Lambda}_s$–$\bar{\Lambda}_a$.

The quantity $\bar{\Lambda}_s$ is a dimensionless symmetric combination of the tidal deformability of each of the components of the binary system. It is defined as:

$$\bar{\Lambda}_s = \frac{\bar{\Lambda}_1 + \bar{\Lambda}_2}{2}, \tag{4.3}$$

where $\bar{\Lambda}_1$ is the dimensionless tidal deformability defined in subsection 2.2.1 of the component 1 of the binary system and $\bar{\Lambda}_2$ is the dimensionless tidal deformability of the component 2 of the system. These quantities are calculated by considering each star separately and treating the tidal effects as is done in subsection 2.2.1. The quantity $\bar{\Lambda}_a$ is

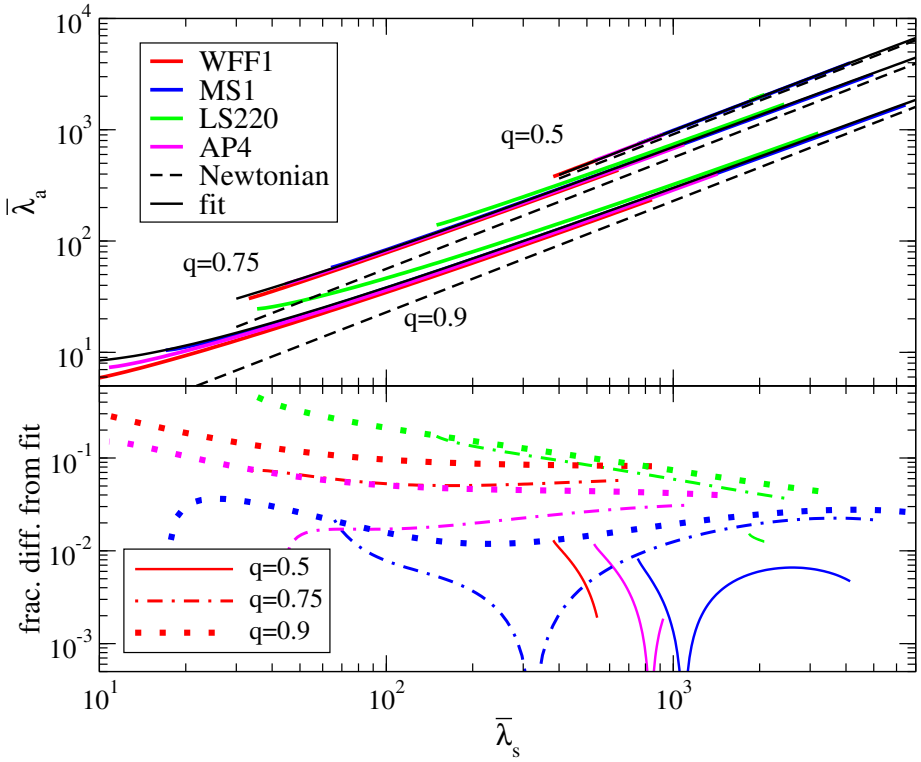

Figure 4.4: Reproduction from Ref. [27]. Top: the universal $\bar{\Lambda}_s$–$\bar{\Lambda}_a$ relation for a binary system of neutron stars for a few realistic equations of state, the Newtonian limit is represented in dashed black lines and the equations are fitted to a fit that can be found in Ref. [27]. The relation is tested for different values of the mass ratio q. Bottom: corresponding fractional error in relation to the fit.

the dimensionless asymmetric combination of the tidal deformabilities:

$$\bar{\Lambda}_a = \frac{\bar{\Lambda}_1 - \bar{\Lambda}_2}{2}. \tag{4.4}$$

The relation $\bar{\Lambda}_s$–$\bar{\Lambda}_a$ is illustrated in Fig. 4.4, reproduced from Ref. [27]. In the figure, $q \equiv \frac{m_1}{m_2}$, where m_a is the mass of the a-th component of the binary system, here, it is considered that the component 2 is the most massive star, meaning $q < 1$. The relation is evaluated for different values of q, and the figure shows that the relation becomes more insensitive to the EoS choice with high values of $\bar{\Lambda}_s$ or low values of q. Also from the figure we can see that the degree of universality of this relation is $\mathcal{O}(10\%)$.

This relation has important applications: currently, one of the most important ways of extracting new neutron star information is through the detection of gravitational waves, examples include Refs. [18, 82–85]. One of the systems generating an observable GW signal is the neutron star-neutron star binary system. However, detecting individual deformabilities from such a system is difficult due to the degeneracy between them when

entering the GW model, this happens because at leading order, the GW phase is sensitive to the combination of the tidal deformabilities, and not to the individual ones.

Using the relation to write, for example $\bar{\Lambda}_a = \bar{\Lambda}_a(q, \bar{\Lambda}_s)$ improves the accuracy in which $\bar{\Lambda}_s$ can be measured; and this relation can be used again to extract $\bar{\Lambda}_a$, making it possible to obtain both of the individual deformabilities. An estimate of the error of measuring these quantities with and without this relation can be found in Ref. [27]. This was used in the first confirmed gravitational wave detection of a NS binary system [45].

There are also other applications of this relation. For example, constraining the EoS families given a GW observation; this can be done because the relation between the tidal deformability of a star and its mass is EoS dependent, thus measuring them simultaneously can be used to extract EoS information [27]. Another applications can be found in [27] and [28]. Examples include:

- Improving the possibility of testing General Relativity through tests of the I-Love-Q relation; this is done by using the binary Love relation to improve measurements of the tidal deformability;
- It can also be used in cosmology to help improve the measurement of cosmological parameters through gravitational waves. Details on how this is done can be found in Refs. [86–89].

I-Love and C

The relations between the I-Love quantities and the compactness C are also EoS-independent for neutron stars. These are two relations: the I-C, and the Love-C, that can be treated individually.

A universal relation between the normalized moment of inertia $\frac{I}{MR^2}$ and the compactness C was first highlighted in Ref. [90] and later treated in Refs. [30], [11] and applied in [13]. A more recent account can be found in Refs. [91] and [92], exploring the relation between both the normalized moment of inertia and the dimensionless moment of inertia $\overline{I}$ defined as in Equation (2.93) with the compactness.

As shown in Ref. [91], the latter relation appears to be more insensitive to the choice of EoS, a comparison between them can be found in the same reference. The relation $\overline{I}$-C is illustrated in Fig. 4.5, for slowly rotating stars. As the figure shows, the

$\overline{I}$-C relation depends very weakly on the equation of state.

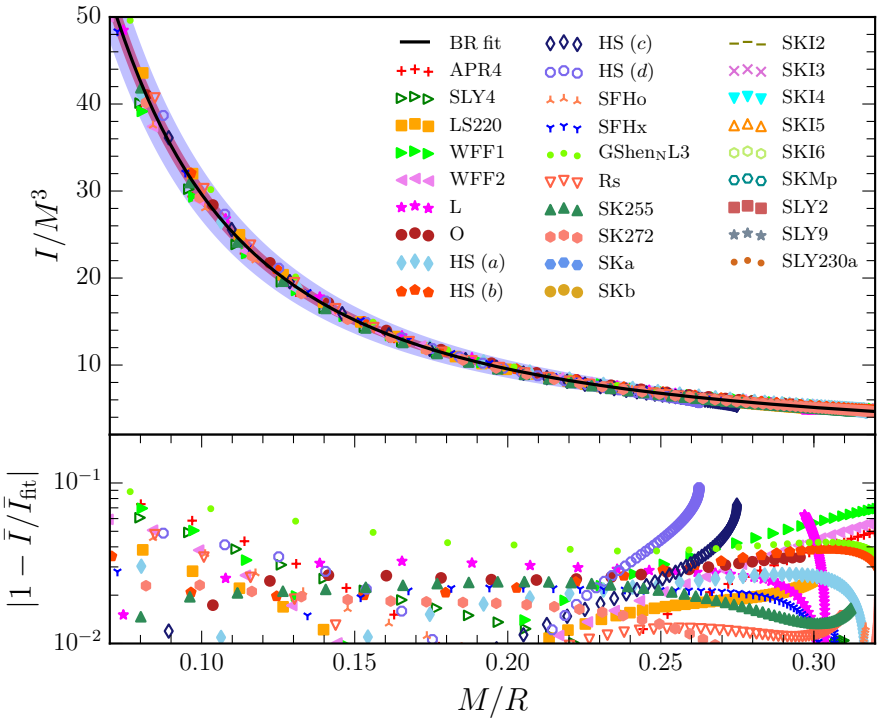

Figure 4.5: Reproduction from Ref. [91]. Top: the universal $\overline{I}$-C relation for a slowly rotating neutron star for a number realistic equations of state, and a fit that can be found in Ref. [91]. Bottom: corresponding fractional error in relation to the fit.

The Love-C relation was first noted in Ref. [80] and later illustrated in [93]. It arises naturally from the Q-C relation [94] (that is not explained here due to its similarity to the $\overline{I}$-C relation) and the I-Love-Q relations. The relation between the dimensionless tidal deformability defined in Eq. (2.72), then with the symbol $\overline{\Lambda}$ and here with $\overline{\Lambda}_2$, and the compactness of the star is illustrated in Fig. 4.6. From the figure it is possible to note that the relation, specifically for neutron stars, is indeed universal.

The $\overline{I}$-C relation can be used to obtain, or at least constrain, the radius of the star given measurements of its moment of inertia and mass from pulsar timing [51]. The analysis on how this can be done can be found in Refs. [13] and [91]. The $\overline{\Lambda}_2$-C relation can be applied to extract the radius of the star through gravitational-wave detections that can provide measurements of the tidal deformability and its mass [80]. Both the methods of extracting the radius with mass measurements are capable of constraining the equation of state because, as mentioned in Chapter 3, and illustrated in Figure 3.3, the mass-radius curve of neutron stars is not EoS-independent and determining points in this curve with a sufficiently low uncertainty can help greatly in determining the right EoS, see Ref. [8]

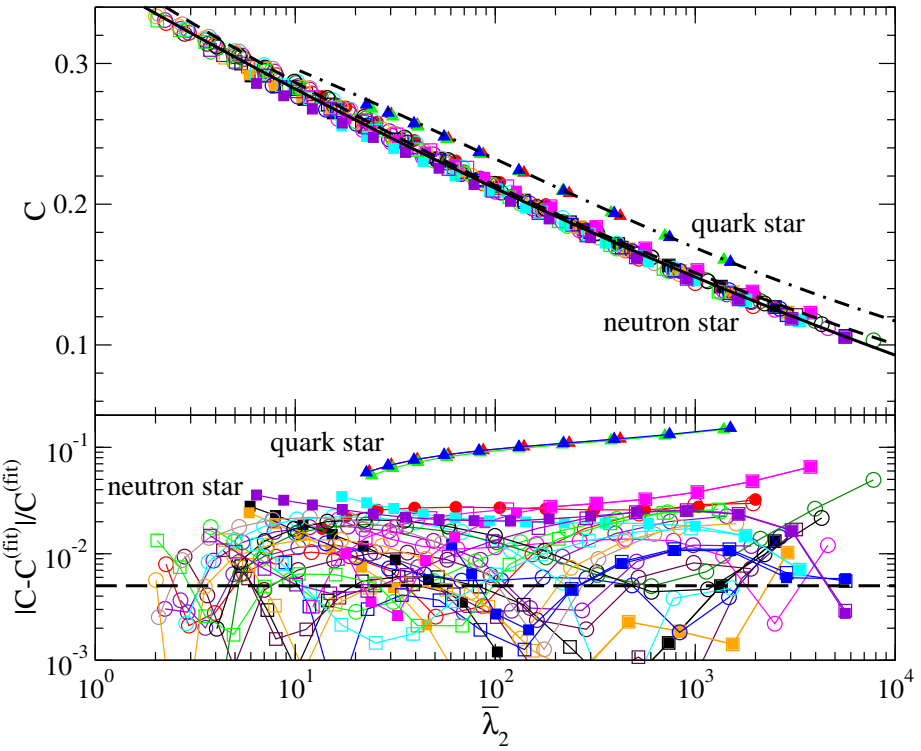

Figure 4.6: Reproduction from Ref. [93]. Top: the universal $\overline{\Lambda}_2$-C relation for neutron stars and quark stars. The relation was analyzed for a number of equations of state; the dashed lines represent the fit in [80] and the solid black line represent the fit that can be found in [93]. Bottom: corresponding fractional error in relation to the fit.

and [30] for a detailed description on how this can be done.

The $\overline{I}$-C relation was also studied for rapidly rotating stars in Refs. [91] and [92]. The reasoning for both these relations and an analytic version and explanation for them can be found in Ref. [95].

$\mathbf{R_M}$-$\mathbf{P(n)}$

The relation R_M-$P(n)$ was first noted by Ref. [30]. It is the relation between the nominal radius R_M which is the radius of a star at a certain mass M and the pressure $P(n)$ at a specific baryon density n.

It was noted, in Ref. [30], that a lot of the realistic equations of state had approximately the same behavior, characterized as having the same adiabatic index $\Gamma = 2$, around the baryon density interval $n_s - 2n_s$, where n_s is the nuclear saturation baryon density, which is the density related to the nuclear saturation mass density ρ_{sat} as $\rho_{\text{sat}} = m_b n_s$, where m_b is the baryon mass. Alongside the fact that when $\Gamma = 2$ the radius is proportional to the square root of the K constant in the polytropic equation of state (3.18), this

suggested the possibility of a relation between the radius and pressure that was not EoS dependent.

This was confirmed by analyzing the nominal radius with $M = M_\odot$ and $M = 1.4\,M_\odot$ and the pressure at the densities $n = n_s$, $1.5n_s$, $2n_s$. The relation between these quantities can be numerically written as the power law [30]:

$$R_M \simeq C(n, M)\ [P(n)]^{0.23-0.26}, \tag{4.5}$$

where $C(n, M)$ is a constant that varies for different values of density and mass. This relation is demonstrated in Fig. 4.7: in the figure the value 0.25 is chosen for the power in equation (4.5) even though the relation holds for a small range of parameters. From Fig. 4.7 it is possible to identify the different values of $C(n, M)$, that can be found in Ref. [30].

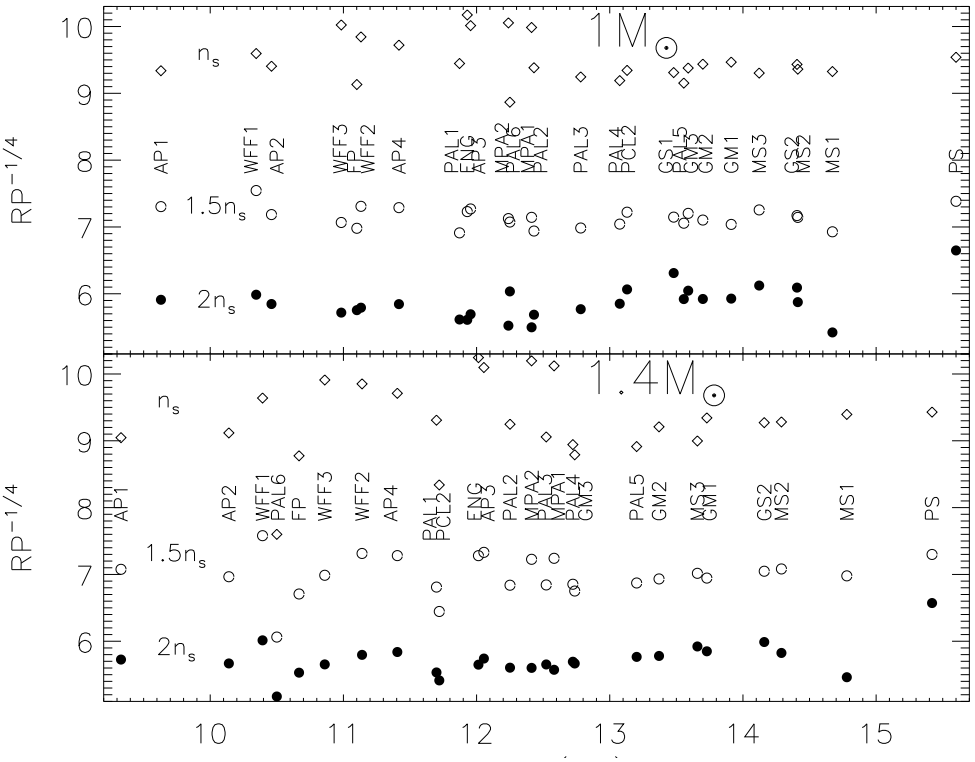

Figure 4.7: Reproduction from Ref. [30]. Top (Bottom): Relation between $R_{M_\odot}(R_{1.4M_\odot})$ and $RP^{0.25}$ for several equations of state considering the pressure P at different values of density, which can be identified by the different symbols.

The relation mentioned in this section differs from others presented so far in the

sense that instead of connecting two or more macroscopic observables it connects a macroscopic quantity, the radius of the star, to a microscopic quantity, the pressure at a fiducial density. As mentioned previously, the microscopic behavior of the matter inside neutron stars is still a mystery, and a direct way to obtain information regarding it from macroscopic observations is extremely useful. This means that it is possible to constrain the equation of state given a radius measurement using directly the inverse relation found in equation (4.5). A complete analysis and further discussion on the reasons for this relation can be found in Ref. [30].

f-Love

The f-Love relation was first highlighted in Ref. [96]. This is the relation between the multipolar fundamental mode oscillation frequency and the multipolar tidal deformability. A universal relation between the moment of inertia and the $l = 2$ (or quadrupolar) f-mode oscillation frequency was discovered by [19], and alongside the I-Love-Q relations, it seems natural that a relation between the quadrupolar f-mode and the quadrupolar tidal deformability (the one present in the I-Love-Q relation and described in Subsection 2.2.1) was also EoS-independent. Besides the analysis of this relation, the other multipolar relations, meaning with different values of l, were also discovered by Ref. [96].

Perturbations to the equilibrium state of a neutron star lead to oscillations that can be described in terms of quasinormal modes (QNM) [97]. These modes are quasinormal and not normal because of the decay that occurs due to the emission of gravitational waves. Each of these modes is characterized by a complex frequency $\omega = \omega_r + i\,\omega_i$, where ω_i is the measure of its decay rate. The f-mode is the fundamental mode, associated with the frequency ω_r. The frequency used in this relation is the scaled lth multipole defined as:

$$\overline{\omega}_l = M\,\omega_l, \tag{4.6}$$

where M is the stellar mass. The jth multipolar tidal deformability is defined in Ref. [43] in terms of the tidal love number as:

$$k_j = \frac{(2j-1)!!}{2}\,C^{2j+1}\overline{\Lambda}_j, \tag{4.7}$$

where $\overline{\Lambda}_j$ is the dimensionless tidal deformability, with the normalization:

$$\overline{\Lambda}_j \equiv \frac{\Lambda_j}{M^{2j+1}}. \tag{4.8}$$

There are several relations between these quantities that arise from the combination of different values of l and j. In Ref. [96], the considered values for l and j are $(2, 3, 4, 5)$. Here, we illustrate only the relation between the $j = 2$ tidal deformability and $l = 2, 3, 4, 5$ oscillation frequencies in Fig. 4.8. The illustrations for different values of j can be found in Ref. [96].

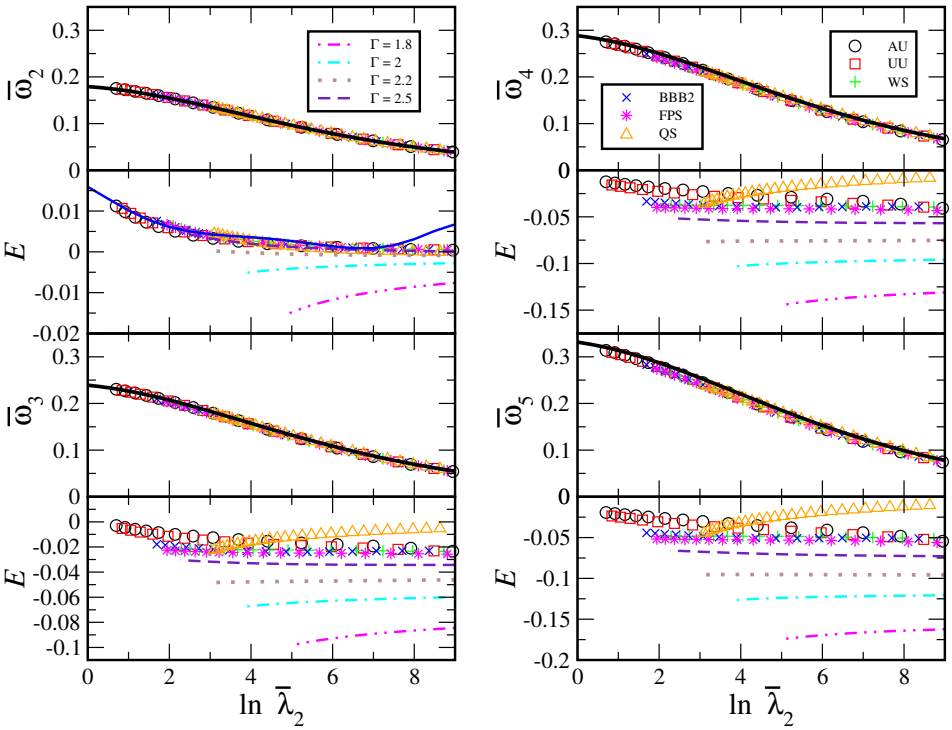

Figure 4.8: Reproduction from Ref. [96]. The relations for $\overline{\omega}_l$-$\overline{\Lambda}_2$ for $l = 2, 3, 4$ and 5 for a few realistic equations of state and polytropic stars with various adiabatic indices and one quark star. The black solid line indicates an incompressible star. Under each relation are the fractional errors E.

From these graphs it is possible to see that the universality increases when $l = j$, which also happens for different values of j. A Newtonian analytical analysis of this relation can be found in Ref. [96].

Other relations

Here we mention a few other universal relations:

- $\tilde{\Lambda}$-$\delta\tilde{\Lambda}$: Relation between the coefficients of the Post-Newtonian expansion of the GW phase [81];
- $\overline{\Lambda}_0^{(0)}$-$\overline{\Lambda}_0^{(k)}$: Relation between the coefficients of the Taylor expansion of the tidal deformabilities [27];
- $\frac{BE}{M}$-C: Relation between the normalized binding energy and the compactness [30];
- $\overline{\Lambda}_l$-$\overline{\Lambda}_j$, $\overline{\sigma}_2$-$\overline{\Lambda}_2$ and $\overline{\eta}_l$-$\overline{\eta}_j$: Relations between the dimensionless forms of the multipolar even tidal deformabilities, $\overline{\Lambda}_l$, between the even quadrupolar tidal deformability $\overline{\Lambda}_2$ and the quadrupolar odd one, $\overline{\sigma}_2$, and between the multipolar shape tidal deformabilities $\overline{\eta}_l$ [28].

4.2 Results

The new relations presented and analyzed here are between the microscopic quantity α_c, defined as the ratio:

$$\alpha_c \equiv \frac{p_c}{\epsilon_c}, \tag{4.9}$$

where p_c and ϵ_c are respectively the pressure and the energy density evaluated at the center of the star, and three macroscopic quantities: the dimensionless tidal deformability $\overline{\Lambda}$, the compactness C and the dimensionless moment of inertia $\overline{I}$.

The ratio α_c is an average measure of the stiffness of the star, in contrast with the sound velocity that can be interpreted as a local parameter of the stiffness. This difference can be seen in Fig. 4.9. In the figure three different equations of state are displayed, one considered to be "soft", composed of APR nuclear matter and color-flavor-locked quark matter (ALF1) [98]; one with $npe\mu$ nuclear matter (SLy) [59], considered neither soft nor stiff and a stiff one, also with $npe\mu$ nuclear matter but relativistic (MPA1) [60].

The angles indicated with the letter ϕ (ϕ_1, ϕ_2 and ϕ_3) are the angles between the tangent line to the point $\frac{\epsilon_c}{c^2} = 3\rho_{\rm sat}$, and the x-axis. The tangent lines are indicative of

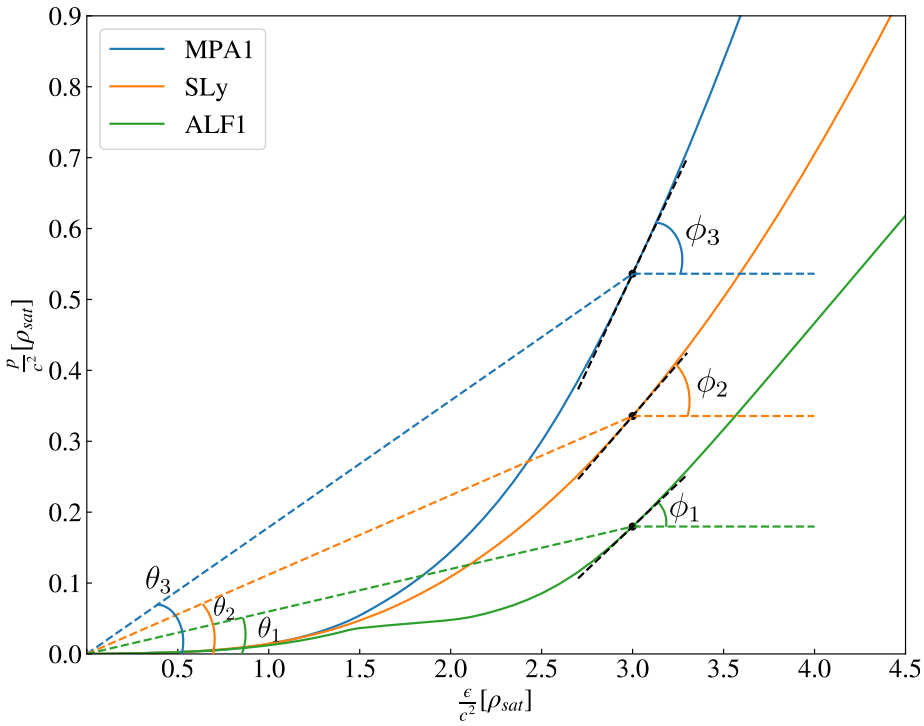

Figure 4.9: The relation $p(\epsilon)$, represented by the solid lines, is presented for three equations of state of different stiffness. The colored dashed lines are to better visualize the angles and the black dotted lines are the tangent lines to the points marked by dots.

the slope of the equation of state at the specific point, meaning how much the pressure is increasing given the energy density at this point. The angles are directly related to the derivative at the point $\frac{dp}{d\epsilon}\big|_{\epsilon_c}$ in the form of $\phi = \arctan\left(\frac{dp}{d\epsilon}\right)$. This derivative is also related to the sound speed through the relation in Eq. (3.26), $c_s^2 = \frac{dp}{d\epsilon}$, meaning the sound speed and the angle are related by $c_s^2 = \tan(\phi)$. In this particular case, the values we find for the speed of sound of each particular EoS (represented by the superscript) are:

$$\begin{aligned} c_s^{(1)}(\epsilon_c) &= 0.4940, \\ c_s^{(2)}(\epsilon_c) &= 0.5449, \\ c_s^{(3)}(\epsilon_c) &= 0.7372. \end{aligned} \tag{4.10}$$

On the other hand, the angles represented by the letter θ are the angles between the lines that connect $\epsilon(0)$ and the point ϵ_c. These lines characterize the general slope of

the equation of state up until the specified point, with general meaning that it describes the total variation of the pressure given an energy density. However, for most equations of state $\epsilon(0) \approx 0$, so that for the following discussion we consider this approximation. The corresponding angles θ_1, θ_2 and θ_3 are related to the ratio $\frac{p(\epsilon_c)}{\epsilon_c}$ by $\theta = \arctan\left(\frac{p(\epsilon_c)}{\epsilon_c}\right)$ Consequently they are related to the quantity α_c by $\alpha_c = \tan(\theta)$. The values we find for this quantity given these specific EoS and the energy density ϵ_c are:

$$\begin{aligned} \alpha_c^{(1)} &= 0.0599, \\ \alpha_c^{(2)} &= 0.1119, \\ \alpha_c^{(3)} &= 0.1788. \end{aligned} \tag{4.11}$$

As shown, this is capable of differentiating the stiffness of each equation of state and being able to determine the value of this quantity from observations can be an important tool in understanding more of the matter inside neutron stars and their EoS.

The quantity $\alpha \equiv \frac{p}{\epsilon}$ is bound to some values; requiring causality, implies [99] that

$$c_s \leq 1. \tag{4.12}$$

The dominant energy condition (see e.g. Ref. [100]), on the other hand, for perfect fluids can be written as $\epsilon \geq |p|$. This leads to:

$$\alpha \leq 1. \tag{4.13}$$

Of course, since in the non-relativistic limit nuclear matter satisfies $p \ll \epsilon$, for the bound $\alpha = 1$ to be achieved, the fluid must first go superluminal; Eq. (4.12) is therefore more restrictive than (4.13). In particular, it is interesting to consider the case of an EoS that is "maximally soft", $p(\epsilon) = 0$, for $\epsilon \leq \epsilon_0$, and "maximally stiff", $p(\epsilon) = \epsilon - \epsilon_0$, for $\epsilon \geq \epsilon_0$, which yields the most compact NS models consistent with causality [101]. The maximally compact configuration, with $C \approx 0.35$, has $\epsilon_c = 3.024\epsilon_0$ and $p_c = 2.034\epsilon_c$, and therefore

$$\alpha_c = 0.670. \tag{4.14}$$

As we will see below, by requiring that the EoS satisfies Eq. (4.12), the bound (4.14) is

approached, rather than (4.13).

4.2.1 Relations for Realistic EoS

Here we present three approximately EoS-independent relations $\alpha_c - \overline{I}$, $\alpha_c - \overline{\Lambda}$ and $\alpha_c - C$ for a set of 40 realistic equations of state. These equations are the ones that can be found in the catalog from Ref. [63], the values and naming used here are also the ones in the catalog. The equations of state are: ALF1-4 [98], AP1-4 [102], BBB2 [103], BGN1H1 [104], BPAL12 [105], BSK19-21 [106], ENG [107], FPS [108], GNH3 [109], GS1-2 [110], H1-7 [111], MPA1 [60], MS1-1b-2 [61], PAL6 [112], PCL2 [113], PS [114], SLy [59]; SQM1-3 [113] and WFF1-3 [62].

In order to present these relations 50 stars were generated each with different central densities for each one of the equations of state. For each star, its mass and radius were determined through the TOV equations (2.22) and (2.23), its moment of inertia through Eqs. (2.92) and (2.93) and its tidal deformability through Eqs. (2.71) and (2.72). Here, we only consider stars with compactness $C \geq 0.05$, which besides setting a lower limit for the compactness, also sets an upper limit for both the deformability and the moment of inertia, the particular values will be mentioned later on.

First we evaluate the relation between the value of α at the center of the star and the compactness of the star. This relation is presented in the top of the images in Fig. 4.10, from which we can see that it is weakly sensitive to the choice of equation of state.

We analyze different polynomial fits for this relation, all in the form of:

$$\alpha_c = \sum_{k=0}^{n} a_k C^k, \tag{4.15}$$

where a_k are the coefficients of the polynomial. The fits here and forward were made using the least squares methods. The values $n = 3$, 4, 5, and 6 are used for this purpose. The relative error, presented in the bottom of the images in Fig. 4.10 is calculated as:

$$E = \frac{|\alpha_{fit} - \alpha_c|}{\alpha_{fit}}, \tag{4.16}$$

where α_{fit} is the value found by substituting the value of C in Eq. (4.15).

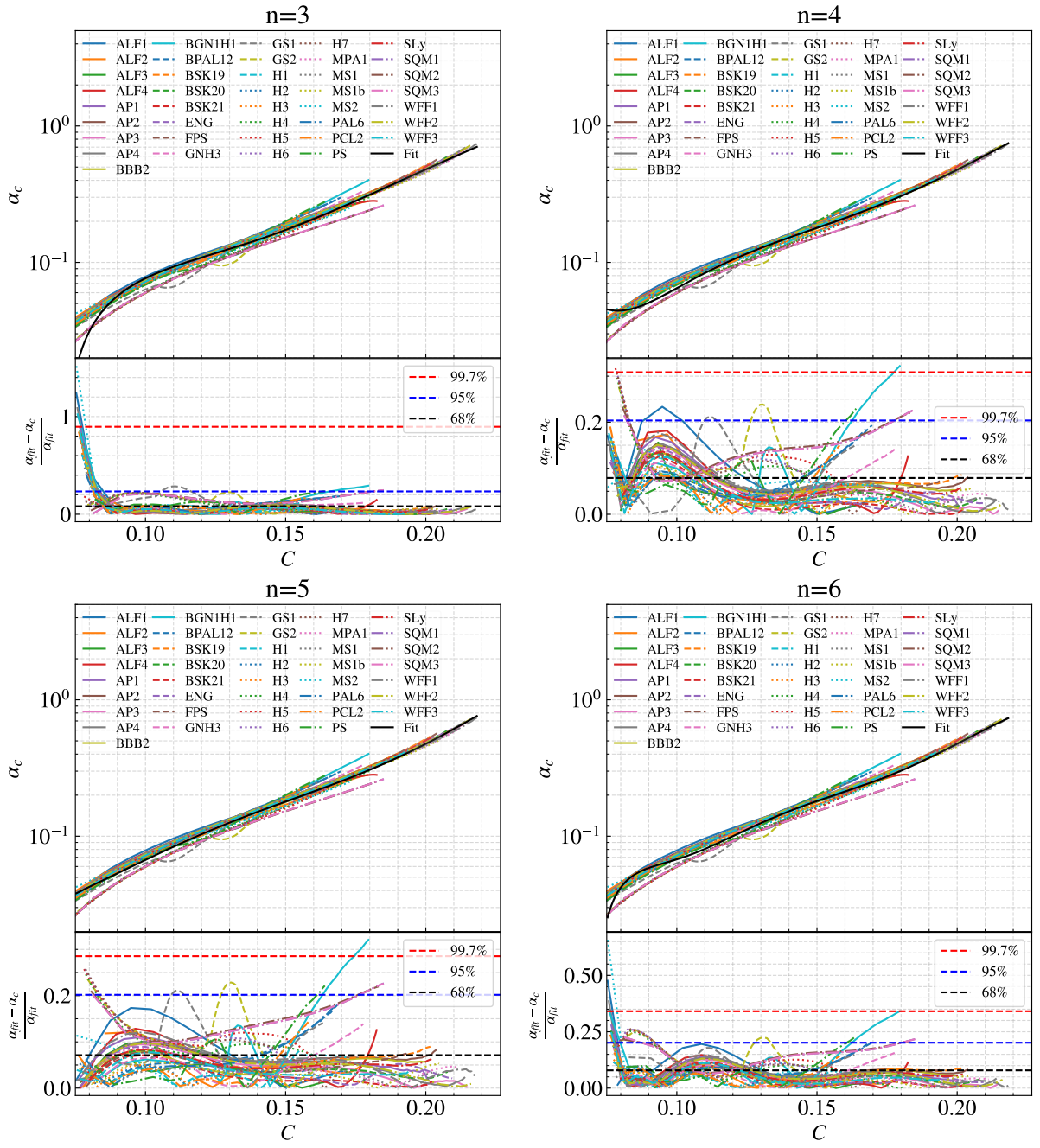

Figure 4.10: Universal $\alpha_c - C$ relation for a set of 40 realistic equations of state. A solid black line represents an n-th order polynomial fit (as in Eq. (4.15)). Bottom panels display the corresponding relative error as described in Eq. (4.16), with the red, blue and black dashed lines representing the value of, respectively, 99.7%, 95% and 68% of the relative error. Only configurations with $C > 0.05$ are considered.

The fits with lower parameters, $n = 3$, 4 do not seem to capture accurately the behavior of the relation at lower values of C and neither does the $n = 6$ fit, the only one, from Fig. 4.10, that seems to the properly demonstrate the general behavior of the relation is also the one with the lower maximum relative error ($\sim 32\%$), $n = 5$; this

one also presents the lower average relative error ($\sim 6.7\%$). Also in this fit 99.7% of the relative error, which is represented by the dashed horizontal red line in the bottom, is under $\sim 28.5\%$, 95%, represented by the blue line is under $\sim 20.2\%$ and 68%, represented by the black line under $\sim 7.1\%$. For $n = 5$ the values of the fit coefficients can be found in Table B.1.

The $\alpha_c - \overline{I}$ relation is presented in upper panels of Figure 4.11. From it we can see that the dependence on the choice of EoS is also weak. In the figure, the $C \geq 0.05$ requirement sets an upper limit in the moment of inertia of $\log \overline{I} \lesssim 4.47$. To fit this relation we try different degrees of a logarithmic polynomial expression in the form of:

$$\log \alpha_c = \sum_{k=0}^{n} b_k (\log \overline{I})^k, \tag{4.17}$$

where b_k are the fit coefficients. The values $n = 3$, 4, 5 and 6 are used for this purpose. The relative error, presented in the bottom of the images in Fig. 4.11 is calculated as presented in Eq. (4.16).

The fits with lower parameters, $n = 3$, 4 show a bigger discrepancy from the curve of the relation at higher values of $\overline{I}$. Both the $n = 5$ and the $n = 6$ fits seem to the properly capture the general behavior of the relation. The one with the lower maximum relative error ($\sim 34.6\%$) is $n = 5$; it also presents the lower average relative error ($\sim 3.9\%$). Also in this fit 99.7% of the relative error, which is represented by the dashed horizontal red line in the bottom, is under $\sim 15.4\%$, 95%, represented by the blue line is under $\sim 9.6\%$ and 68%, represented by the black line, under $\sim 5\%$. For $n = 5$ the values of the fit coefficients can be found in Table B.2.

The $\alpha_c - \overline{\Lambda}$ relation is presented in upper panels of Figure 4.12. In the figure, the $C \geq 0.05$ requirement sets an upper limit in the tidal deformability of $\log \overline{\Lambda} \lesssim 12.3$. From it we can see that the dependence on the choice of EoS is weak, except for the equations of state SQM1-3. SQM1-3 EoS are modeled for quark stars, instead of neutron stars and from this figure it is apparent that these stars obey a different relation than the one found for NS. This has similarities to the difference found in the universal relation between $\overline{\Lambda}$ and $\overline{I}$ in Fig. 4.6. Here we first fit the relation including these equations then excluding them. To do this we try different degrees of a logarithmic polynomial expression in the form of:

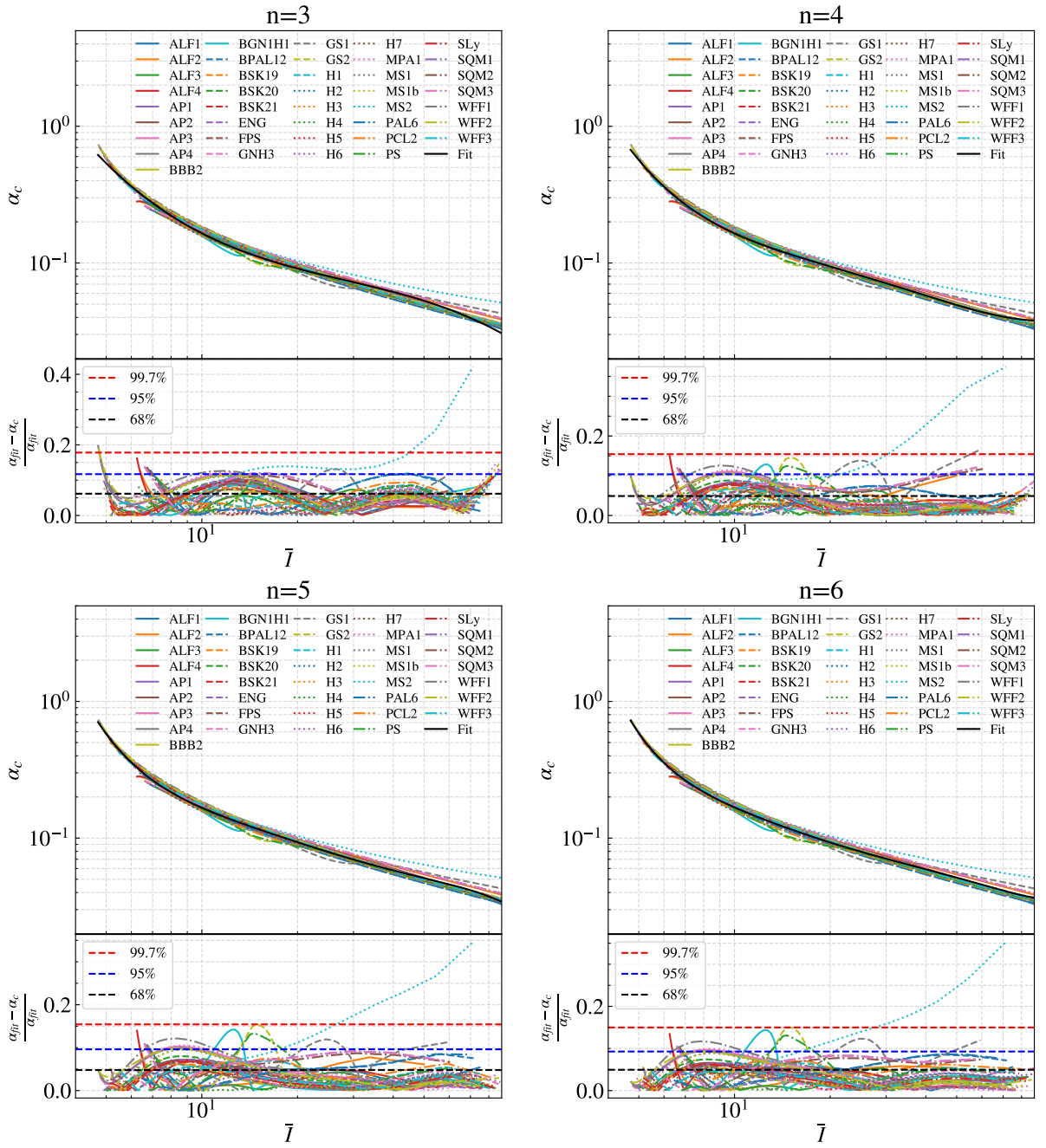

Figure 4.11: Quasi universal $\overline{I} - \alpha_c$ relation for a set of 40 realistic equations of state. A solid black line represents an n-th order polynomial fit (as in Eq. (4.17)). Bottom panels display the corresponding relative error as described in Eq. (4.16), with the red, blue and black dashed lines representing the value of, respectively, 99.7%, 95% and 68% of the relative error. Only configurations with $C > 0.05$ are considered.

$$\log \alpha_c = \sum_{k=0}^{n} c_k (\log \overline{\Lambda})^k, \tag{4.18}$$

where c_k are the fit coefficients. The values $n = 3$, 4, 5 and 6 are used for this purpose.

The relative error, presented in the bottom of the images in Fig. 4.11 is calculated as presented in Eq. (4.16).

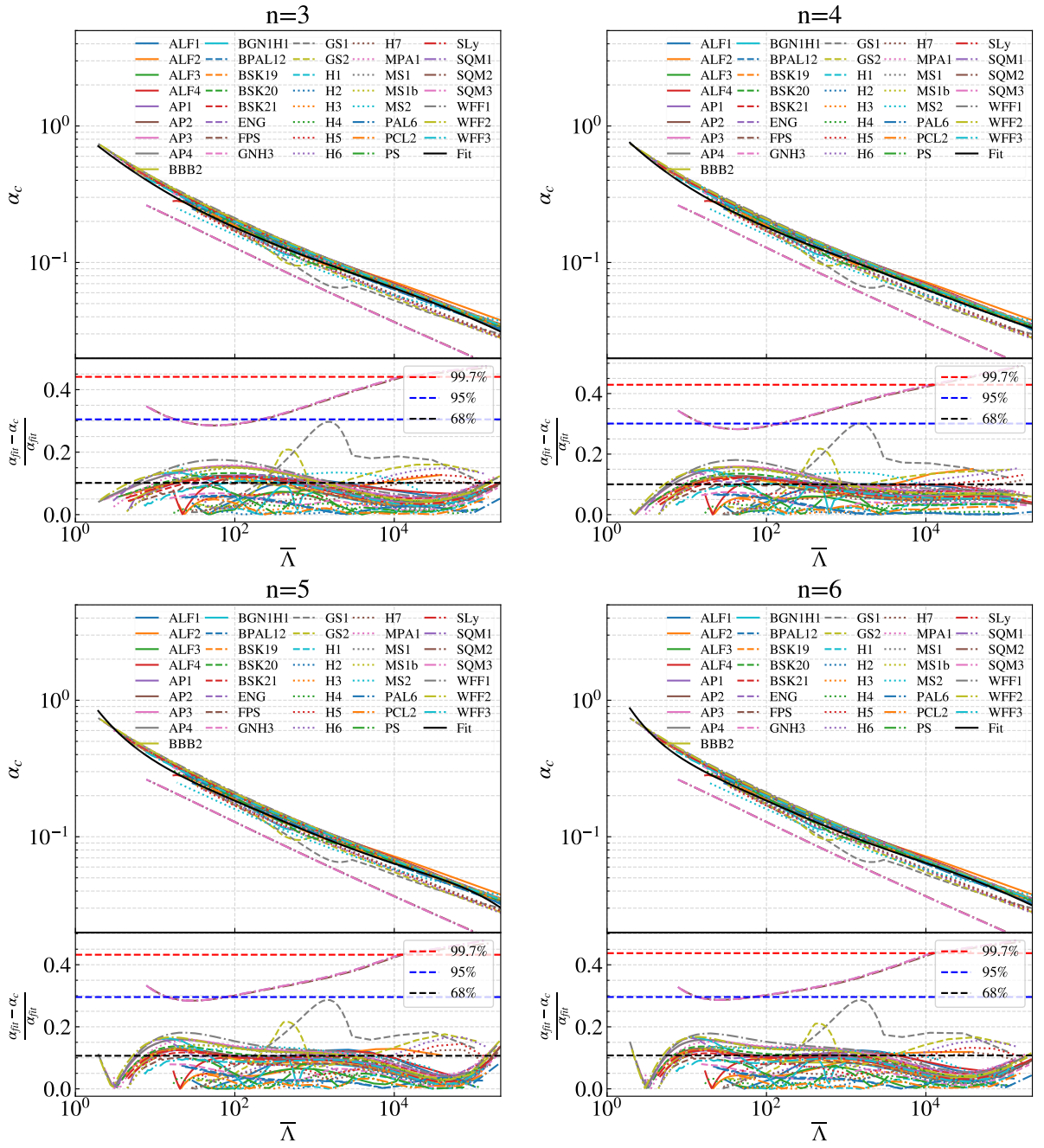

Figure 4.12: Approximately universal $\overline{\Lambda} - \alpha_c$ relation for a set of 40 realistic equations of state. A solid black line represents an n-th order polynomial fit (as in Eq. (4.18)). Bottom panels display the corresponding relative error as described in Eq. (4.16), with the red, blue and black dashed lines representing the value of, respectively, 99.7%, 95% and 68% of the relative error. Only configurations with $C > 0.05$ are considered.

Here the fit with the lower maximum relative error is the one that generally tends towards the lower part of the plot. This one, with maximum relative error ($\sim 47.5\%$) is

$n = 3$. It also has average relative error $\sim 9.05\%$. Also in this fit 99.7% of the relative error, which is represented by the dashed horizontal red line in the bottom, is under $\sim 44.1\%$, 95%, represented by the blue line is under $\sim 30.5\%$ and 68%, represented by the black line, under $\sim 10.2\%$. For $n = 3$ the values of the fit coefficients can be found in Table B.3.

If we consider the $\alpha_c - \overline{\Lambda}$ relation only for neutron stars, meaning, excluding equations of state that describe quark matter, we obtain Fig. 4.13. In this case, the fit with lower maximum relative error $\sim 30\%$ is $n = 4$ which has the lower average relative error $\sim 5.4\%$, with 99.7% of the relative errors under $\sim 28\%$, 95% under $\sim 14\%$ and 68% under $\sim 6.7\%$. The values for this fit can be found in B.4.

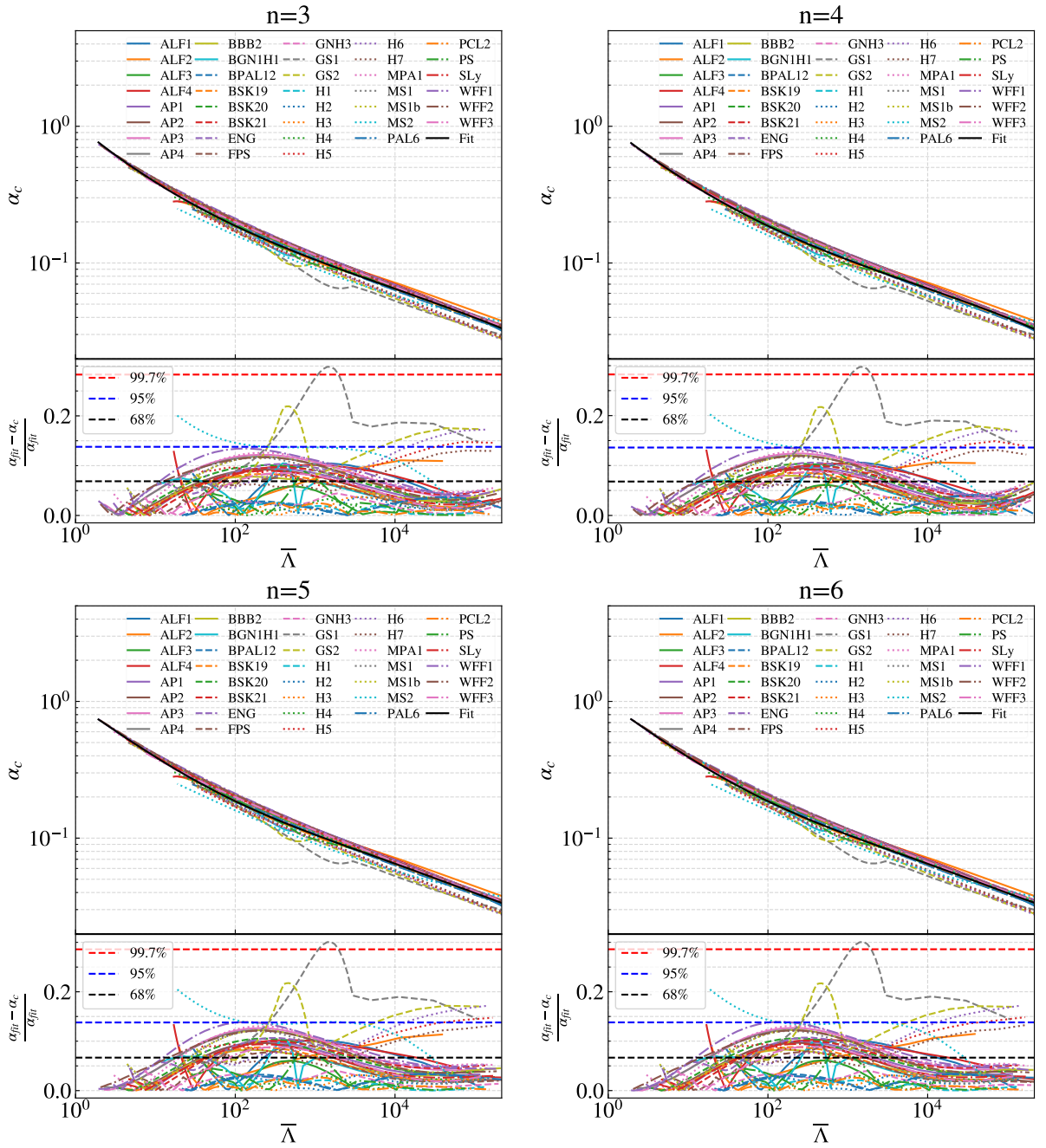

Figure 4.13: Approximately universal $\overline{\Lambda} - \alpha_c$ relation for a set of 37 realistic equations of state. A solid black line represents an n-th order polynomial fit (as in Eq. (4.18)). Bottom panels display the corresponding relative error as described in Eq. (4.16), with the red, blue and black dashed lines representing the value of, respectively, 99.7%, 95% and 68% of the relative error. Only configurations with $C > 0.05$ are considered.

4.2.2 Relations for Phenomenological Equations of State

Besides presenting the relation for tabulated realistic equations of state, we also present them for a set of 15,000 phenomenological equations of state. These equations

were generated using the GPP parametrization, described in Sec. 3.1.1. Comparison with another set of 10,000 spectral EoS will be performed in Sec. 4.2.5

The process of generating these EoS was to randomly generate values for each of the free parameters of the parametrization. The relation between parameters K_1 and Γ_1 is constrained by the equations that describe the last interval of the SLy crust, and the first interval of the core. As the densities for the intervals mentioned are $\rho_{\rm SLy} < \rho < \rho_0$, where $\rho_{\rm SLy} = 5.317 \times 10^{11}$ g/cm^3 is the last density of the crust from Table A.1, and $\rho_0 < \rho < \rho_1$, we have a requirement that the dividing density ρ_0 is in the interval:

$$\rho_{\rm SLy} < \rho_0 < \rho_1. \tag{4.19}$$

Using Eq. (3.36) we find that:

$$K_{\rm SLy}\,\Gamma_{\rm SLy}\,\rho_0^{\Gamma_{\rm SLy}-1} = K_1\,\Gamma_1\,\rho_0^{\Gamma_1-1}, \tag{4.20}$$

where the subscript SLy indicates the last item from the Table A.1. From this equation we can isolate ρ_0:

$$\rho_0 = \left(\frac{K_{\rm SLy}\,\Gamma_{\rm SLy}}{K_1\,\Gamma_1}\right)^{1/(\Gamma_{\rm SLy}-\Gamma_1)}. \tag{4.21}$$

With the requirement in Eq. (4.19) we find that if $\Gamma_1 > \Gamma_{\rm SLy}$, the parameter K_1 is restricted as:

$$\frac{K_{\rm SLy}\,\Gamma_{\rm SLy}}{\Gamma_1\,\rho_1^{\Gamma_1-\Gamma_{\rm SLy}}} < K_1 < \frac{K_{\rm SLy}\,\Gamma_{\rm SLy}}{\Gamma_1\,\rho_{\rm SLy}^{\Gamma_1-\Gamma_{\rm SLy}}}, \tag{4.22}$$

and on the other hand if $\Gamma_1 < \Gamma_{\rm SLy}$:

$$\frac{K_{\rm SLy}\,\Gamma_{\rm SLy}}{\Gamma_1\,\rho_{\rm SLy}^{\Gamma_1-\Gamma_{\rm SLy}}} < K_1 < \frac{K_{\rm SLy}\,\Gamma_{\rm SLy}}{\Gamma_1\,\rho_1^{\Gamma_1-\Gamma_{\rm SLy}}}. \tag{4.23}$$

This means that the portrayed four free parameters parametrization has effectively only three free parameters, as the area for the allowed values of K_1 is limited. This is displayed in Fig. 4.14.

In order to decide the interval in which the parameters Γ_i, with $i = 1$, 2, and 3

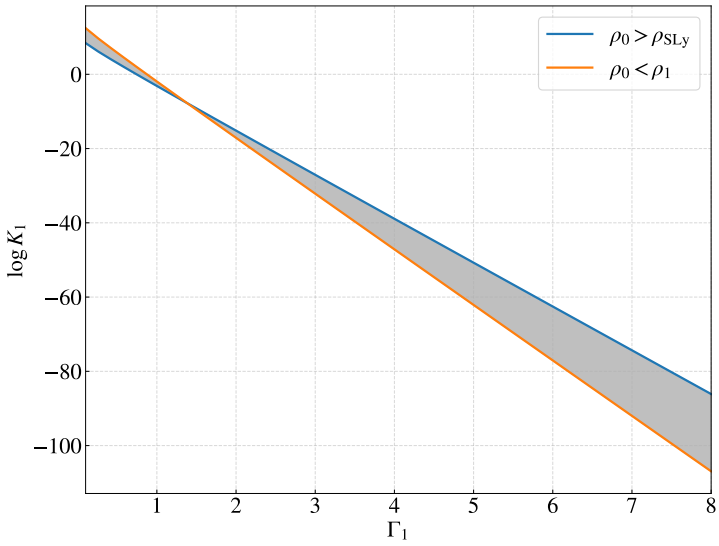

Figure 4.14: The allowed area for $\log K_1$, as limited by Eqs. (4.22) and (4.23).

should be generated, we take the interval in which they are contained in Table A.2, which is $\Gamma_1 \in [2,4]$, $\Gamma_2 \in [2,4]$ and $\Gamma_3 \in [1.5,4]$ and expand it. We generate random values for Γ_i and $\log K_1$. The interval for Γ_2 and Γ_3 was $[-2,8]$; for Γ_1 it was $[0,8]$ (excluding $\Gamma_1 = \Gamma_{SLy}$ as that would result in an infinite power in Eq. (4.21) and negative numbers as $\log K_1$ depends on $\log \Gamma_1$); lastly, $\log K_1$ is generated between the restrictions in Eq. 4.22 given the value of $\log \Gamma_1$. We generated 5,000 EoS in this interval in order to test the possible constraints due to causality and the requirement that $M_{max} \geq 2M_\odot$. The result of this analysis is presented in Figs. 4.15, 4.16, 4.17 and 4.18.

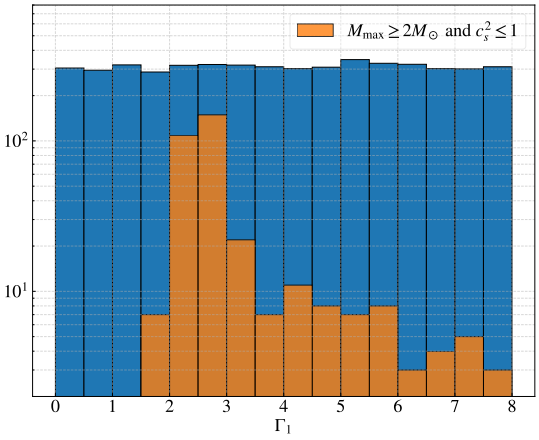

Figure 4.15: Histogram of the randomly generated values of Γ_1 in blue and in orange the histogram of values that satisfy causality and the requirement $M_{max} \geq 2M_\odot$.

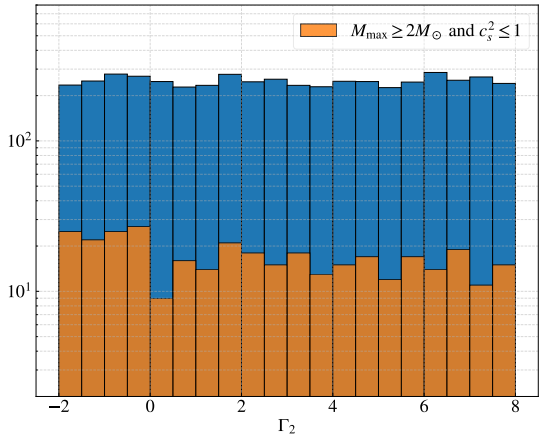

Figure 4.16: Histogram of the randomly generated values of Γ_2 in blue and in orange the histogram of values that satisfy causality and the requirement $M_{max} \geq 2M_\odot$.

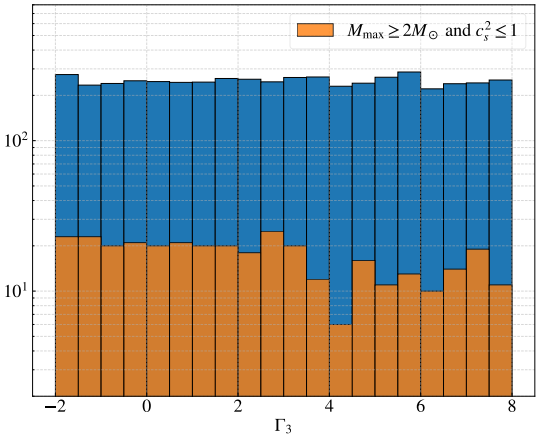

Figure 4.17: Histogram of the randomly generated values of Γ_3 in blue and in orange the histogram of values that satisfy causality and the requirement $M_{\max} \geq 2M_\odot$.

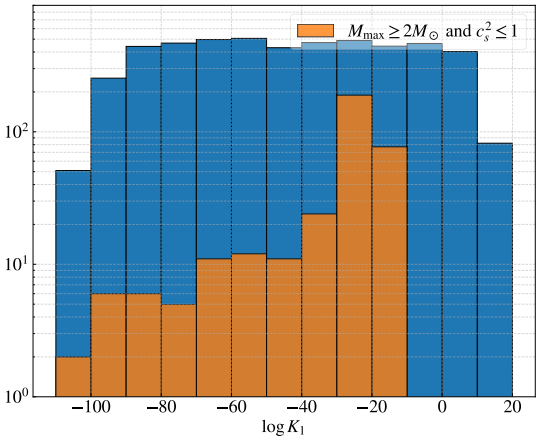

Figure 4.18: Histogram of the randomly generated values of $\log K_1$ in blue given the intervals in Eqs. (4.22) and (4.23) and in orange the histogram of values that satisfy causality and $M_{\max} \geq 2M_\odot$.

From the histograms of Γ_2 and Γ_3 we find that causality and the maximum mass requirements do not restrict the possible values for these parameters. For Γ_1 and consequently K_1, however, these requirements do change the allowed interval. In the case of Γ_1, no value below $\Gamma_{\rm SLy}$ was able to generate an EoS that fulfilled the specific constraints. To generate the 15,000 phenomenological EoS we use the intervals Γ_1 in $[\Gamma_{\rm SLy}, 8]$, $\Gamma_{2,3}$ from $[-2, 8]$ and $\log K_1$ the one described in Eq. (4.22). Besides this, we also require:

- Causality, by imposing that $c_s^2 \leq 1$ throughout the star up to the density that generates the maximum mass;
- That the configuration with the highest mass, generates a star with $M_{\max} \geq 2\,M_\odot$, value that is in correspondence to measured masses of neutron stars [63, 115].

The equations of state generated can be represented by two graphs: one of the different $\epsilon(p)$ relations and the correspondent mass-radius curves. These are presented in Figs. 4.19 and 4.20. Also in this figures we highlight the EoS that satisfy $\overline{\Lambda}_{1.4M_\odot} \leq 800$ and both this and $M_{\max} \leq 2.3M_\odot$; it is clear that although these restrictions do not greatly restrict the $\epsilon(p)$ space, they do restrict the mass-radius space. The upper limit on $\overline{\Lambda}_{1.4M_\odot}$ is the 90% credible upper bound derived in Ref. [22]; the upper limit on the $M_{\max}$ is a reasonable condition for the maximum mass coming from analysis of GW170817 and its electromagnetic counterpart [116–118].

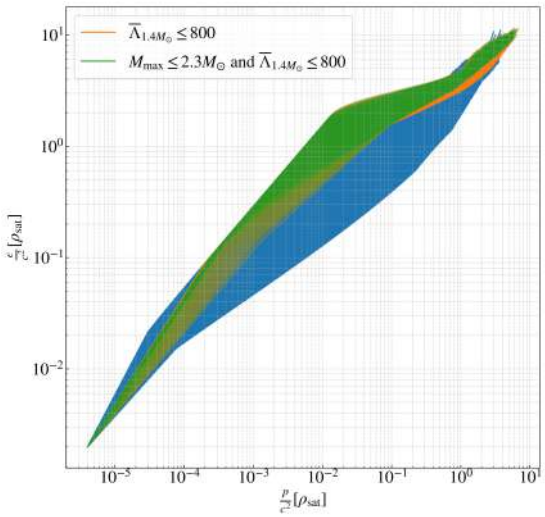

Figure 4.19: Curves, in blue, representing the $\epsilon(p)$ relations for 15,000 phenomenological equations of state, where both ϵ and p are in unities of the nuclear saturation mass density $\rho_{\rm sat}$. Highlighted in orange are the ones that satisfy $\overline{\Lambda}_{1.4M_\odot} \leq 800$ and in green the ones that satisfy both this and $M_{\max} \leq 2.3M_\odot$.

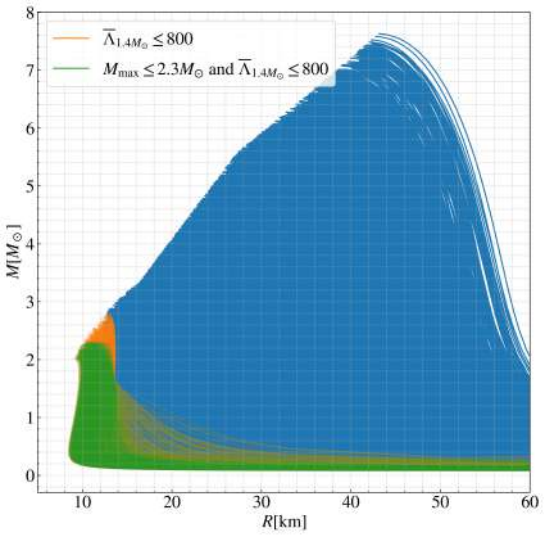

Figure 4.20: Representation of the mass-radius curves for 15,000 phenomenological EoS. Each curve was made by generating 50 stars with different central densities up to the one that generates the most massive star. Highlighted in orange are the ones that satisfy $\overline{\Lambda}_{1.4M_\odot} \leq 800$ and in green the ones that satisfy both this and $M_{\max} \leq 2.3M_\odot$.

From this we can move on to analyze the $\alpha_c - C/\bar{I}/\bar{\Lambda}$ relations with this space of equations of state, considering the entire space, with no further restrictions. The fits presented here are done in the same manner as described in Sec. 4.2.1 where only configurations with $C > 0.05$ are considered.

The relation between $\alpha_c - C$ is presented in Fig. 4.21 fitted to different values of n in Eq. (4.15). The fit with the lower maximum relative error is $n = 6$, $\sim 51.8\%$, with 90% of errors below $\sim 15.5\%$ and average relative error of $\sim 4.18\%$. However, from the figure, we can see that the difference between the fits is very small. The coefficient values for all the fits presented in Fig. 4.21 can be found in Table B.5. From this table we can see that the coefficient a_0 is small in all the different order fits and because of this, it can be set to 0. As this does not affect the errors, we choose not to do so.

The relation between $\alpha_c - \overline{I}$ is presented in Fig. 4.22 fitted to different values of n in Eq. (4.17). The fit with the lower maximum relative error is $n = 6$, $\sim 23.76\%$, with 90% of errors below $\sim 6.8\%$ and average relative error of $\sim 2.82\%$. The coefficient values for all the fits presented in Fig. 4.22 can be found in Table B.6.

The relation between $\alpha_c - \overline{\Lambda}$ is presented in Fig. 4.23 fitted to different values of n

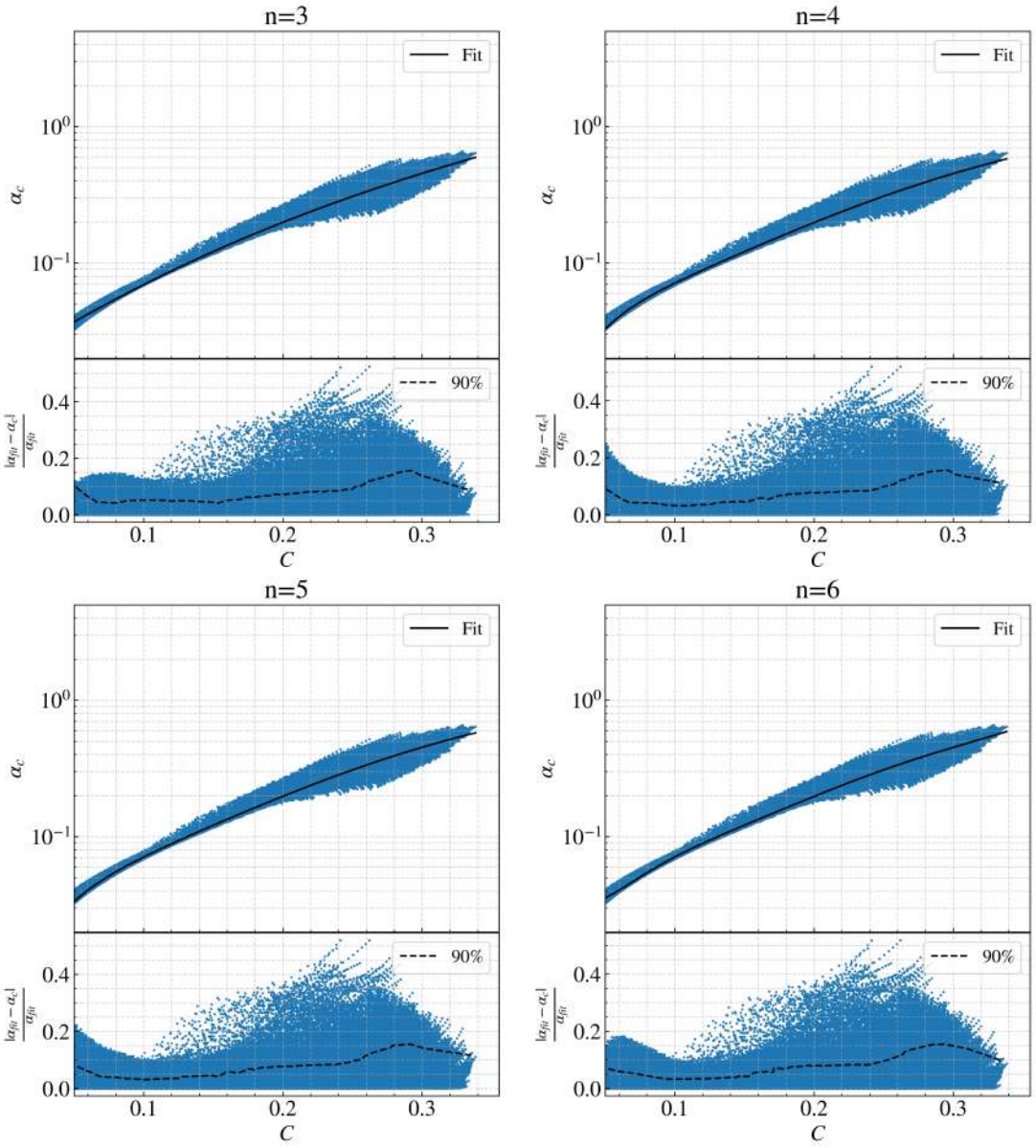

Figure 4.21: Approximately universal$\alpha_c - C$ relation for a set of 15,000 phenomenological equations of state. A solid black line represents an n-th order polynomial fit (as in Eq. (4.15)). Bottom panels display the corresponding relative error as described in Eq. (4.16), with the black dashed line representing 90% of the relative error in the particulars intervals. Only configurations with $C > 0.05$ are considered.

in Eq. (4.18). The fit with the lower maximum relative error is $n = 4$, $\sim 25.0\%$, with 90% of errors below $\sim 7.3\%$ and average relative error of $\sim 2.52\%$. The coefficient values for all the fits presented in Fig. 4.23 can be found in Table B.7. From the table we can see that the higher order coefficients are extremely small; this means a lower order fit than $n = 3$ may still be able to properly fit this relation.

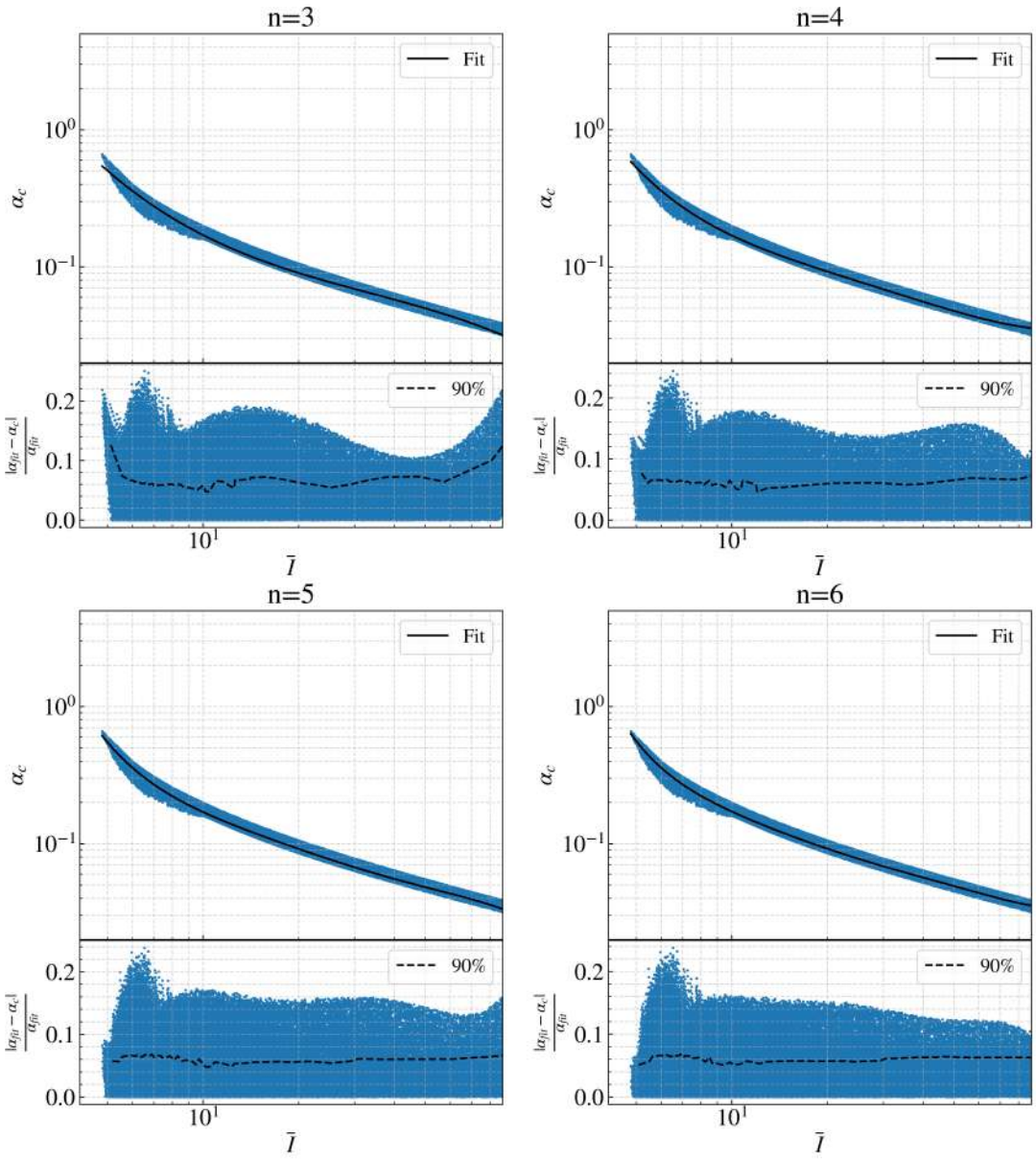

Figure 4.22: Approximately universal$\alpha_c - \bar{I}$ relation for a set of 15,000 phenomenological equations of state. A solid black line represents an n-th order polynomial fit (as in Eq. (4.17)). Bottom panels display the corresponding relative error as described in Eq. (4.16), with the black dashed line representing 90% of the relative error in the particulars intervals. Only configurations with $C > 0.05$ are considered.

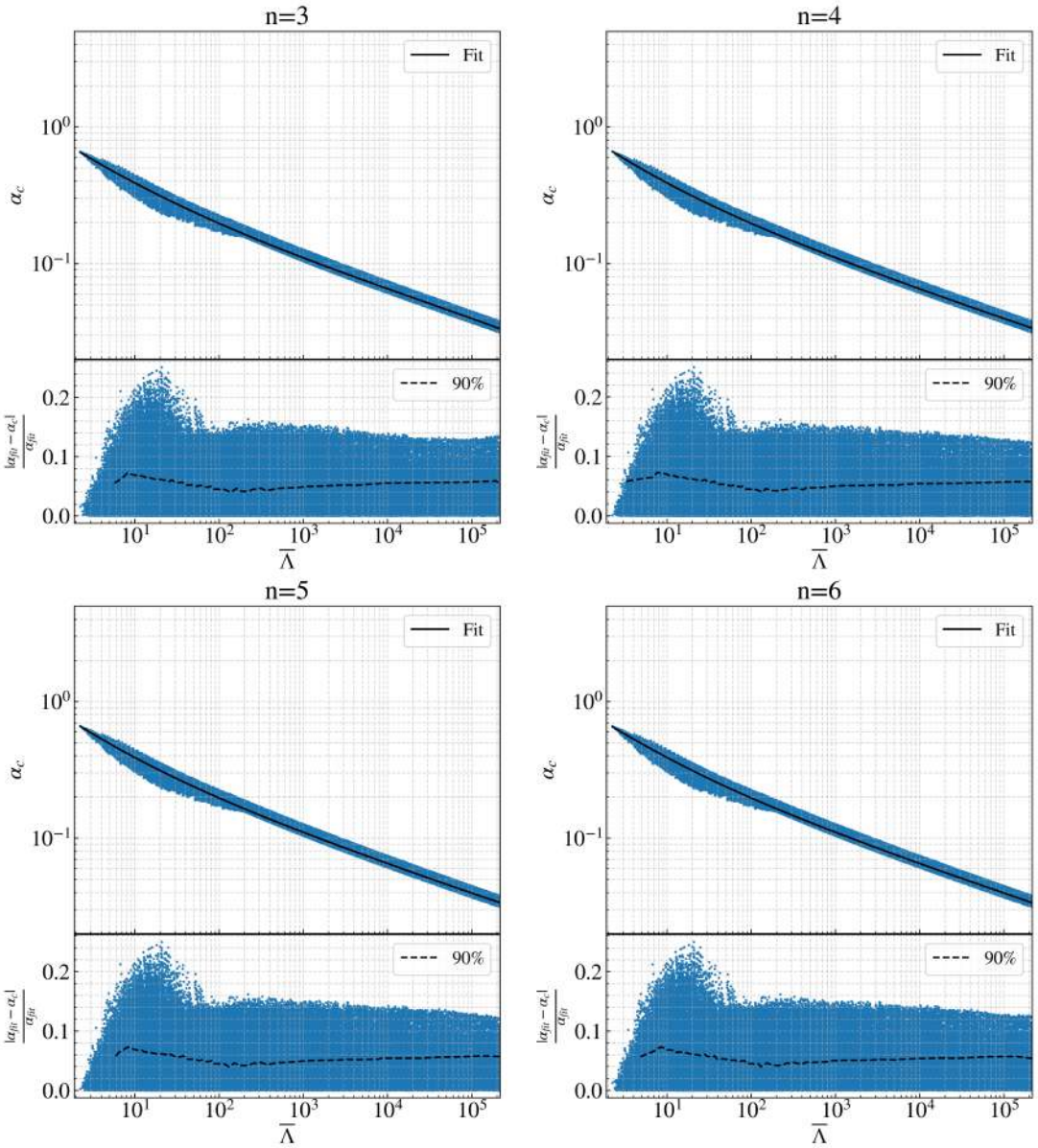

Figure 4.23: Approximately universal$\alpha_c - \overline{\Lambda}$ relation for a set of 15,000 phenomenological equations of state. A solid black line represents an n-th order polynomial fit (as in Eq. (4.18)). Bottom panels display the corresponding relative error as described in Eq. (4.16), with the black dashed line representing 90% of the relative error in the particulars intervals. Only configurations with $C > 0.05$ are considered.

4.2.3 Effects of Constraints on the Maximum Mass and Tidal Deformability

We can impose on the EoS space the constraints highlighted in Figs. 4.19 and 4.20. We consider both only setting the upper limit $\overline{\Lambda}_{1.4M_\odot} \leq 800$ (Ref. [22]) and setting the upper limit on both the tidal deformability and the upper limit $M_{\max} \leq 2.3M_\odot$ [116–118].

The effect this has on the $\alpha_c - C/\overline{\Lambda}/\overline{I}$ relations can be seen in Fig. 4.24. The fits used here are the ones that capture the tendencies of the relation with the lowest number of parameters. For $\alpha_c - C$ we use $n = 4$, $\alpha_c - \overline{\Lambda}$ is fitted with $n = 3$ and $\alpha_c - \overline{I}$ is fitted to $n = 5$. From Fig. 4.24 we can see that these restrictions do not change the profile of these relations significantly.

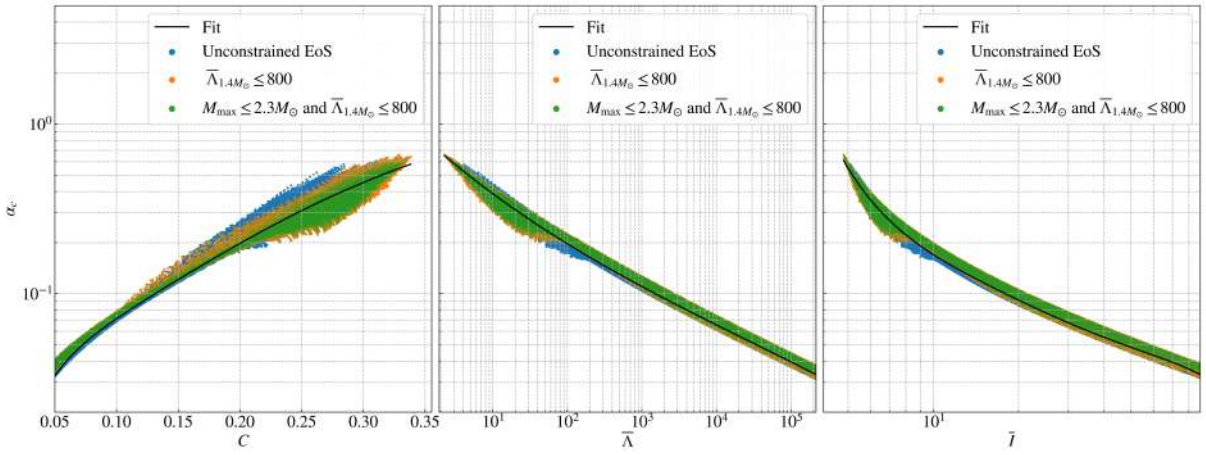

Figure 4.24: Approximately universal$\alpha_c - C/\overline{\Lambda}/\overline{I}$ relations for a set of 15,000 phenomenological equations of state, with regions that satisfy $\overline{\Lambda}_{1.4M_\odot} \leq 800$ and both this and $M_{\max} \leq 2.3M_\odot$. A solid black line represents the fits of 4/3/5-order respectively. Only configurations with $C > 0.05$ are considered.

4.2.4 Effects of Requiring Monotonicity in the Speed of Sound

We can also require that the sound speed c_s^2 is monotonically increasing with the pressure, which is not an mandatory physical condition, but is being explored here to evidence the possible impacts on the relations. We demonstrate this behavior by categorizing equations of state that have this characteristic as type 1. The requirement also leads to α_c being monotonically increasing. The effect this has on the EoS space and the space of the mass-radius curves can be visualized in Figs. 4.25 and 4.26, that show that this requirement does not restrict the EoS space.

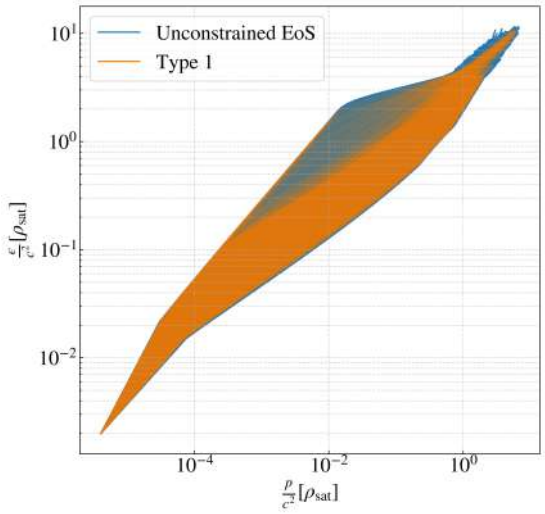

Figure 4.25: Curves representing the $\epsilon(p)$ relations for 15,000 phenomenological equations of state, where both ϵ and p are in unities of the nuclear saturation mass density ρ_{sat}. The orange curves indicate the type 1 EoS, meaning the ones were the speed of sound is monotonically increasing.

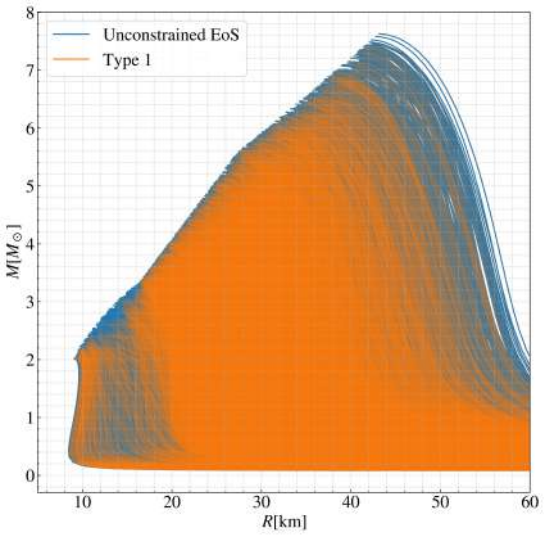

Figure 4.26: Representation of the mass-radius curves for 15,000 phenomenological equations of state. Each curve was made by generating 50 stars with different central densities up to the density corresponding to the maximum mass. The orange curves indicate the type 1 EoS, meaning the ones were the speed of sound is monotonically increasing.

The $\alpha_c - C/\overline{\Lambda}/\overline{I}$ relations for EoS that have monotonically increasing speed of sound compared to the general space is shown in Fig. 4.27. Even though imposing this seems to have little effect on the EoS space, it has a big impact on the relations. It is apparent that the widening that occurs for higher values of α_c are directly related to the behavior of non-monotonicity in the speed of sound.

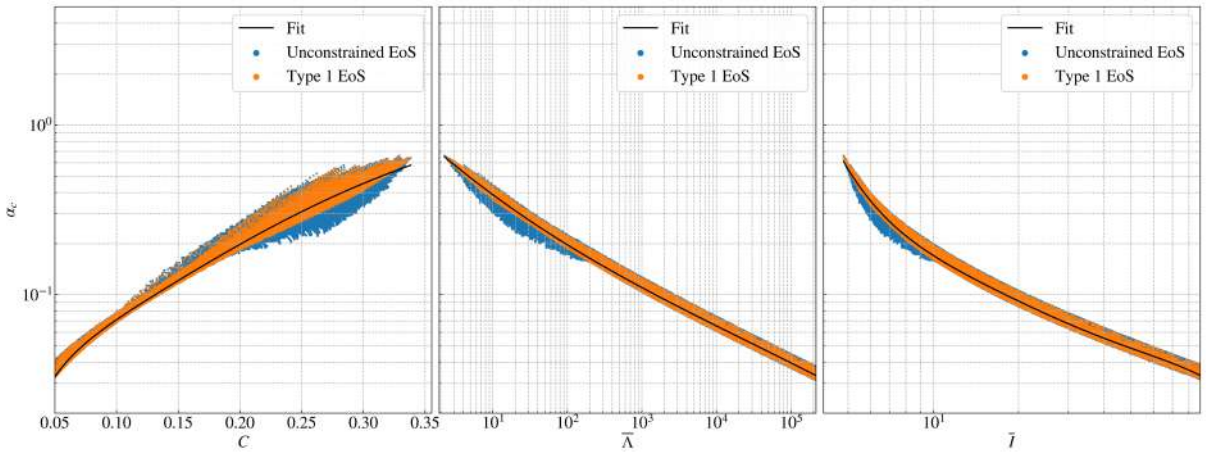

Figure 4.27: Approximately universal$\alpha_c - C/\overline{\Lambda}/\overline{I}$ relations for a set of 15,000 phenomenological equations of state, with regions that satisfy the requirement of monotonicity in the speed of sound. A solid black line represents the fits of 4/3/5-order respectively. Only configurations with $C > 0.05$ are considered.

4.2.5 Impact of Parametrization Choice

To analyze the impact of the parametrization choice on the $\alpha_c - C/\overline{\Lambda}/\overline{I}$ relations we can generate phenomenological EoS utilizing a different parametrization. Here, we choose the spectral parametrization, described in Sec. 3.1.2.

To generate these equations we use a different method than the one presented in Sec. 4.2.2. This is because that method was not an effective way of generating these EoS, likely due to the fact that a small change in the parameters generate a big change in the equation of state. Here, we opted for a random walk in the space of spectral EoS.

The first equation of state is generated by taking the SLy equation of state parameters $\gamma_i^{\rm SLy}$, $i \in [0, 3]$, presented in Table A.3, and changing each one of the free parameters γ_i, $i \in [0, 3]$ by up to 5% of the original SLy values. The following are generated by changing the parameters of the last EoS generated by up to 5% of the original SLy parameters. This means that the n-th EoS parameters γ_i are generated by:

$$\gamma_i^n = \gamma_i^{n-1} + r\,\gamma_i^{\rm SLy}, \tag{4.24}$$

where $r \in [-0.05, 0.05]$ is a randomly generated number. The equation is accepted if it satisfies the requirements:

- Causality, by imposing that $c_s^2 \leq 1$ throughout the star up to the density that

generates the maximum mass;

- That the configuration with the highest mass, generates a star with $M_{\rm max} \geq 2\,M_{\odot}$, value that is in correspondence to measured masses of neutron stars [63], [115];
- That the tidal deformability $\overline{\Lambda}_{1.4M_{\odot}} \leq 800$, which is the 90% credible upper bound derived in Ref. [22].

With this, 10,000 EoS were generated, with the distribution of the parameters presented in Figs. 4.28, 4.29, 4.30 and 4.31

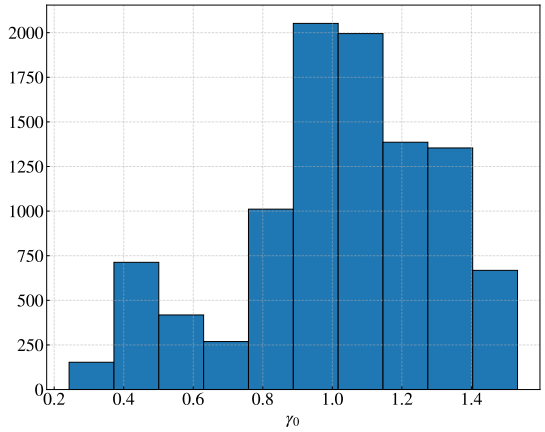

Figure 4.28: Histogram of the values of γ_0 generated with the random walk.

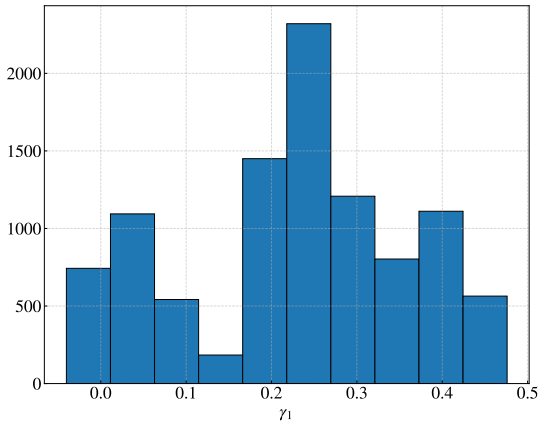

Figure 4.29: Histogram of the values of γ_1 generated with the random walk.

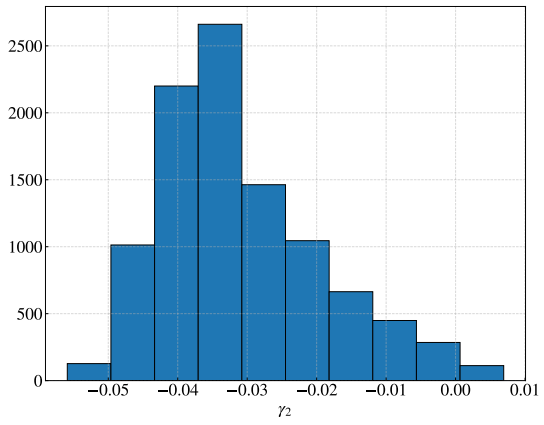

Figure 4.30: Histogram of the values of γ_2 generated with the random walk.

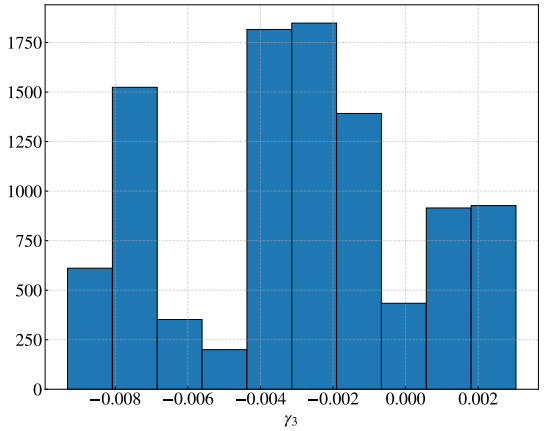

Figure 4.31: Histogram of the values of γ_3 generated with the random walk.

We can now compare the relation for the set of equations of state with $\overline{\Lambda}_{1.4M_{\odot}} \leq 800$ generated with the GPP parametrization — which amounts to about $\sim 2,300$ EoS— and the spectral parameterized EoS. The space of EoS of both these cases is presented in Figs.

4.32 and 4.33. As the method used to generate the EoS were different in both cases, it is understandable that the number of EoS generated by the spectral parametrization was not high enough to populate the entire space occupied by the EoS generated with the GPP parametrization. However, it was capable of populating areas that the GPP EoS were not. This is likely due to the fact that the random walk method chosen to generate the EoS with the spectral parametrization populates the EoS space slowly, whereas the method used to generate the EoS with the GPP parametrization is quick to populate the EoS space as the parameters are chosen at random.

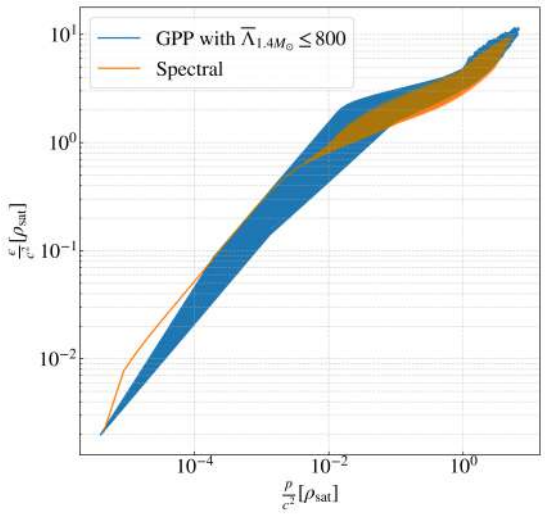

Figure 4.32: Curves representing the $\epsilon(p)$ relations for 10,000 phenomenological equations of state generated with the spectral parametrization and the GPP EoS space with the restriction on the tidal deformability. Both ϵ and p are in unities of the nuclear saturation mass density ρ_{sat}.

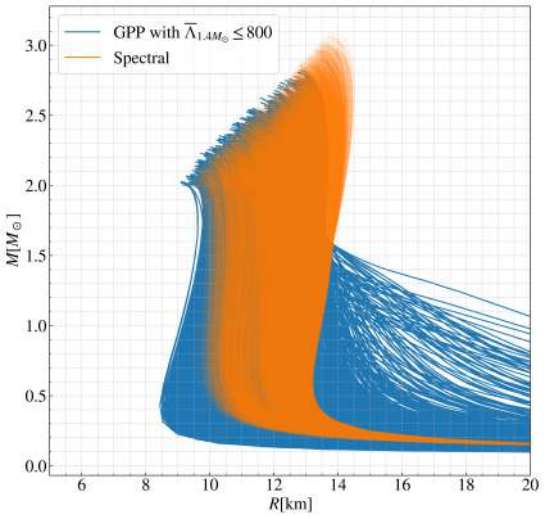

Figure 4.33: Representation of the mass-radius curves for 10,000 phenomenological equations of state generated with the spectral parametrization and the GPP EoS space with the restriction on the tidal deformability. Each curve was made by generating 50 stars with different central densities up to the density corresponding to the maximum mass.

The $\alpha_c - C/\overline{\Lambda}/\overline{I}$ relations for the spectral and GPP with $\overline{\Lambda}_{1.4M_\odot} \leq 800$ generated EoS is shown in Fig. 4.34. From it we can see that the relations for the spectral parametrization are tighter than the ones from GPP even with the same restrictions on the observables.

4.2.6 Comparison with other Relations

As demonstrated previously, the speed of sound and α_c are both measures of the stiffness of a neutron star. Because of this, it is natural to consider if the $\alpha_c - C/\overline{\Lambda}/\overline{I}$

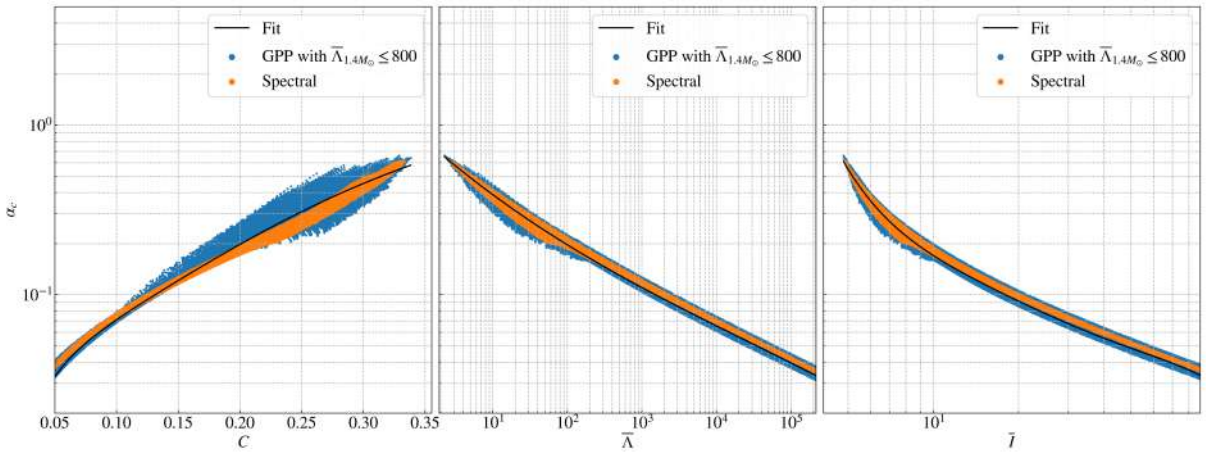

Figure 4.34: Approximately universal$\alpha_c - C/\overline{\Lambda}/\overline{I}$ relations for 10,000 phenomenological equations of state generated with the spectral parametrization and the GPP EoS space with the restriction on the tidal deformability. A solid black line represents the fits of 4/3/5-order respectively. Only configurations with $C > 0.05$ are considered.

relations are also valid if we consider the squared speed of sound c_s^2 at the center of the star instead of α_c.

This is tested with the set of $\sim 25,000$ phenomenological EoS generated both with the GPP and spectral parametrization in Fig. 4.35. From it is clear that the relations involving the central speed of sound c_s^2 are much more EoS-dependent than the $\alpha_c - C/\overline{\Lambda}/\overline{I}$ relations, meaning it presents no universality.

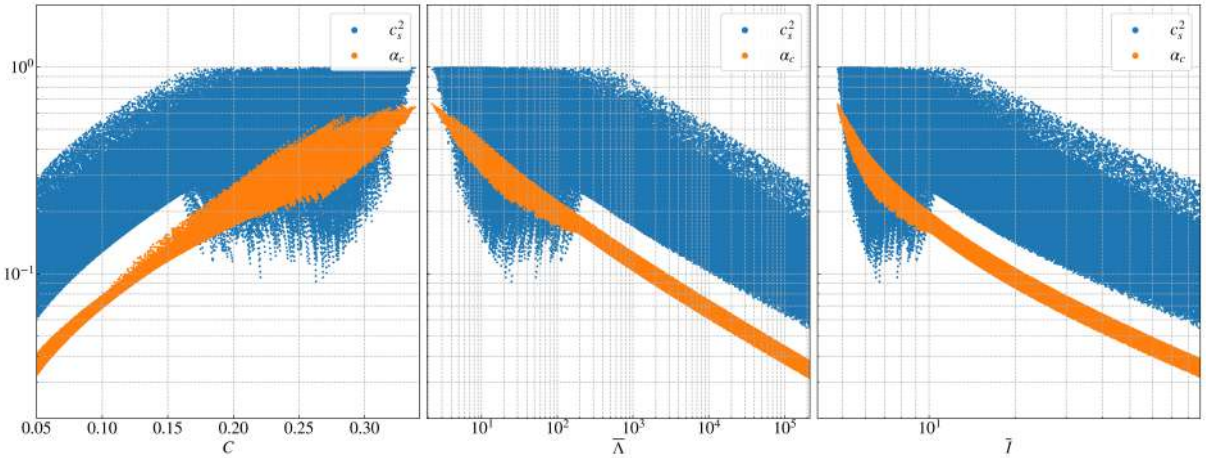

Figure 4.35: Comparison between the $\alpha_c - C/\overline{\Lambda}/\overline{I}$ relations and $c_s^2 - C/\overline{\Lambda}/\overline{I}$ for 25,000 phenomenological equations of state generated with both the spectral and the GPP parametrizations. Only configurations with $C > 0.05$ are considered.

It has been shown in Ref. [30] and presented here in Sec. 4.1 that the radius of a star with a fixed mass, or equivalently its compactness, is well correlated with the pressure at densities of (1-2)$\rho_{\rm sat}$ as can be seen in Fig. 4.7. As a consequence of the Love-C (and

I-C) relations [30, 80, 90, 91], a similar correlation is expected between the dimensionless tidal deformability (or moment of inertia) and pressure at 1-2 $\rho_{\rm sat}$. This is illustrated for a $1.4M_\odot$ neutron star in the first row of Fig. 4.36 for our set of phenomenological EoS generated with the GPP parametrization (gray), with the spectral parametrization (blue) and realistic tabulated (orange) EoS. The correlation is stronger for realistic EoS, but much weaker for the larger set of phenomenological EoS.

On the other hand, around nuclear saturation density, the ratio ϵ/ρ between energy density and mass density is not expected to differ appreciably from 1. As a consequence, a similar relation is expected between α around nuclear saturation density and the radius (and also the compactness, tidal deformability and moment of inertia) of a NS with fixed mass. This is presented in the second row of Fig. 4.36 for a $1.4M_\odot$ neutron star.

Due to these relations, it is natural to consider whether the $\alpha_c - C/\overline{\Lambda}/\overline{I}$ relations we present here might be a consequence of this well known relation, extrapolated for the higher densities present in the NS core. We show, on the the third row of Fig. 4.36, the relations between α_c and $R_{1.4}$, $C_{1.4}$ and $\overline{\Lambda}_{1.4}$. Also in this figures are fits such as presented in Eqs. (4.15) and (4.18) for $C_{1.4}$ and $\overline{\Lambda}_{1.4}$ respectively and

$$\log \alpha_c \; = \; \sum_{k=0}^{n} a_k (\log \; R)^k, \tag{4.25}$$

where a_k are the fit coefficients, for $R_{1.4}$. The correlation between this quantities is much stronger at the stellar center than around $2\rho_{\rm sat}$. It appears then that the relations $\alpha_c - C/\overline{\Lambda}/\overline{I}$ are more fundamental than the ones presented in the upper rows of Fig. 4.36.

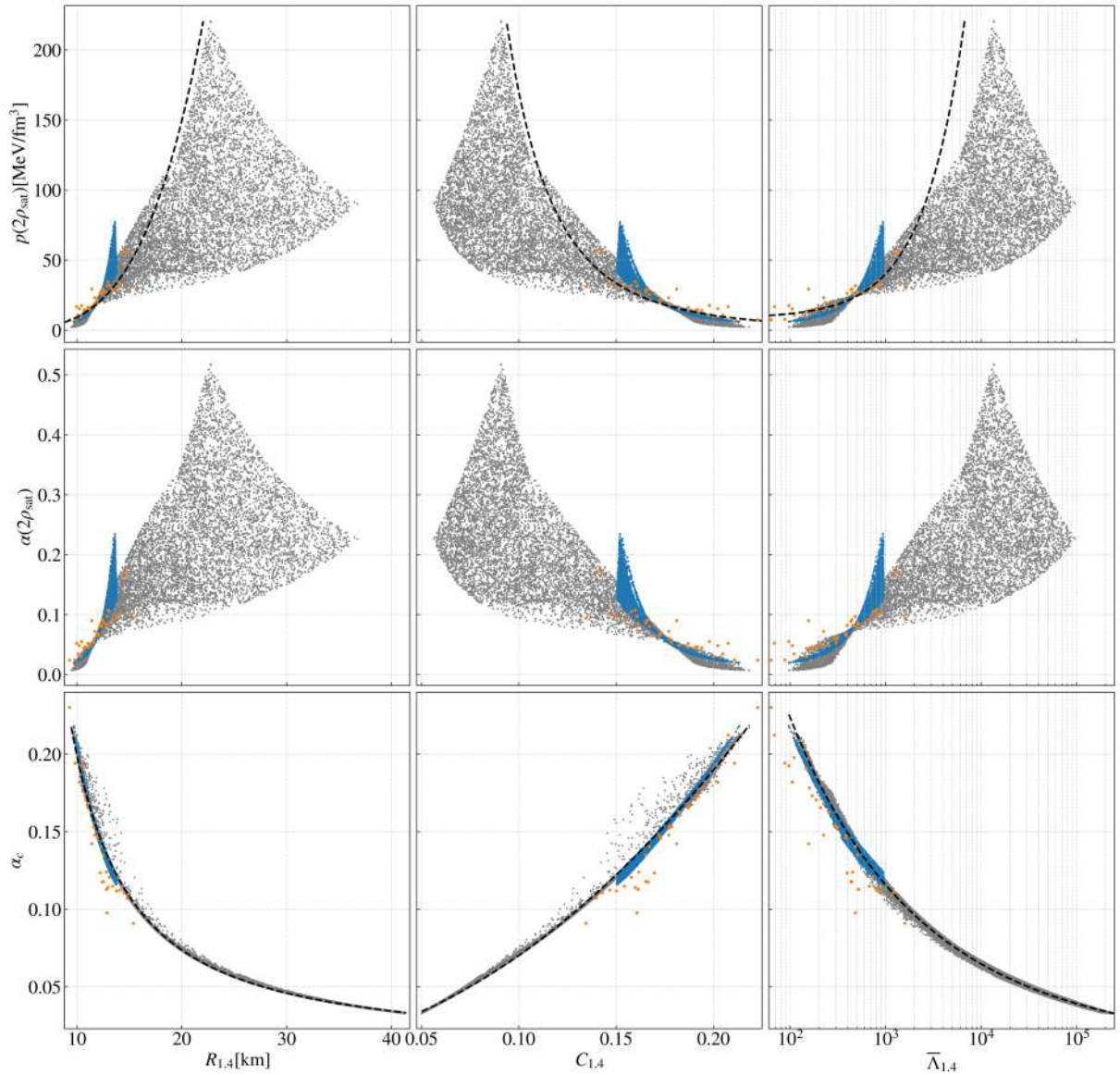

Figure 4.36: *Top row*: Pressure at twice nuclear saturation density as a function of radius, compactness and dimensionless tidal deformability of a $1.4M_\odot$ NS for our set of phenomenological EoS generated with the GPP parametrization (gray), with the spectral parametrization (blue) and realistic tabulated (orange) EoS. A black dashed line represents the fitting formulae $p(2\,\rho_{\rm sat})^{-1/4}\,R_{1.4} = 5.72$ km MeV$^{-1/4}$ fm$^{3/4}$ [30] (first panel), $p(2\rho_{\rm sat})^{1/4}\,C_{1.4} = 0.361$ MeV$^{1/4}$ fm$^{-3/4}$, which is a rescaling of the first (second panel), and $\overline{\Lambda} = 31.59\,p(2\rho_{\rm sat})/({\rm MeVfm}^{-3}) - 272.36$ [47] (third panel). *Middle row.* Same as first row, but for α at twice nuclear saturation density. *Bottom row.* Same as first row, but for α_c. Black dashed lines represent the fitting formulae B.8. Only configurations with $C > 0.05$ are considered.

Chapter 5

Conclusions

Neutron stars are objects in which matter is at its most extreme apart from the beginning of the universe. Understanding these objects can be very informative of the nature of matter at high densities and can provide important tests of General Relativity. Because of this, since its prediction and subsequent discovery, several models to describe the neutron star interior — through the equation of state — have been created (e.g. Refs. [59–62, 98, 102–114]. And due to the difficulties of obtaining either experimental or theoretical information on the validity of any particular EoS, extensive efforts to extract this information via observations have been made (examples include Refs. [7–21]). An important part of being able to measure accurately different macroscopic properties of neutron stars are the universal relations. They allow, for example, the measurements of the individual tidal deformabilities of a binary system of neutron stars through GW detection [27] and the determination of quantities that are not yet measured, such as the moment of inertia, through the measurements of the tidal deformability or the quadrupole moment [29]. Besides this, universal relations that connect microscopic and macroscopic quantities can be useful to determine important information and behavior on the interior of neutron stars (e.g. Ref. [30]).

In this thesis we presented three new EoS-independent relations in neutron stars between the ratio of the pressure and energy density at the center of the star α_c and three macroscopic quantities, the compactness C, the dimensionless tidal deformability $\overline{\Lambda}$ and the moment of inertia $\overline{I}$. In Chapter 2 we described the necessary theoretical basis to calculate the macroscopic quantities C, $\overline{\Lambda}$ and $\overline{I}$: the equilibrium and perturbation configurations of neutrons stars. In Chapter 3 we described the general difficulties of

determining the neutron star equation of state, the importance of EoS parametrizations and described two parametrizations, the generalized piecewise polytropic [65] and the spectral [66] parametrizations. Chapter 4 is divided in two sections: Section 4.1 is a general overview of universal relations in the form of a literature survey, where a few known relations are presented. Section 4.2 is where the original contributions of this thesis are presented and elaborated.

First, we describe the interpretation of the microscopic quantity present in the EoS-independent relations, $\alpha_c = p_c/\epsilon_c$ as an average measure of the stiffness of a neutron star. Then, we move on to analyzing the relations between this quantity, evaluated at the center of the star α_c, and the macroscopic quantities $C/\overline{\Lambda}/\overline{I}$ for a set of 40 realistic equations of state found in [63], we do this by presenting fits to represent these relations. The fits can be used to portray the dependence on the EoS each relation has; this is presented here with values of the maximum error. We find that the $\alpha_c - C$ relation has the maximum relative error of 32% with respect to the fit, with 99.7% of the relative error under 28.5%. For the $\alpha_c - \overline{I}$ relation we find that it has a maximum relative error of 35% with respect to the fit and 99.7% of its relative error is under 15.4%. For the $\alpha_c - \overline{\Lambda}$ relation we find that its maximum relative error with respect to the fit is 47.5%, which is considerably higher due to the apparent different relation that quark stars obey; if we remove the EoS that describe these stars, we find the maximum relative error is of 30%, and 99.7% of the relative error is under 28%.

After this, we analyzed these relations for a set of 15,000 phenomenological EoS generated with the GPP parametrization. Preceding this we discuss the process of generating these equations and analyze the space of parameters of the GPP parametrization and present new restrictions in this space, showing that the four free parameters parametrization has, in reality, effectively only three free parameters. The $\alpha_c - C/\overline{\Lambda}/\overline{I}$ relations for this set of equations of state is, as expected, wider than for the set of realistic EoS. The fit of the relation between $\alpha_c - C$ has the maximum relative error of 51.8% with respect to the fit and 90% of the relative error under 15.5%. The fit of the correlation between $\alpha_c - \overline{I}$ has the maximum relative error of 23.8% with respect to the fit and 90% of the relative error under 6.8%. The fit of the correlation between $\alpha_c - \overline{\Lambda}$ has the maximum relative error of 25% with respect to the fit and 90% of the relative error under 7.3%.

The next step we took was to analyze the robustness of these relations given

different assumptions. First we consider the effect of setting an upper limit $\overline{\Lambda}_{1.4} \leq 800$ on the tidal deformability by itself and latter adding an upper limit of $M_{\max} \leq 2.3 M_{\odot}$ on the maximum mass. Neither of these requirements appears to change the general profile of the three relations. Then we consider the effect of requiring monotonicity of c_s^2; this seems to tighten the three relations: it is apparent that the non-monotonicity on the speed of sound causes widening in the region of high compactness. Following this we considered how dependent on the EoS parametrization these relations are. To do this we generated 10,000 phenomenological equations of state using the spectral parametrization with the requirement that $\overline{\Lambda}_{1.4} \leq 800$, previously describing the process of generating these equations. We compare the relation for this set of EoS with the set of GPP-generated EoS with the same upper limit requirement on the tidal deformability. We find that the relations hold for the spectral parametrization, being even tighter than the one presented with the GPP equations of state, which is likely the result of the smaller EoS space generated by the set of the EoS generated with the spectral parametrization.

Lastly we analyzed the universality of these relations against different relations between macroscopic and microscopic quantities. We find that it depends considerably less on the EoS than the relations between the speed of sound in the center of the star and the quantities $C/\overline{\Lambda}/\overline{I}$, that has great EoS-dependence. We also find that for our set of equations of state, the known correlation between the radius of a neutron star at a specific mass and the pressure evaluated near the nuclear saturation density [30] appears to be much less robust than the relation between α_c and the radius at a specific mass. We also analyze the possibility that the origin of the $\alpha_c - C/\overline{\Lambda}/\overline{I}$ lies in this known relation; which does not appear to be the case, with the relation of α evaluated near the nuclear saturation density being much more EoS-dependent than the relations we present.

There are several possible extensions to the work presented here. A clear path is to determine how well these relations can be used to estimate the value of α_c given a measurement of one of the observables in the relation. One can also, for example, explore these relations for neutron stars under different configurations: analyzing magnetized neutron stars and considering rapidly rotating NSs. Another possible extension is analyzing the possibility of other macroscopic quantities also being universally related to α_c, for example the frequency of the fundamental quadrupolar mode. On the other hand, it is possible to consider an extension under the nuclear physics scope, by asking questions

such as: What can a specific value for α_c tell us about the behavior of the matter inside the star? These are some of the interesting avenues intended to future research.

Bibliography

[1] W. Baade and F. Zwicky. Remarks on Super-Novae and Cosmic Rays. *Physical Review*, 46(1):76–77, July 1934.

[2] Richard C. Tolman. Static Solutions of Einstein's Field Equations for Spheres of Fluid. *Physical Review*, 55(4):364–373, February 1939. Publisher: American Physical Society.

[3] J. R. Oppenheimer and G. M. Volkoff. On Massive Neutron Cores. *Physical Review*, 55(4):374–381, February 1939. Publisher: American Physical Society.

[4] Robert F. Tooper. Adiabatic Fluid Spheres in General Relativity. *The Astrophysical Journal*, 142:1541, November 1965. ADS Bibcode: 1965ApJ...142.1541T.

[5] Jeffrey M. Cohen, William D. Langer, Leonard C. Rosen, and A. G. W. Cameron. Neutron Star Models based on an Improved Equation of State. *Astrophysics and Space Science*, 6(2):228–239, February 1970.

[6] Gerhard Borner and Jeffrey M. Cohen. Rotating Neutron Star Models and Pulsars. *The Astrophysical Journal*, 185:959–974, November 1973. ADS Bibcode: 1973ApJ...185..959B.

[7] W. David Arnett and Richard L. Bowers. A Microscopic Interpretation of Neutron Star Structure. *The Astrophysical Journal Supplement Series*, 33:415, April 1977. ADS Bibcode: 1977ApJS...33..415A.

[8] Lee Lindblom. Determining the Nuclear Equation of State from Neutron-Star Masses and Radii. *The Astrophysical Journal*, 398:569, October 1992.

[9] Scott Koranda, Nikolaos Stergioulas, and John L. Friedman. Upper Limits Set by Causality on the Rotation and Mass of Uniformly Rotating Relativistic

Stars. *The Astrophysical Journal*, 488:799–806, October 1997. ADS Bibcode: 1997ApJ...488..799K.

[10] Bennett Link, Richard I. Epstein, and James M. Lattimer. Pulsar Constraints on Neutron Star Structure and Equation of State. *Physical Review Letters*, 83(17):3362–3365, October 1999. Publisher: American Physical Society.

[11] M. Bejger and P. Haensel. Moments of inertia for neutron and strange stars: limits derived for the Crab pulsar. *Astronomy & Astrophysics*, 396(3):917–921, December 2002. arXiv: astro-ph/0209151.

[12] Joshua A. Faber, Philippe Grandclement, Frederic A. Rasio, and Keisuke Taniguchi. Measuring Neutron Star Radii with Gravitational Wave Detectors. *Physical Review Letters*, 89(23):231102, November 2002. arXiv: astro-ph/0204397.

[13] James M. Lattimer and Bernard F. Schutz. Constraining the Equation of State with Moment of Inertia Measurements. *The Astrophysical Journal*, 629(2):979, August 2005. Publisher: IOP Publishing.

[14] Slavko Bogdanov, George B. Rybicki, and Jonathan E. Grindlay. Constraints on Neutron Star Properties from X-Ray Observations of Millisecond Pulsars. *The Astrophysical Journal*, 670(1):668, November 2007. Publisher: IOP Publishing.

[15] Tanja Hinderer and Eanna E. Flanagan. Constraining neutron star tidal Love numbers with gravitational wave detectors. *Physical Review D*, 77(2):021502, January 2008. arXiv: 0709.1915.

[16] Feryal Özel and Dimitrios Psaltis. Reconstructing the neutron-star equation of state from astrophysical measurements. *Physical Review D*, 80(10):103003, November 2009. Publisher: American Physical Society.

[17] Jocelyn S. Read, Charalampos Markakis, Masaru Shibata, Koji Uryu, Jolien D. E. Creighton, and John L. Friedman. Measuring the neutron star equation of state with gravitational wave observations. *Physical Review D*, 79(12):124033, June 2009. arXiv: 0901.3258.

[18] Charalampos Markakis, Jocelyn S. Read, Masaru Shibata, Koji Uryu, Jolien D. E. Creighton, John L. Friedman, and Benjamin D. Lackey. Neutron star equation of

state via gravitational wave observations. *Journal of Physics: Conference Series*, 189:012024, October 2009. arXiv: 1110.3759.

[19] H. K. Lau, P. T. Leung, and L. M. Lin. Inferring physical parameters of compact stars from their f-mode gravitational wave signals. *The Astrophysical Journal*, 714(2):1234–1238, April 2010. Publisher: American Astronomical Society.

[20] Feryal Özel, Gordon Baym, and Tolga Güver. Astrophysical measurement of the equation of state of neutron star matter. *Physical Review D*, 82(10):101301, November 2010. Publisher: American Physical Society.

[21] Andrew W. Steiner, James M. Lattimer, and Edward F. Brown. The Equation of State from Observed Masses and Radii of Neutron Stars. *The Astrophysical Journal*, 722(1):33–54, October 2010. arXiv: 1005.0811.

[22] LIGO Scientific Collaboration, Virgo Collaboration, B. P. Abbott, R. Abbott, et al. GW170817: Observation of Gravitational Waves from a Binary Neutron Star Inspiral. *Physical Review Letters*, 119(16):161101, October 2017. Publisher: American Physical Society.

[23] T. E. Riley, A. L. Watts, S. Bogdanov, P. S. Ray, R. M. Ludlam, S. Guillot, Z. Arzoumanian, C. L. Baker, A. V. Bilous, D. Chakrabarty, K. C. Gendreau, A. K. Harding, W. C. G. Ho, J. M. Lattimer, S. M. Morsink, and T. E. Strohmayer. A NICER View of PSR J0030+0451: Millisecond Pulsar Parameter Estimation. *The Astrophysical Journal*, 887(1):L21, December 2019. Publisher: American Astronomical Society.

[24] M. C. Miller, F. K. Lamb, A. J. Dittmann, S. Bogdanov, Z. Arzoumanian, K. C. Gendreau, S. Guillot, A. K. Harding, W. C. G. Ho, J. M. Lattimer, R. M. Ludlam, S. Mahmoodifar, S. M. Morsink, P. S. Ray, T. E. Strohmayer, K. S. Wood, T. Enoto, R. Foster, T. Okajima, G. Prigozhin, and Y. Soong. PSR j0030+0451 mass and radius from NICER data and implications for the properties of neutron star matter. *The Astrophysical Journal*, 887(1):L24, dec 2019.

[25] Thomas E. Riley, Anna L. Watts, Paul S. Ray, Slavko Bogdanov, Sebastien Guillot, Sharon M. Morsink, Anna V. Bilous, Zaven Arzoumanian, Devarshi Choudhury, Julia S. Deneva, and et al. A nicer view of the massive pulsar psr j0740+6620

informed by radio timing and xmm-newton spectroscopy. *The Astrophysical Journal Letters*, 918(2):L27, Sep 2021.

[26] M. C. Miller, F. K. Lamb, et al. The Radius of PSR J0740+6620 from NICER and XMM-Newton Data. *arXiv:2105.06979 [astro-ph, physics:gr-qc, physics:nucl-ex, physics:nucl-th]*, May 2021. arXiv: 2105.06979.

[27] Kent Yagi and Nicolas Yunes. Binary Love Relations. *Classical and Quantum Gravity*, 33(13):13LT01, July 2016. arXiv: 1512.02639.

[28] Kent Yagi. Multipole Love Relations. *Physical Review D*, 89(4):043011, February 2014. arXiv: 1311.0872.

[29] Kent Yagi and Nicolas Yunes. I-Love-Q. *Science*, 341(6144):365–368, July 2013. arXiv: 1302.4499.

[30] J. M. Lattimer and M. Prakash. Neutron Star Structure and the Equation of State. *The Astrophysical Journal*, 550:426–442, March 2001.

[31] S. Chandrasekhar. The highly collapsed configurations of a stellar mass. *Monthly Notices of the Royal Astronomical Society*, 91:456–466, March 1931.

[32] L. Landau. Origin of Stellar Energy. *Nature*, 141(3564):333–334, February 1938.

[33] A. Einstein. Die Grundlage der allgemeinen Relativitätstheorie. *Annalen der Physik*, 354(7):769–822, 1916.

[34] R.C. Tolman. *Relativity, Thermodynamics and Cosmology.* International series of monographs on physics. Clarendon Press, 1934.

[35] E. M. Lifshitz L. D. Landau. *The Classical Theory of Fields, Third Revised English Edition 2.* Course of Theoretical Physics. Pergamon Press, 2 edition, 1971.

[36] Albert Einstein. Die Feldgleichungen der Gravitation. *Sitzungsberichte der Königlich Preußischen Akademie der Wissenschaften (Berlin)*, pages 844–847, January 1915.

[37] Tullio Regge and John A. Wheeler. Stability of a schwarzschild singularity. *Physical Review*, 108:1063–1069, Nov 1957.

[38] Eric Poisson and Clifford M. Will. *Gravity: Newtonian, Post-Newtonian, Relativistic*. Cambridge University Press, 2014.

[39] A. E. H. Love. *Some Problems of Geodynamics*. Cambridge University Press, 1911.

[40] Kip S. Thorne. Tidal stabilization of rigidly rotating, fully relativistic neutron stars. *Physical Review D*, 58(12):124031, November 1998. Publisher: American Physical Society.

[41] Tanja Hinderer. Tidal Love Numbers of Neutron Stars. *The Astrophysical Journal*, 677(2):1216–1220, April 2008.

[42] Michele Maggiore. *Gravitational Waves. Vol. 2: Astrophysics and Cosmology*. Oxford University Press, 3 2018.

[43] Thibault Damour and Alessandro Nagar. Relativistic tidal properties of neutron stars. *Physical Review D*, 80(8):084035, October 2009. arXiv: 0906.0096.

[44] Taylor Binnington and Eric Poisson. Relativistic theory of tidal Love numbers. *Physical Review D*, 80(8):084018, October 2009. arXiv: 0906.1366.

[45] The LIGO Scientific Collaboration, the Virgo Collaboration, B. P. Abbott, R. Abbott, et al. GW170817: Measurements of Neutron Star Radii and Equation of State. *Physical Review Letters*, 121(16):161101, October 2018. arXiv: 1805.11581.

[46] Tanja Hinderer and Andreas Guerra Chaves. Probing the equation of state of neutron star matter with gravitational waves from binary inspirals in light of GW170817: a brief review. *Journal of Physics G: Nuclear and Particle Physics*, 46(12):123002, December 2019. arXiv: 1912.01461.

[47] Yeunhwan Lim and Jeremy W. Holt. Neutron star tidal deformabilities constrained by nuclear theory and experiment. *Physical Review Letters*, 121(6):062701, August 2018. arXiv: 1803.02803.

[48] Tanja Hinderer, Benjamin D. Lackey, Ryan N. Lang, and Jocelyn S. Read. Tidal deformability of neutron stars with realistic equations of state and their gravitational wave signatures in binary inspiral. *Physical Review D*, 81(12):123016, June 2010. arXiv: 0911.3535 version: 1.

[49] Thibault Damour, Alessandro Nagar, and Loic Villain. Measurability of the tidal polarizability of neutron stars in late-inspiral gravitational-wave signals. *Physical Review D*, 85(12):123007, June 2012. arXiv: 1203.4352.

[50] Kip S. Thorne. Multipole expansions of gravitational radiation. *Rev. Mod. Phys.*, 52:299–339, Apr 1980.

[51] M. Kramer and N. Wex. The double pulsar system: a unique laboratory for gravity. *Classical and Quantum Gravity*, 26(7):073001, February 2009. Publisher: IOP Publishing.

[52] James B. Hartle. Slowly Rotating Relativistic Stars. I. Equations of Structure. *The Astrophysical Journal*, 150:1005, December 1967.

[53] James B. Hartle and David H. Sharp. Variational Principle for the Equilibrium of a Relativistic, Rotating Star. *Astrophysical Journal*, 147:317, January 1967.

[54] Eric Poisson. *A Relativist's Toolkit: The Mathematics of Black-Hole Mechanics*. Cambridge University Press, 2004.

[55] P. Haensel, A.Y. Potekhin, and D.G. Yakovlev. *Neutron Stars 1: Equation of State and Structure*. Astrophysics and Space Science Library. Springer New York, 2007.

[56] John Antoniadis, Paulo C. C. Freire, Norbert Wex, Thomas M. Tauris, Ryan S. Lynch, Marten H. van Kerkwijk, Michael Kramer, Cees Bassa, Vik S. Dhillon, Thomas Driebe, and et al. A massive pulsar in a compact relativistic binary. *Science*, 340(6131), Apr 2013.

[57] P. B. Demorest, T. Pennucci, S. M. Ransom, M. S. E. Roberts, and J. W. T. Hessels. A two-solar-mass neutron star measured using Shapiro delay. *Nature*, 467(7319):1081–1083, October 2010.

[58] H. T. Cromartie, E. Fonseca, S. M. Ransom, P. B. Demorest, Z. Arzoumanian, H. Blumer, P. R. Brook, M. E. DeCesar, T. Dolch, J. A. Ellis, R. D. Ferdman, E. C. Ferrara, N. Garver-Daniels, P. A. Gentile, M. L. Jones, M. T. Lam, D. R. Lorimer, R. S. Lynch, M. A. McLaughlin, C. Ng, D. J. Nice, T. T. Pennucci, R. Spiewak, I. H. Stairs, K. Stovall, J. K. Swiggum, and W. W. Zhu. Relativistic

Shapiro delay measurements of an extremely massive millisecond pulsar. *Nature Astronomy*, 4(1):72–76, January 2020.

[59] F. Douchin and P. Haensel. A unified equation of state of dense matter and neutron star structure. *Astronomy & Astrophysics*, 380(1):151–167, Dec 2001.

[60] Horst Müller and Brian D. Serot. Relativistic mean-field theory and the high-density nuclear equation of state. *Nuclear Physics A*, 606(3-4):508–537, Sep 1996.

[61] H. Müther, M. Prakash, and T.L. Ainsworth. The nuclear symmetry energy in relativistic brueckner-hartree-fock calculations. *Physics Letters B*, 199(4):469–474, 1987.

[62] R. B. Wiringa, V. Fiks, and A. Fabrocini. Equation of state for dense nucleon matter. *Physical Review C*, 38:1010–1037, Aug 1988.

[63] Feryal Özel and Paulo Freire. Masses, radii, and the equation of state of neutron stars. *Annual Review of Astronomy and Astrophysics*, 54(1):401–440, Sep 2016.

[64] Jocelyn Read, Benjamin Lackey, Benjamin Owen, and John L. Friedman. Constraints on a phenomenologically parametrized neutron-star equation of state. *Physical Review D*, 79(12):124032, jun 2009.

[65] Michael F. O'Boyle, Charalampos Markakis, Nikolaos Stergioulas, and Jocelyn S. Read. Parametrized equation of state for neutron star matter with continuous sound speed. *Physical Review D*, 102:083027, Oct 2020.

[66] Lee Lindblom. Spectral representations of neutron-star equations of state. *Physical Review D*, 82:103011, Nov 2010.

[67] Eemeli Annala, Tyler Gorda, Aleksi Kurkela, Joonas Nättilä, and Aleksi Vuorinen. Evidence for quark-matter cores in massive neutron stars. *Nature Physics*, 16(9):907–910, Jun 2020.

[68] Werner Israel. Event Horizons in Static Vacuum Space-Times. *Physical Review*, 164(5):1776–1779, December 1967.

[69] Werner Israel. Event horizons in static electrovac space-times. *Communications in Mathematical Physics*, 8(3):245–260, September 1968.

[70] B. Carter. Axisymmetric Black Hole Has Only Two Degrees of Freedom. *Physical Review Letters*, 26(6):331–333, February 1971.

[71] Kent Yagi and Nicolás Yunes. I-love-q relations in neutron stars and their applications to astrophysics, gravitational waves, and fundamental physics. *Physical Review D*, 88(2), Jul 2013.

[72] Bruno Giacomazzo, Luciano Rezzolla, and Nikolaos Stergioulas. Collapse of differentially rotating neutron stars and cosmic censorship. *Physical Review D*, 84(2), Jul 2011.

[73] Kent Yagi, Leo C. Stein, George Pappas, Nicolas Yunes, and Theocharis A. Apostolatos. Why I-Love-Q. *Physical Review D*, 90(6):063010, September 2014. arXiv: 1406.7587.

[74] Daniela D. Doneva, Stoytcho S. Yazadjiev, Nikolaos Stergioulas, and Kostas D. Kokkotas. Breakdown of i-love-q universality in rapidly rotating relativistic stars. *The Astrophysical Journal*, 781(1):L6, December 2013. Publisher: American Astronomical Society.

[75] George Pappas and Theocharis A. Apostolatos. Effectively universal behavior of rotating neutron stars in general relativity makes them even simpler than their Newtonian counterparts. *Physical Review Letters*, 112(12):121101, March 2014. arXiv: 1311.5508.

[76] Sayan Chakrabarti, Térence Delsate, Norman Gürlebeck, and Jan Steinhoff. I-Q relation for rapidly rotating neutron stars. *Physical Review Letters*, 112(20):201102, May 2014. arXiv: 1311.6509.

[77] B. Haskell, R. Ciolfi, F. Pannarale, and L. Rezzolla. On the universality of i-love-q relations in magnetized neutron stars. *Monthly Notices of the Royal Astronomical Society: Letters*, 438(1):L71–L75, Dec 2013.

[78] Kent Yagi and Nicolás Yunes. I-love-q anisotropically: Universal relations for compact stars with scalar pressure anisotropy. *Physical Review D*, 91(12), Jun 2015.

[79] Grégoire Martinon, Andrea Maselli, Leonardo Gualtieri, and Valeria Ferrari. Rotating protoneutron stars: Spin evolution, maximum mass, and i-love-q relations. *Physical Review D*, 90(6), Sep 2014.

[80] Andrea Maselli, Vitor Cardoso, Valeria Ferrari, Leonardo Gualtieri, and Paolo Pani. Equation-of-state-independent relations in neutron stars. *Physical Review D*, 88(2):023007, July 2013. arXiv: 1304.2052.

[81] Kent Yagi and Nicolás Yunes. Approximate universal relations among tidal parameters for neutron star binaries. *Classical and Quantum Gravity*, 34(1):015006, December 2016. Publisher: IOP Publishing.

[82] Walter Del Pozzo, Tjonnie G. F. Li, Michalis Agathos, Chris Van Den Broeck, and Salvatore Vitale. Demonstrating the feasibility of probing the neutron-star equation of state with second-generation gravitational-wave detectors. *Physical Review Letters*, 111(7), Aug 2013.

[83] Leslie Wade, Jolien D. E. Creighton, Evan Ochsner, Benjamin D. Lackey, Benjamin F. Farr, Tyson B. Littenberg, and Vivien Raymond. Systematic and statistical errors in a bayesian approach to the estimation of the neutron-star equation of state using advanced gravitational wave detectors. *Physical Review D*, 89(10):103012, May 2014. arXiv: 1402.5156.

[84] Benjamin D. Lackey and Leslie Wade. Reconstructing the neutron-star equation of state with gravitational-wave detectors from a realistic population of inspiralling binary neutron stars. *Physical Review D*, 91(4), Feb 2015.

[85] Michael McNeil Forbes, Sukanta Bose, Sanjay Reddy, Dake Zhou, Arunava Mukherjee, and Soumi De. Constraining the neutron-matter equation of state with gravitational waves. *Physical Review D*, 100(8):083010, October 2019. arXiv: 1904.04233.

[86] B. F. Schutz. Determining the Hubble constant from gravitational wave observations. *Nature*, 323(6086):310–311, September 1986.

[87] Chris Messenger and Jocelyn Read. Measuring a cosmological distance-redshift relationship using only gravitational wave observations of binary neutron star coalescences. *Physical Review Letters*, 108(9):091101, February 2012. arXiv: 1107.5725.

[88] T. G. F. Li, W. Del Pozzo, and C. Messenger. Measuring the redshift of standard sirens using the neutron star deformability. *arXiv:1303.0855 [astro-ph, physics:gr-qc]*, March 2013. arXiv: 1303.0855.

[89] Walter Del Pozzo, Tjonnie G. F. Li, and Chris Messenger. Cosmological inference using only gravitational wave observations of binary neutron stars. *Physical Review D*, 95(4):043502, February 2017. arXiv: 1506.06590.

[90] D. G. Ravenhall and C. J. Pethick. Neutron Star Moments of Inertia. *The Astrophysical Journal*, 424:846, April 1994. ADS Bibcode: 1994ApJ...424..846R.

[91] Cosima Breu and Luciano Rezzolla. Maximum mass, moment of inertia and compactness of relativistic stars. *Monthly Notices of the Royal Astronomical Society*, 459(1):646–656, June 2016.

[92] Kalin V. Staykov, Daniela D. Doneva, and Stoytcho S. Yazadjiev. Moment-of-inertia–compactness universal relations in scalar-tensor theories andr2gravity. *Physical Review D*, 93(8), Apr 2016.

[93] Kent Yagi and Nicolas Yunes. Approximate Universal Relations for Neutron Stars and Quark Stars. *Physical Review ports*, 681:1–72, April 2017. arXiv: 1608.02582.

[94] M Urbanec, J. C Miller, and Z Stuchlík. Quadrupole moments of rotating neutron stars and strange stars. *Monthly Notices of the Royal Astronomical Society*, 433(3):1903–1909, Jun 2013.

[95] Nan Jiang and Kent Yagi. Analytic I-Love-C relations for realistic neutron stars. *Physical Review D*, 101(12):124006, June 2020. arXiv: 2003.10498 version: 2.

[96] T. K. Chan, Y.-H. Sham, P. T. Leung, and L.-M. Lin. Multipolar universal relations between f-mode frequency and tidal deformability of compact stars. *Physical Review D*, 90(12):124023, December 2014. arXiv: 1408.3789.

[97] Kostas D. Kokkotas and Bernd G. Schmidt. Quasi-Normal Modes of Stars and Black Holes. *Living Reviews in Relativity*, 2(1):2, December 1999. arXiv: gr-qc/9909058 version: 1.

[98] Mark Alford, Matt Braby, Mark Paris, and Sanjay Reddy. Hybrid stars that masquerade as neutron stars. *The Astrophysical Journal*, 629(2):969–978, Aug 2005.

[99] A. M. Anile. *Relativistic Fluids and Magneto-fluids: With Applications in Astrophysics and Plasma Physics*. Cambridge Monographs on Mathematical Physics. Cambridge University Press, 1990.

[100] Sean Carroll. *Spacetime and geometry: an introduction to General Relativity*. Benjamin Cummings, 2004.

[101] Scott Koranda, Nikolaos Stergioulas, and John L. Friedman. Upper limits set by causality on the rotation and mass of uniformly rotating relativistic stars. *The Astrophysical Journal*, 488(2):799–806, oct 1997.

[102] A. Akmal, V. R. Pandharipande, and D. G. Ravenhall. Equation of state of nucleon matter and neutron star structure. *Phys. Rev. C*, 58:1804–1828, Sep 1998.

[103] M. Baldo, I. Bombaci, and G. F. Burgio. Microscopic nuclear equation of state with three-body forces and neutron star structure. *Astronomy and Astrophysics*, 328:274–282, December 1997.

[104] Shmuel Balberg and Avraham Gal. An effective equation of state for dense matter with strangeness. *Nuclear Physics A*, 625(1-2):435–472, Oct 1997.

[105] W. Zuo, I. Bombaci, and U. Lombardo. Asymmetric nuclear matter from an extended brueckner-hartree-fock approach. *Phys. Rev. C*, 60:024605, Jul 1999.

[106] A. Y. Potekhin, A. F. Fantina, N. Chamel, J. M. Pearson, and S. Goriely. Analytical representations of unified equations of state for neutron-star matter. *Astronomy & Astrophysics*, 560:A48, December 2013.

[107] L. Engvik, E. Osnes, M. Hjorth-Jensen, G. Bao, and E. Ostgaard. Asymmetric Nuclear Matter and Neutron Star Properties. *Astrophysical Journal*, 469:794, October 1996.

[108] B. Friedman and V. R. Pandharipande. Hot and cold, nuclear and neutron matter. *Nucl. Phys. A*, 361:502–520, 1981.

[109] N. K. Glendenning. Neutron stars are giant hypernuclei ? *Astrophysical Journal*, 293:470–493, June 1985.

[110] Norman K. Glendenning and Jürgen Schaffner-Bielich. First order kaon condensate. *Phys. Rev. C*, 60:025803, Jul 1999.

[111] Benjamin D. Lackey, Mohit Nayyar, and Benjamin J. Owen. Observational constraints on hyperons in neutron stars. *Phys. Rev. D*, 73:024021, Jan 2006.

[112] M. Prakash, T. L. Ainsworth, and J. M. Lattimer. Equation of state and the maximum mass of neutron stars. *Phys. Rev. Lett.*, 61:2518–2521, Nov 1988.

[113] M. Prakash, J. R. Cooke, and J. M. Lattimer. Quark-hadron phase transition in protoneutron stars. *Physical Review D*, 52(2):661–665, July 1995.

[114] V.R. Pandharipande and R.A. Smith. A model neutron solid with $\pi 0$ condensate. *Nuclear Physics A*, 237(3):507–532, 1975.

[115] James M. Lattimer. The Nuclear Equation of State and Neutron Star Masses. *Annual Review of Nuclear and Particle Science*, 62(1):485–515, November 2012. arXiv: 1305.3510.

[116] Ben Margalit and Brian D. Metzger. Constraining the maximum mass of neutron stars from multi-messenger observations of GW170817. *The Astrophysical Journal*, 850(2):L19, nov 2017.

[117] Luciano Rezzolla, Elias R. Most, and Lukas R. Weih. Using gravitational-wave observations and quasi-universal relations to constrain the maximum mass of neutron stars. *The Astrophysical Journal*, 852(2):L25, jan 2018.

[118] Milton Ruiz, Stuart L. Shapiro, and Antonios Tsokaros. Gw170817, general relativistic magnetohydrodynamic simulations, and the neutron star maximum mass. *Phys. Rev. D*, 97:021501, Jan 2018.

Appendix A

Table EoS

Presented here are the fit values for some of the parametrized realistic equations of state presented in Ref. [65] and Ref. [66].

ρ_i (g/cm^3)	K_i (cgs)	Γ_i	Λ_i (g/cm^3)	a_i
0	$5.214\text{e}-9$	1.611	0	0
6.285e5	$5.726\text{e}-8$	1.440	-1.354	$-1.861\text{e}-5$
1.826e6	$1.662\text{e}-6$	1.269	-6.025e3	$-5.278\text{e}-4$
3.350e11	$-7.957\text{e}29$	-1.841	1.193e9	$1.035\text{e}-2$
5.317e11	$1.746\text{e}-8$	1.382	7.077e8	$8.208\text{e}-3$

Table A.1: From Ref. [65], a GPP fit to the SLy equation of state found in Ref. [59]. This was designed to reproduce the values from the article Ref. [59] at low densities.

EOS	$\log K_1$	Γ_1	Γ_2	Γ_3
APR	-33.210	3.169	3.452	3.310
BHF	-35.016	3.284	2.774	2.616
FPS	-32.985	3.147	2.652	2.120
H4	-23.310	2.514	2.333	1.562
KDE0V	-30.250	2.967	2.835	2.803
KDE0V1	-29.232	2.900	2.809	2.747
MPA1	-40.301	3.662	3.057	2.298
MS1	-30.170	2.998	2.123	1.955
MS1b	-33.774	3.241	2.136	1.963
QHC19	-36.879	3.419	2.760	2.017
RS	-25.150	2.636	2.677	2.647
SK255	-25.990	2.693	2.729	2.667
SK272	-27.597	2.804	2.793	2.733
SKI2	-24.202	2.575	2.639	2.656
SKI3	-26.457	2.729	2.680	2.708
SKI4	-31.008	3.029	2.759	2.651
SKI5	-23.109	2.505	2.708	2.727
SKI6	-31.089	3.036	2.762	2.653
SKMP	-27.116	2.766	2.741	2.698
SKOP	-26.089	2.693	2.660	2.579
SLY2	-31.070	3.026	2.871	2.760
SLY230A	-33.385	3.184	2.895	2.588
SLY4	-31.350	3.045	2.884	2.773
SLY9	-30.657	3.005	2.796	2.652
WFF1	-34.394	3.240	3.484	3.695

Table A.2: From Ref. [65], fit parameters for the core region of a set of realistic EOS matched to the SLy(4) crust in Table A.1 at the density ρ_0 defined in (3.37).

EOS	γ_0	γ_1	γ_2	γ_3
SLy	0.9865	0.1110	-0.0301	0.0022
FPS	1.1561	-0.0468	0.0081	-0.0010
WFF1	0.6785	0.2626	-0.0215	-0.0008
MPA1	1.0215	0.1653	-0.0235	-0.0004
MS1	0.9189	0.1432	0.0122	-0.0094
MS1b	1.2132	-0.0648	0.0561	-0.0111
H4	1.0526	0.1695	-0.1200	0.0150

Table A.3: From Ref. [66], spectral fits of the standard $\epsilon = \epsilon(p)$ form of a set of realistic neutron-star equations of state. These fits were made to match the lower density part of each specific EoS at the pressure p_0 defined in (3.44).

Appendix B

Fit Coefficient Tables

Presented here are the tables containing the values for the fit coefficients used throughout this work.

a_0	a_1	a_2	a_3	a_4	a_5
93.004×10^{-4}	89.475×10^{-2}	-11.9	1.3378×10^{2}	-5.5227×10^{2}	8.766×10^{2}

Table B.1: Fit coefficients of a 5-th order polynomial fit to the $\alpha_c - C$ relation for a set of 40 realistic EoS. The values used here were restricted to 5 significant figures.

b_0	b_1	b_2	b_3	b_4	b_5
25.114	-40.279	24.803	-7.7737	1.2131	-75.105×10^{-3}

Table B.2: Fit coefficients of a 5-th order logarithmic polynomial fit to the $\alpha_c - \overline{I}$ relation for a set of 40 realistic EoS. The values used here were restricted to 5 significant figures.

c_0	c_1	c_2	c_3
-26.032×10^{-3}	-0.4985	35.384×10^{-3}	-14.339×10^{-4}

Table B.3: Fit coefficients of a 3-rd order logarithmic polynomial fit to the $\alpha_c - \overline{\Lambda}$ relation for a set of 40 realistic EoS. The values used here were restricted to 5 significant figures.

c_0	c_1	c_2	c_3	c_4
16.191×10^{-3}	-0.46772	0.02346	-22.462×10^{-5}	-3.5524×10^{-5}

Table B.4: Fit coefficients of a 4-th order logarithmic polynomial fit to the $\alpha_c - \overline{\Lambda}$ relation for a set of 37 realistic EoS. The values used here were restricted to 5 significant figures.

n	a_0	a_1	a_2	a_3	a_4	a_5	a_6
3	18.355×10^{-3}	27.612×10^{-2}	1.5615	77.8809	—	—	—
4	-17.182×10^{-3}	1.3117	−8.4592	47.166	−53.75	—	—
5	-6.1723×10^{-3}	0.90421	−3.0053	13.604	42.629	−104.57	—
6	70.315×10^{-3}	−2.5229	55.78	−485.41	2276.7	−5152.6	4532.6

Table B.5: Fit coefficients of polynomial fits to the $\alpha_c - C$ relation for a set of 15,000 phenomenological EoS. The values used here were restricted to 5 significant figures.

n	b_0	b_1	b_2	b_3	b_4	b_5	b_6
3	4.9531	−5.3362	1.3432	−0.12747	—	—	—
4	9.7476	−12.553	5.278	−1.0485	0.078206	—	—
5	18.746	−29.432	17.602	−5.4264	0.83526	−0.051045	—
6	35.829	−67.818	52.74	−22.197	5.2386	−0.65446	0.033747

Table B.6: Fit coefficients of logarithmic polynomial fits to the $\alpha_c - \overline{I}$ relation for a set of 15,000 phenomenological EoS. The values used here were restricted to 5 significant figures.

n	c_0	c_1	c_2	c_3	c_4	c_5	c_6
3	−0.12009	−0.39439	0.017279	-56.271×10^{-5}	—	—	—
4	−0.084571	−0.42467	0.02575	−0.001501	3.548×10^{-5}	—	—
5	−0.093826	−0.41448	0.021753	-79.405×10^{-5}	-2.1793×10^{-5}	-1.7245×10^{-6}	—
6	−0.13057	−0.36445	−0.0038252	0.005556	-83.853×10^{-5}	5.3917×10^{-5}	-1.3079×10^{-6}

Table B.7: Fit coefficients of a logarithmic polynomial fit to the $\alpha_c - \overline{\Lambda}$ relation for a set of 15,000 phenomenological EoS. The values used here were restricted to 5 significant figures.

Relation	d_0	d_1	d_2
$\alpha_c - R_{1.4}$	3.3379	−2.7036	0.24016
$\alpha_c - C_{1.4}$	0.01372	0.25105	3.148
$\alpha_c - \overline{\Lambda}_{1.4}$	0.051614	−0.37015	0.0073207

Table B.8: Fit coefficients of a 2-nd order polynomial fits to the $\alpha_c - R_{1.4}/C_{1.4}/\overline{\Lambda}_{1.4}$ relation for the set of EoS presented in Fig. 4.36. The first row was fitted to the fit presented in Eq. (4.25), the second fitted to the fit presented in Eq. (4.15) and the third one fitted to Eq. (4.18). The values used here were restricted to 5 significant figures.